Modélisation multi-échelle des tissus secs : Application à l'impact

Pietro del Sorbo

2018-ENAM-0003

École doctorale n° 432 : Science des Métiers de l'ingénieur

Doctorat ParisTech

T H È S E

pour obtenir le grade de docteur délivré par

l'École Nationale Supérieure d'Arts et Métiers

Spécialité "Mécanique"

présentée et soutenue publiquement par

Pietro DEL SORBO

le 21 janvier 2019

Modélisation multi-échelle des tissus secs: Application à l'impact

Directeur de thèse : **Ivan IORDANOFF**
Co-encadrement de la thèse : **Jérémie GIRARDOT, Frederic DAU**

Jury

M. Philippe BOISSE,	Professeur des Universités, INSA Lyon - LaMCoS	Président
M. François BOUSSU,	Professeur des Universités, ENSAIT - GEMTEX	Rapporteur
M. Subramani SOCKALINGAM,	Assistant Professor, Dept. of Mech. Eng., Univ. of SC	Rapporteur
M. Erasmo CARRERA,	Professeur des Universités, Politecnico di Torino - DIMEAS	Examinateur
M. Cuong HA-MINH,	Maître de Conférence, ENS Paris-Saclay – LMT	Examinateur
M. Nicolas CARRERE,	Ingénieur, Safran Composite	Invité

T
H
È
S
E

Arts et Métiers ParisTech - Campus de Bordeaux
I2M, UMR CNRS 5295

I would like to dedicate this thesis to my loving parents ...

Abstract

Les structures composites sont actuellement utilisées dans différents domaines industriels, civils et militaires tels que l'aéronautique, l'automobile, la mécanique, l'éolien et l'espace. Le grand avantage offert par ces structures en termes de résistance élevée, de rigidité élevée par rapport au poids influence directement les choix de conception et de production. C'est pourquoi il est d'une importance capitale de comprendre quels types de phénomènes vont affecter leur comportement mécanique et fournir des outils de prédiction efficaces pour la conception des structures et des matériaux.

Dans ce contexte général, le projet FULLCOMP vise à développer des outils d'analyse intégrés pour améliorer la conception de structures composites et avancées. Financé par la Commission européenne dans le cadre d'un programme Marie Sklodowska-Curie Innovative Training, 12 étudiants au doctorat ont été recrutés pour élaborer des outils d'analyse. Le spectre complet de la conception des composites est traité, comme la fabrication, la surveillance de la santé, la défaillance, la modélisation, les approches multi-échelles et les essais. Ce consortium est composé de sept universités : Politecnico di Torino (Italie), Université de Bristol (Royaume-Uni), École Nationale Supérieure d'arts et Métiers (Bordeaux, France), Université de Hanovre (Allemagne), Université de Porto (Portugal), Université de Washington (USA), RMIT (Australie), d'un institut de recherche : l'institut luxembourgeois de technologie) et d'une société (Elan-Ausy, Hambourg, Allemagne).

Les travaux de thèse présentés dans ce manuscrit s'inscrivent dans le cadre des études développées au sein de l'École Nationale Supérieure d'Arts et Métiers et traite de l'analyse numérique des structures de protection.

Les panneaux balistiques et les composites balistiques sont généralement utilisés comme couches de protection des objets entrant en collision à grande vitesse. Ainsi, les composites dits 'balistiques' se retrouvent dans les systèmes de protection du combattant ou encore dans les blindages pour armes de moyen calibre et autres applications.

Par rapport aux composites structuraux, la fraction volumique des fibres est ici plus élevée et peut atteindre 90%. La faible teneur en résine conduit à une adhérence inter-pli relativement faibles qui favorise la dissipation de l'énergie par délaminage lors de l'impact. Une autre particularité de ces matériaux est l'utilisation de fibres spécifiques comme le

para-aramide ou le UHMWPE (Ultra High Molecular Weight Poly-Ethylene). Ces fibres sont préférées au carbone et au verre traditionels en raison de leur capacité à résister aux déformations transversales extrêmes qui surviennent lors de l'impact, sans altérer leurs propriétés mécaniques longitudinales.

Généralement, des tissages taffetas bidirectionnels sont utilisées pour les fibres de para-amide tandis que les fibres UHMWPE sont utilisées sous forme unidirectionnelle. Les panneaux balistiques des structures blindées sont enfin constitués de plusieurs couches et constituent en tant que composants autonomes ou en tant que couches secondaires selon le degré de protection voulu.

Les propriétés balistiques de ces structures dépendent d'une multitude de paramètres qui sont directement liés à la nature multi-échelle du tissu. En effet, une couche de tissu est composée de faisceaux de fibres, appelés torons, agencés entre eux selon une configuration géométrique (le tissage) pour créer une structure finale 2D/3D. Les types de fibres, leur densité, la géométrie de tissage, le nombre de couches ont ainsi un effet important sur le comportement mécanique de la structure et ses performances balistiques. C'est la raison pour laquelle une bonne compréhension des mécanismes de déformation et d'endommagement aux différentes échelles (fibre, toron, tissu) est cruciale pour garantir la résistance balistique et orienter les concepteurs vers des solutions optimisées.

La première partie de cette étude propose une analyse des travaux existants dans le domaine de l'impact sur tissus secs vis à vis de la modélisation.

La réponse du tissu sec à un objet entrant en collision à grande vitesse est complexe et fortement influencée par sa nature multi-échelle. Géométrie de tissage, nombre de couches, matériau des fibres, ne sont que quelques-uns des paramètres qui affectent la réponse balistique globale. Ce niveau de complexité est pris en compte par les modèles numériques dans lesquels les phénomènes qui ne peuvent pas être explicitement modéliser sont implicitement inclus dans un comportement mécanique homogénéisé. Par exemple, lorsqu'un tissu est modélisé comme une plaque continue (on parle alors d'une échelle de travail macroscopique) et un comportement non linéaire lié à la géométrie de tissage. La même procédure peut s'appliquer aux torons dont le comportement est représenter par un comportement continu qui doit reproduire celui d'un faisceau de fibres alignées (on parle alors d'une échelle de travail mésoscopique). L'échelle dite 'microscopique' représente chaque fibres du toron et ne nécessite pas à priori d'opération d'homogénéisation.

Les modèles macroscopiques sont les plus efficaces du point de vue du temps de calcul, cependant ils sont limités dans la représentation des plis et de la rupture de la couche. À l'échelle microscopique, les modèles numériques sont très précis dans la description des phénomènes, mais sont pénalisés par un énorme coût en temps de calcul. Les modèles numériques mésoscopiques sont ainsi les plus populaires parmi les chercheurs en raison de leur capacité à représenter avec précision l'évolution de l'impact avec des temps de calcul raisonnable.

L'état de l'art actuel sur la modélisation mésoscopique des tissus secs soumis à un impact haute vitesse est résumé dans les travaux de Nilakantan [71]. Ici, la prédiction numérique de la résistance balistique et de la vitesse critique d'une couche de Kevlar S760 est obtenue et s'est avérée remarquablement proche des données expérimentales. L'auteur pointe en revanche un verru scientifique important en soulignant la nécessité de représenter physiquement le comportement transversal du toron afin d'éliminer l'étalonnage numérique des paramètres du modèle continue.

Dans la continuité de ces récents résultats et discussions qui se basent sur un état de l'art le plus exhaustif possible sur le sujet, le but identifié de cette thèse sera de fournir un modèle mésoscopique d'un tissu où le comportement transversal du fil sera physiquement et le plus précisément modélisé.

Ce comportement transverse doit au préalable être analysé. L'essai de l'impact transverse sur toron est retenu afin d'analyser uniquement l'effet du comportement transverse de l'ensemble des fibres alignées au départ. Il s'agit la de la première contribution de ce travail de thèse qui se traduit par une analyses numériques à l'échelle microscopiques. Afin de réduire les coûts de calcul, une approche numérique basée sur la méthode des éléments discrets a été proposée. L'interaction des fibres et les propriétés inertielles sont traitées et leur comportement longitudinal est modélisé par des ressorts en série. Cette approche numérique a été validée à l'échelle de la fibre par comparaison avec la théorie de Smith et au niveau du toron en utilisant des résultats numériques préexistants.

Deux cas d'impact différents d'un fil Kevlar KM2 600 impacté transversalement ont été réalisées.

La première simulation s'est concentrée sur l'étude des phénomènes qui se produisent une fois que l'onde longitudinale et l'onde transversale se sont propagées, on parle ainsi d'impact en 'temps longs'. Dans ce cas, le modèle initial se révèle suffisant pour décrire correctement les mécanismes d'absorption à l'impact et notamment la rupture finale qui est influencée par la propagation d'onde au sein de la de la section du toron. La deuxième simulation s'est orienté vers le cas d'impact en 'temps court' lorsque les ondes longitudinales ne jouent plus de rôle dans les mécanismes de déformations. Dans ce cas, la section transversale du fil joue un rôle principal dans l'évolution des énergies, l'état de tension du toron et la cinématique globale. Au vue des résultats, il apparaît que le concept de vitesse critique introduit par Smith doit être revisité en tenant compte des effest aux temps courts et donc du comportement transverse pour les simulations mésoscopiques.

Le modèle à cet échelle là doit donc être suffisamment riche pour inclure les mécanismes observés à l'échelle inférieure. La deuxième contribution de ce travail de thèse est donc la construction d'un modèle de comportement basé sur une loi constitutive hyperélastique basé sur des invariants mathématiques judicieusement choisis, dont les paramètres seront identifiés par une analyse à l'échelle de la fibre. Ce modèle a été implémenté en tant qu'UMAT dans le logiciel commercial LS-DYNA.

La technique proposée consiste à résoudre trois problèmes microscopiques d'un VER de fibres. En tirant parti de l'analyse numérique et analytique, il a été possible de relier les propriétés tridimensionnelles du toron à la mécanique du niveau des fibres. De plus, la formulation hyper-élastique permet de fournir des critères de rupture basés sur des modes de déformation plutôt que sur des états de tensions. Grâce à cette approche, une façon physique de modéliser la rupture multi-axial a été introduite.

Ce modèle a été validé à l'aide des résultats microscopiques précédents et aussi comparé par rapport à l'approche linéaire élastique classique de la littérature. Les résultats ont montré un bon accord avec les résultats microscopiques pour les analyses à long terme et à court terme. L'avantage principal de cette approche est donc la construction d'un modèle sans hypothèses numériques à priori sur le comportement transverse du toron, mais bien vi une anlayse à l'échelle inférieure. A ce stade, le modèle hyper-élastique mésoscopique peut être appliqué au niveau du tissu afin de tester ses capacités dans un cas réel d'impact sur structure tissée

Un tissu taffetas Kevlar S706 impacté par un projectile sphérique indéformable à été simulé à l'échelle mésoscopique en utilisant le modèle hyper-élastique précédant. Deux scénarios d'impact ont été considérés, à savoir un scénario sous-balistique et un scénario de perforation à faible vitesse.

Les résultats actuels montrent que l'approche proposée pour les deux régimes est au moins aussi bonne que l'approche linéaire élastique tout en offrant de nouvelles possibilités en termes de modélisation des défaillances prenant en compte les mécanismes de rupture aux plus petites échelles, de post-traitement et de stabilité de la solution.

Table of contents

List of figures

List of tables

Chapter 1

Introduction

Composite structure are currently used in different industrial, civil and military fields such as aeronautics, automotive, mechanical, wind energy, and space. The great advantage offered by these structures in terms of high strength, high stiffness to weight ratios is directly influenced by the design and production choices. For this reason is of paramount importance to understand what type of phenomena are going to effect their mechanical behaviour and provide effective prediction tools for structural and material design.
In this general context, the FULLCOMP project aims to develop integrated analysis tools to improve the design of composite and advanced structures. The FULLCOMP project, funded by the European Commission under a Marie Sklodowska-Curie Innovative Training Networks, recruited 12 PhD students to develop integrated analysis tools to improve the design of composite structures. The full spectrum of the design of composites is dealt with, such as manufacturing, health-monitoring, failure, modeling, multiscale approaches, testing, prognosis, and prognostic. The FULLCOMP consortium is composed of 7 Universities - Politecnico di Torino (Italy), University of Bristol (UK), Ecole Nationale Superieure d'arts et Metiers (Bordeaux, France), University of Hannover (Germany), University of Porto (Portugal), University of Washington (USA), RMIT (Australia)- 1 research institute (Luxembourg Institute of Technology) and 1 company (Elan-Ausy, Hamburg, Germany).
The following work is part of the studies developed at the Ecole Nationale Superieure d'arts et Metiers and deals with the numerical analysis of protective structures.
Namely ballistic panels and ballistic composites are generally employed as protective layers from high velocity colliding objects. Ballistic composites can be found in military helmets, vehicle armors for medium-calibre weapons and other applications, Figure 1.1.

Compared to structural composites, here fiber volume fraction is higher and can reach values of 90%.The low content of matrix brings to a relatively weak interply adhesion and favourites energy dissipation by delamination during the impact. Another peculiarity are

Fig. 1.1 Examples of applications for protective structures.

the para-aramid and UHMWPE (Ultra High Molecular Weight Poly-ethylene) fibers are usually employed as reinforcements. These fibers are preferred to carbon due to their ability to withstand extreme transverse deformation which occur during the impact without fail or altering their longitudinal mechanical properties. The composite reinforcements architecture directly derives from soft body armour design. Generally 2D plain woven para-aramid fabrics are employed while UHMWPE fibers are used in unidirectional form.

The second type of structures which are normally employed in protection systems are soft ballistic panels made from various layers of dry woven para-aramid or UHMWPE fibers. These are usually adopted as stand alone components or secondary layers according to the protection grade provided, Figure 1.2. The ballistic properties of these structures depend on a multitude of parameters which are directly related to the multiscale nature of a fabric. A woven fabric layer is comprised of fiber bundles, named yarns, interlaced into a precise geometrical configuration to create a 2D/3D final structure, Figure 1.3. The fiber types, yarn denier, weaving geometry, number of layers have all an important effect on the final mechanical behaviour of the structure and its ballistic performance. For this reason a good comprehension of how design and process choices performed at the different scales (fiber-yarns-fabric) affect the global structural performance is crucial to guarantee the best protection-to-weight ratio.

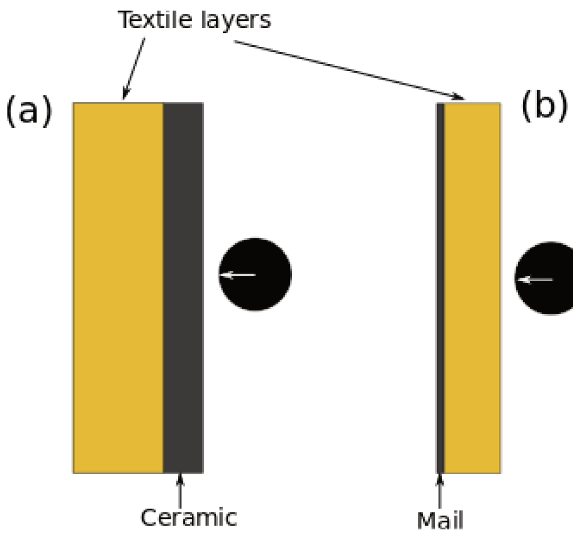

Fig. 1.2 Dry fabrics employment in High velocity, rifle bullets, (a) and low velocity, hand gun bullets, (b) protection systems.

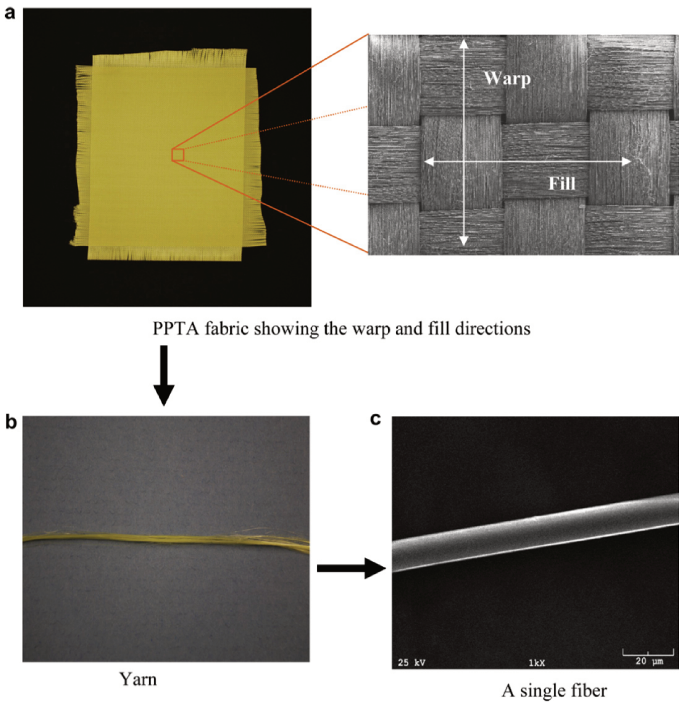

Fig. 1.3 Multiscale structure of a Kevlar fabric layer: (a) fabric, (b) yarn, (c) fiber [64].

The first objective of this dissertation is to provide a predictive numerical model of a dry fabric under high velocity impact (HVI). The proposed model have to be able to represent all the macroscopic phenomena observed experimentally when a textile structures is impacted. Moreover, all the information required for the correct evaluation of the projectile residual speed after an impact and the structure ballistic properties should be included in the model.

The first part of the manuscript is dedicated to the state of the art and the introduction to the subject. Here a general perspective of the materials, experimental observations and numerical models of protective fabric layers under HVI is presented.
In the second part, the microscopic numerical models of yarn structures and their relative numerical approach will be presented. These analyses have been used instead of classical experimental approach to perform qualitative and quantitative physical observation of yarns behaviour under high velocity impact. Thanks to this approach much more data have been recorded which can be used for yarn models verification.
The third part will be dedicated to the introduction to the yarn continuum model and its parameter identification process. The same impact scenarios computed using microscopic approaches will be performed and the results will be compared to classical and microscopic solutions.
In the final part the proposed constitutive model will be employed at the fabric level where its robustness and effectiveness will be tested.

Chapter 2

Ballistic performance of polymeric fibers and their fabrics: state of the art

In this chapter the state of the art of dry fabrics under high velocity impact and their modelization will be presented.
In the first section, aramid fibers adopted in woven fabrics for ballistic application will be introduced. Some generalities will be followed by the presentation of their inner nanoscopical structure and mechanical properties.
The second section is dedicated to the study of a fabric under high velocity impact and an exhaustive description of the phenomena observed during the impact is presented.
The third section is dedicated to the different numerical strategies adopted to study this problem.
The last section focus on the problem of a single yarn transverserly impacted by a projectile. Here the classical analytical solution and its limitations will be presented.

2.1 Aramid fibers for ballistic applications

High performance polymeric fibers employed in ballistic protective structures usually are of two different types, namely aramid and Ultra High Molecular Weight Polyethylene (UHMWPE)[17, 51].
The United States Federal Trade Commission describes the aromatic polyamide based fibres under the generic term aramid as a manufactured fibre in which the fibre forming substance is a long chain synthetic polyamide with at least 85% of the amide (-CO-NH-) linkages attached directly to two aromatic rings. As an example, Kevlar chemical structure is presented in Fig. 2.1. One of the earliest examples of this fibers class was the poly-m-phenyleneisophthalamide,

launched by Dupont in 1967 and commercially know as Nomex. Some years later, the discoveries in the field led to the commercialization of poly (p-phenylene terephthalamide), also known as Kevlar [38, 51]. Today commercially available para-aramid synthetic fibers are produced by DuPont (Kevlar) and Teijin (Twaron) and are widely employed in different protection systems as dry woven fabric layers or woven textile reinforcement (Fig. 2.2 (a)).

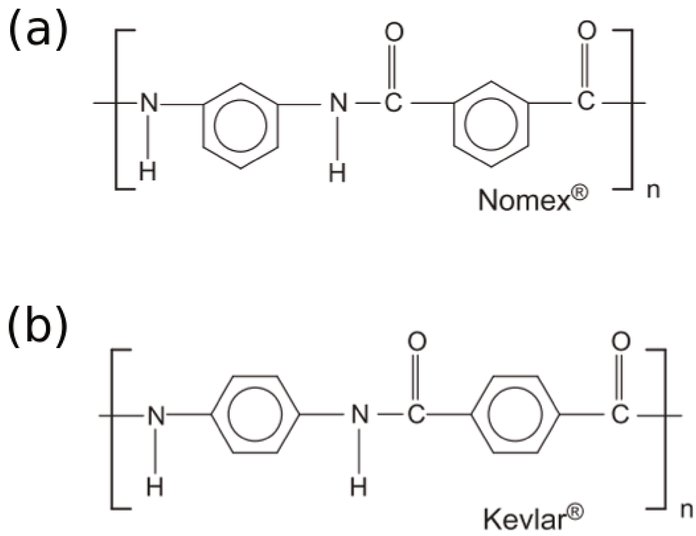

Fig. 2.1 Chemical structure of Nomex (a) and Kevlar (b) macromolecules.

UHMWPE fibers are based on simple and flexible polyethylene chains and they are even called high-performance polyethylene (HPPE) fibres or high-modulus polyethylene (HMPE) fibres. The idea of a superstrong polyethylene fiber was developed in the 1930s, however just in the 1979 DSM invented and patented the process required for the production. These fibers are commercially known under the name of Dyneema and Spectra. They are classically employed as unidirectional layers in flexible or rigid forms, as showed in Fig. 2.2 (b). Since this dissertation focus on dry woven protective fabrics, the current section and the entire work of this thesis will be dedicated to aramid fibers.

2.1.1 Manufacturing

Aramid fibers are synthesized in solution from the para-phenylenediamine and terephthaloyl chloride in a condensation reaction [17, 51]. A solvent is then added to the reaction result in order to prepare the solution that undergoes the dry-jet wet-spinning process. In Fig. 2.3 the spinning process is illustrated. It starts with the extrusion of the solution through a

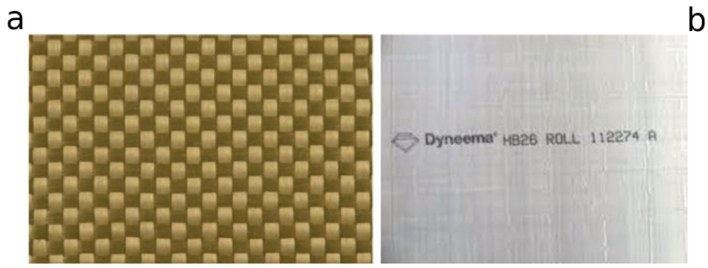

Fig. 2.2 Dry woven fabrics of aramid fibers (a) and unidirectional layer of UHMWPE (b).

spinneret. Under shear the crystal domains become elongated and oriented in the direction of the deformation. The extruded polymer is then forced through a coagulating medium and mechanically drawn in the fiber form.

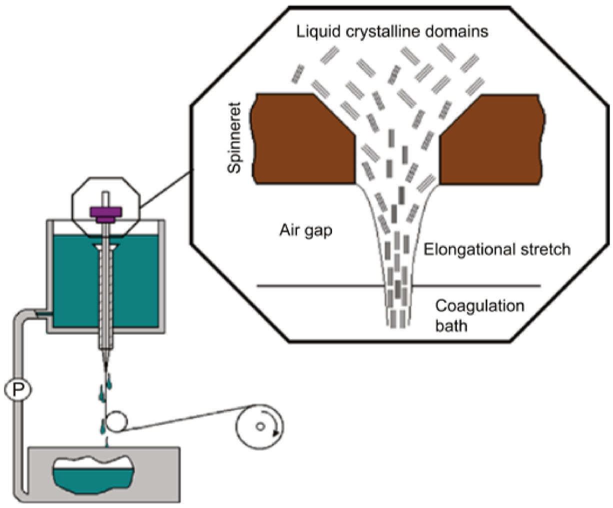

Fig. 2.3 Dry-jet wet-spinning process adopted for aramid fibers production [17].

The mechanical properties and the resultant inner structure of aramid fibers are drastically influenced by the spinning parameters and posttreating conditions. According to the process, different type of fibers have been produced and the analysis of their mechanical properties can give an idea about its influence on the global fiber performance, Fig. 2.4.

2.1.2 Mechanical properties

Unique mechanical properties of aramid fibers set them apart from the others types of organic and inorganic fibers. Kevlar exhibits higher longitudinal stiffness and strength than Nylon while on a weight basis is stronger than steel and much stiffer than glass. Moreover,

Type	Tenacity (mN/tex)	Initial modulus (N/tex)	Elongation at break (%)
Kevlar® 29	2030	49	3.6
Kevlar® 49	2080	78	2.4
Kevlar® 149	1680	115	1.3
Nomex®	485	7.5	35
Twaron®	2100	60	3.6
Twaron® High-Modulus	2100	75	2.5
Technora®	2200	50	4.4

Fig. 2.4 Longitudinal mechanical properties of some of the commercially available aramid fibers [17].

aramid fibers flexible nature make them ideal candidates for weaving and impact application compared to glass or carbon ones which result to be more fragile. They are also resistant to organic solvents, fuels, lubricants and exposure to flame [17, 51].
Physical properties of aramid fibers directly discern from their inner nanoscopical structure. Aramid fibers multiscale nature is presented in Fig. 2.5.
A single fiber can be considered as an assembly of thread-like entities comprised of parallel sheets of aligned and hydrogen bonded molecular chains named fibrils. Here the molecular chains are oriented along the fiber longitudinal axis while weak van der Walls forces acts among this thread-like entities.

Longitudinal elongation

It is clear from this nanoscopic arrangement that an highly anisotropic mechanical behaviour is expected at the fiber level. The longitudinal direction presents the best mechanical performance due to strong chemical bonds of the polymeric chains.
Mechanical properties of aramid fibers have been studied by different authors.
As an example, Lim and Cheng studied Kelvar and Twaron fibers longitudinal behaviour in low and high strain rate regime using a quasi-static tensile test and a miniaturized Kolsky bar [20, 64]. A linear relation among the stress and the strains resulted from the experiments. Longitudinal fiber modulus and their ultimate strengths resulted to be insensitive to strain rate, as shown in Fig. 2.6, while an important dispersion on the ultimate fiber strength was observed. This observation underlines the statistical response of these fibers and was explained by the presence of defects along the fiber length which can alter their resistance. The same explanation was provided for the ultimate strength sensitivity to the fiber length.

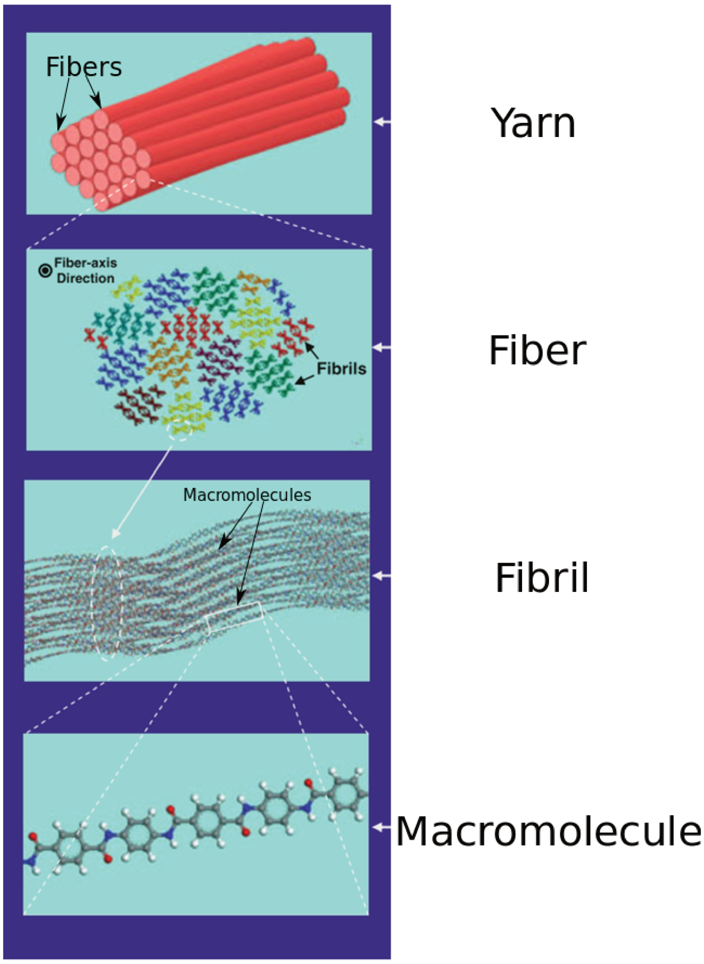

Fig. 2.5 Aramid fiber multiscale nanoscopic structure [44].

The longer the fiber was, the higher the possibility of occurring into a defect, which reduce the global fiber strength, was.

Transverse compression

Transverse compression tests were conducted by Lim, Cheng and Sockalingham who showed how aramid fibers transverse deformation results into a non-linear mechanical behaviour [18–20, 64, 98, 100].
Cheng performed a transverse compression test on a single Kevlar KM2 fiber, Fig. 2.7.
A nominal stress $\bar{\sigma}$ was defined as the ratio among the force per unit length f and the fiber diameter ϕ and reported as a function of a nominal strain $\bar{\varepsilon}$, defined as the ratio among the imposed displacement δ and the fiber diameter ϕ. The same experimental procedure was proposed by Sockalingam [98] where a new definition of true strain and true stress was

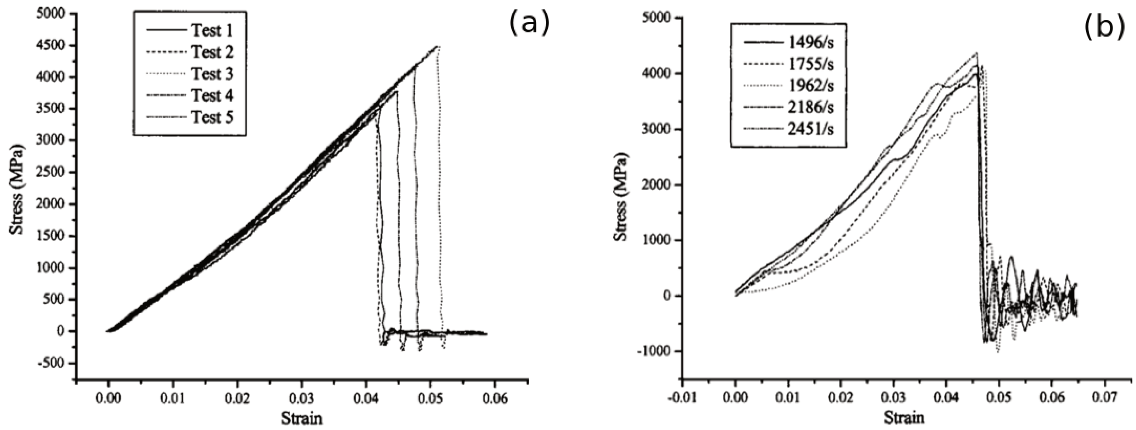

Fig. 2.6 Static (a) and Dynamic stress strain relation obtained for a Kevlar KM2 fiber from longitudinal elongation tests [20].

adopted to emphasize the material nonlinearities and remove the effect of the geometrical ones from the experimental curves. The experimental results showed how this non-linear behaviour was related to fibrils reorganization and fiber damage.

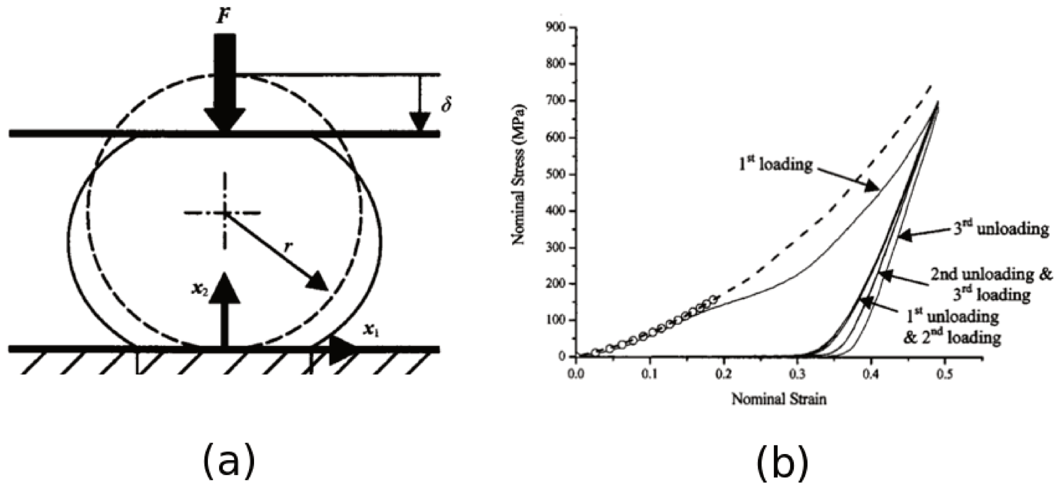

Fig. 2.7 Single fiber transverse compression experiment (a) and curves (b) obtained by Cheng [20].

Multiaxial strain effects on fiber failure

The degradation of fiber longitudinal properties due to fiber transverse deformation and multiaxial stress states assumes a central role in impact applications and have been discussed in different works. This subject is of particular interest since it has been related to yarns

premature failure.
Abbott et al. remarked a reduction of Kevlar 49 yarns longitudinal properties after twisting [1]. The strength loss evaluated under the hypothesis of an ideal helically twisted yarn structures was not sufficient to explain the observed one. In order to clarify the effect of twisting on tensile strength of Kevlar yarns, single fibers were extracted from twisted filaments and tested to tension. A remarkable loss of strength was found from the experiments, as shown in Fig. 2.8. In order to clarify the source of this damage, residual longitudinal properties of virgin filaments after shear, bending and transverse load was evaluated. It was shown that transverse compression is the type of load which alter the most fiber longitudinal properties. Similar results were found by Lim and Bazhenov were imperfectly compressed Kevlar fibers shown significant reduction of about 50% in their axial strength [9, 64] (Fig. 2.9).

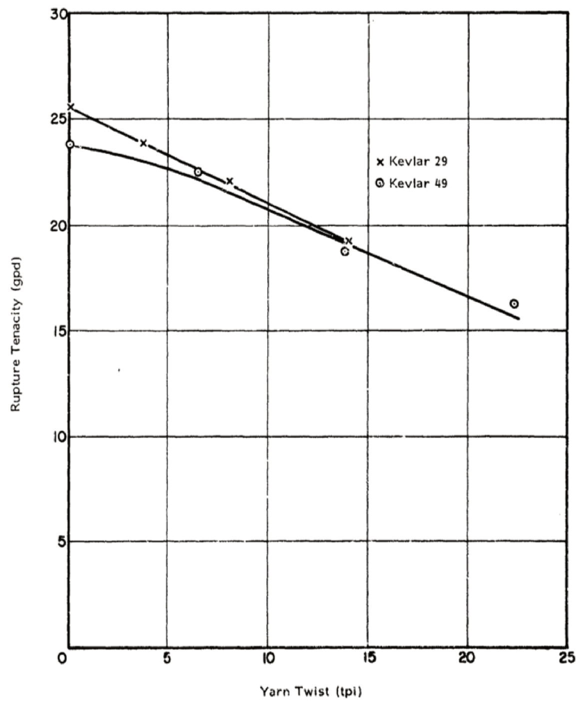

Fig. 2.8 Reduction of Kevlar 49 fiber longitudinal strength after yarn twisting [1].

Deteresa shown that the level of torsional shear strain incurred by an aramid fiber has a definite effect on the residual axial strength [37]. Kevlar 49 was able to incur a torsional shear strain up to 10% before its axial tension failure stress was noticeably reduced. Upon further increasing levels of torsional strain, a linear reduction in residual tensile strength was determined, as illustrated in Fig. 2.10.
Sockalingam evaluated the longitudinal properties degradation induced by multiaxial stress

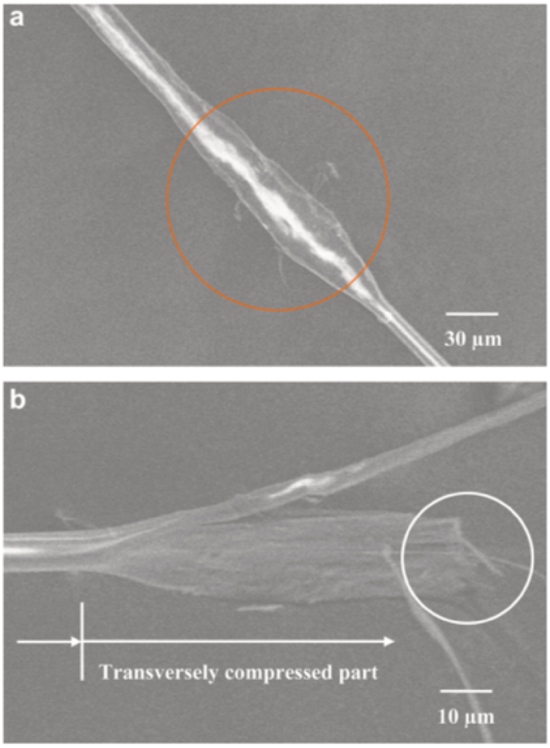

Fig. 2.9 Fiber damage induced by transverse deformation [64].

state due to bending, transverse compression and torsion on a Kevlar KM2 fiber [102]. Results showed that kinking associated to axial compression reduces the fibers tensile strenght by 7%. Moreover fibers subjected to 40% average true compressive strains had a 5.5% degradation in average tensile strength compared to virgin fibers.

Hudspeth presented an experimental study to elucidate about the effects of a multiaxial stress state on the Kevlar fiber failure during an impact[55]. The fiber was posed under tension in contact with a cal 0.30 FSP (Fragment Simulating Projectile) modified indenter which was driven in the vertical direction up to the point where the filament collapsed. It was remarked that longitudinal failure strain was a function of the final angle for which the fiber fails. According to the author, this demonstrates the importance of three-dimensional stress state in fiber failure initialization. The higher the failure angle was the higher would be the stress state induced at the contact zone.

The same experimental procedure was performed successively for different fiber types and indenter shapes [57]. Five different fibers, namely Kevlar KM2, Spectra 130d, Dyneema SK62, Dyneema SK76, Zylon 555, were transversely loaded using a razor shape, a FSP and a

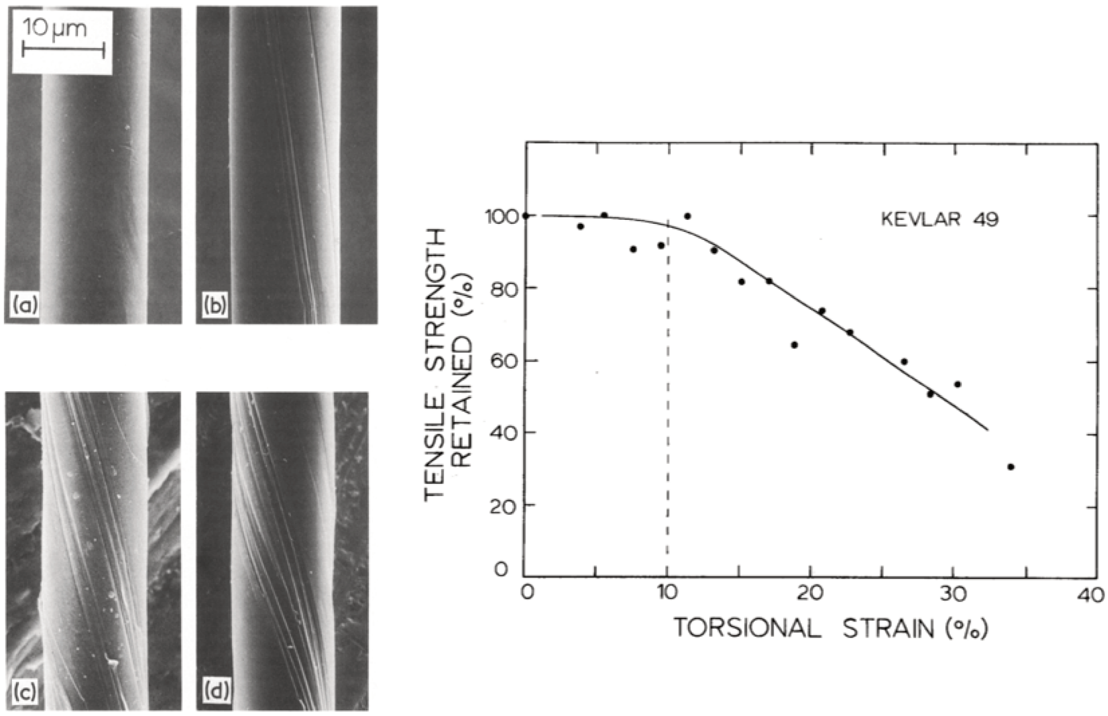

Fig. 2.10 Fiber damage induced by fiber torsion [37].

round indenter. No effect of the failure angle on the longitudinal failure strain was identified for Razor shape and round indenters. The longitudinal failure strain was similar of those recorded by quasi-static longitudinal tension tests for the round-indenter while a much lower value was obtained for the razor shaped one. This results was explained by the extreme stress concentration induced by the razor near the contact zone. Results of the FSP coherent with those presented in the first article. The longitudinal failure strain was a decreasing function of the failure angle for all the analyzed fibers. Moreover its value was very similar to that obtained for the round shape indenter when failure angle was low, while it got close to that recorded for the razor when the failure angle was high.
Post-mortem fiber structure were analyzed in order to get information about the fiber failure mechanisms, Fig. 2.11. Round shape indenter induced fibrillation based failure while razor induced one appears to be much more localized. FSP failure mechanisms follow the transition observed for the longitudinal limit strain. Fibrillation appears for low failure angles while localization and shear failure appears for higher angles.

The previously mentioned studies put a mark on the importance of multiaxial strain state in fiber failure initialization. This type of loading continuously occurs during an impact due

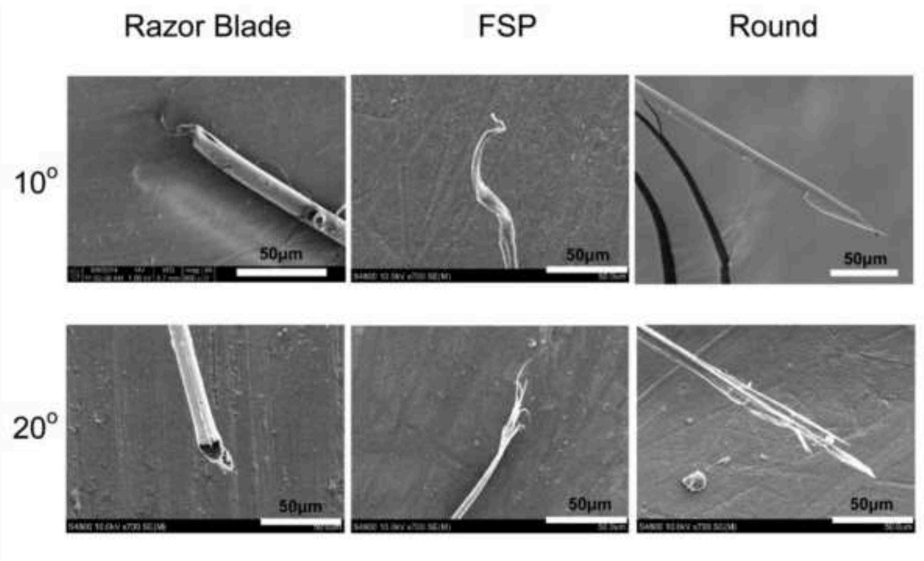

Fig. 2.11 Post-mortem inspection of Kevlar KM2 fibers [57].

to yarn-to-projectile and yarn-to-yarn contacts and it is important to take them into account in any type of predicting model.

2.2 Dry fabrics for ballistic protection

2.2.1 Introduction

The previously presented fibers are not used as stand alone components but arranged into the final bidimensional/ threedimensional structure which takes the name of fabric. A technical textile is defined as a textile product whose design has been driven by functional properties and technical performance rather than aesthetic or decorative aims [51, 85]. Most part of these products consist of yarns or fibers assemblies whose stable internal structure is able to provide useful mechanical strength to the system.
Fabrics are currently adopted in different industrial fields which include geotechnical, automotive, aerospace, medical and civil applications.
The aim of a technical garment developed for ballistic protection is to protect the underlaying structure from a colliding object launched at high speed while limiting to the minimum its global weight contribution and the natural movements of the protected individual.
Textile fabrics are usually woven but other production techniques as knitting, net making, non woven processes can be even used. The majority of ballistic fabrics are of a coarse loose plain-woven construction comprised of multifilament yarns with minimum twist. An example of these structures is presented in Fig. 2.12. This configuration provides the best

overall performance in therms of ballistic protection [112, 117].
Generally, multilayer structures comprised of 5 up to 22 layers are employed. Into a body armor, each body layer is allowed to move independently and the pack is secured by stitching quilting lines or squares to maintain a degree of flexibility. This allows the wearer to bend, turn, and make arm movements. It is necessary to seal the ballistic vest inside a waterproof and light-tight cover, as the presence of moisture and UV light can reduce the ballistic performance.

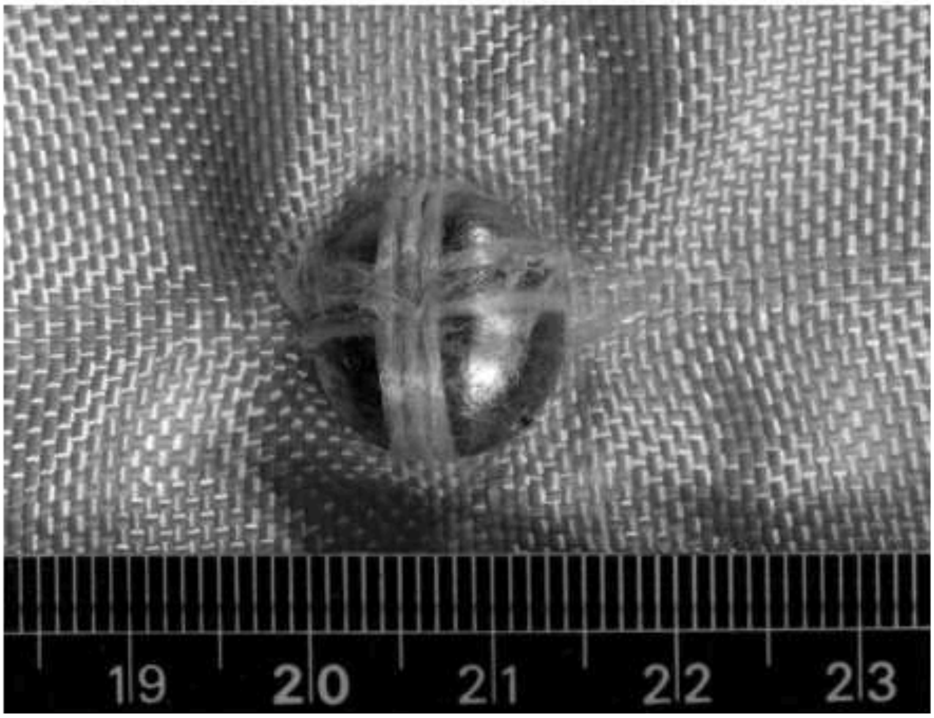

Fig. 2.12 Plain weave textile layer of an impacted body armor [85].

2.2.2 Response to High Velocity Impact

The general problem of a flexible fabric impacted using a projectile has been studied by different authors using experiments, analytical and numerical models [15, 99, 106]. The global phenomenon can be actually resumed as an energy transfer among the bullet and the structure where the impact energy is absorbed by the fabric under different forms.
Fabric internal energy, fabric kinetic energy and friction are the most important form of impact energy dissipation [31, 39]. The amount of energy and its partition among the different modes depends by plenty of factors which are related to the fabric type, the bullet and the impact condition. While the next part will be focused on the presentation of those elements,

here the general response of a fabric to an impact will be introduced.

The goal of the structure design is to avoid the penetration of a single or multiple layers and then completely absorb the energy of the impact.
Different type of measurement have been employed to quantify the ballistic performance of a fabric. One of these measurements is the "ballistic limit", even called "V50", which is defined as the projectile striking velocity for which the fabric is penetrated with a probability of the 50% [29, 32]. This is actually a point of the $V_0 - V_{100}$ curve which represents the probability of a fabric to be penetrated from a given bullet at different speeds, Fig. 2.13.
A second way is to report the energy absorbed during the impact as a function of the initial speed of the projectile [16, 28, 63, 93, 107]. An example of these curve is presented in Fig. 2.14.

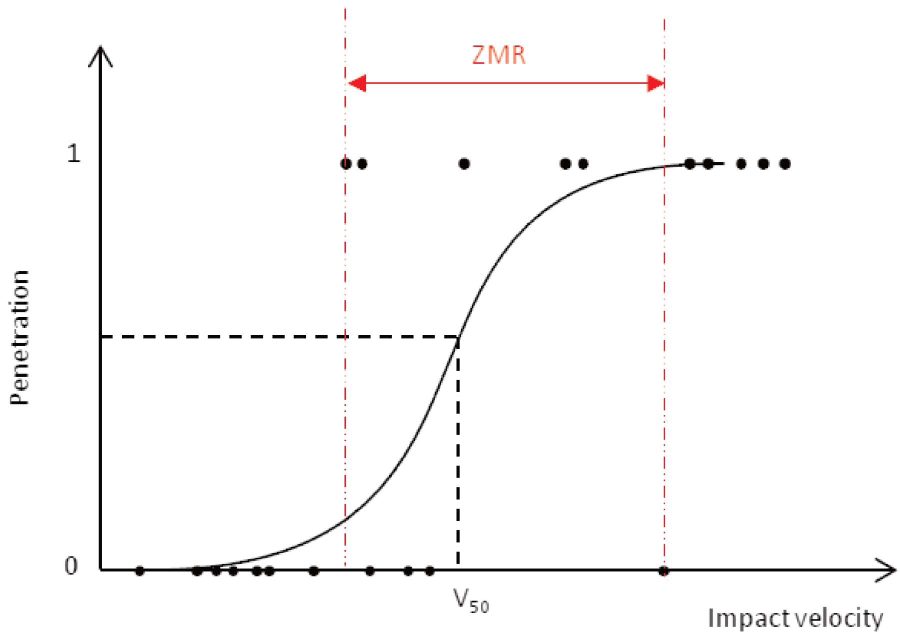

Fig. 2.13 $V_0 - V_{100}$ curve from ballistic impact test.

As the V0-V100 curves, these are specific for a particular impact case. Then different curves will be obtained if another projectile type, fabric geometry or fiber material would be adopted.
The advantage of using the second type of measurement compared to other curves [32, 61] is that the fabric ballistic performance sensitivity to the projectile initial velocity is immediately evident.
The graph can be split in three different zones according to the fabric response:

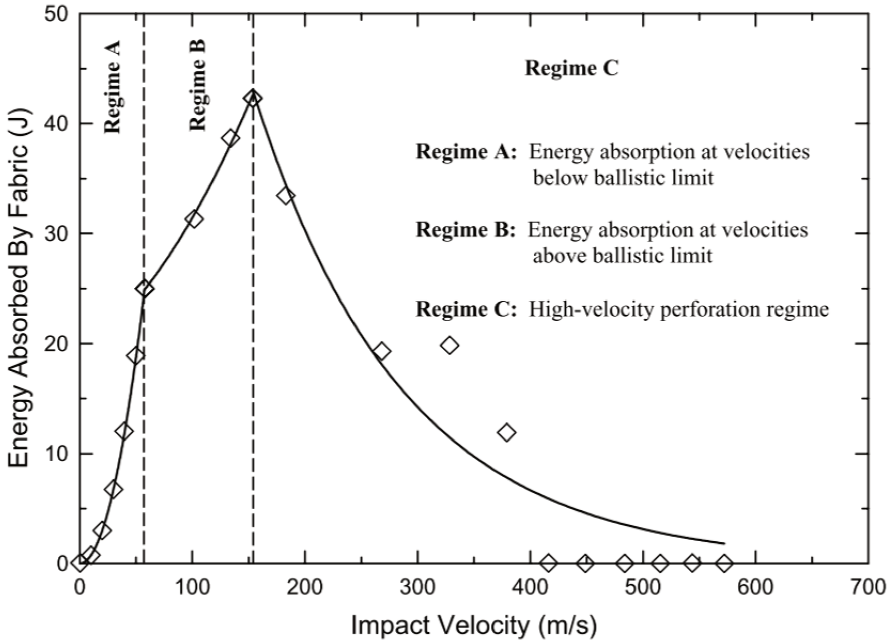

Fig. 2.14 Residual projectile energy after the impact as a function of the initial striking speed obtained by Tan for a conical projectile [107].

- Non-penetration zone (Regime A);
- Low velocity perforation zone (Regime B);
- High velocity perforation zone (Regime C).

Non-penetrating impact

For the non-penetrating case, the fabric is able to withstand to the impact, then the whole projectile striking energy is absorbed by the fabric.

When the projectile impacts the textile, a longitudinal strain waves is initialized within the structure which propagates at the sound speed down the yarns axes whose are directly in contact with the bullet [22, 23, 97]. These particular yarns are named "primary" and are those which are majorly stressed (Fig. 2.15).
After longitudinal wave has been propagated, primary yarns start to move along the impact direction and their displacement is transmitted to the other yarns, named secondary, due to yarn-to-yarn interaction.

Thanks to this mechanism, the deflection moves outside the impact zone at a specific speed while the primary yarns keep on following the projectile. The whole process results in

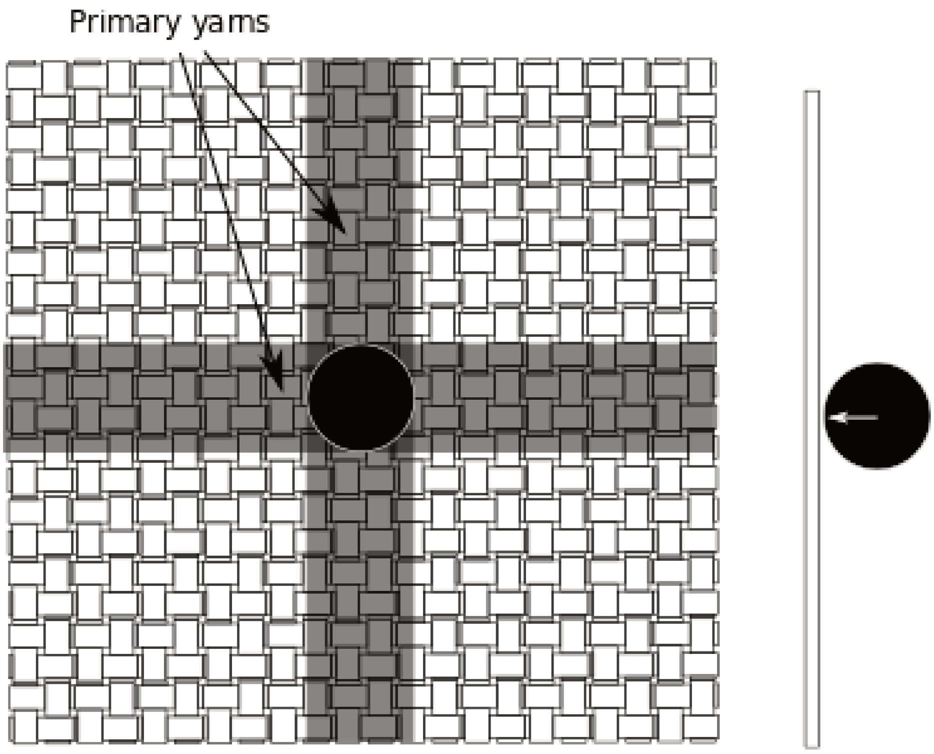

Fig. 2.15 Primary yarns in a fabric impacted by a spherical projectile.

a pyramidal or conical deflected zone, illustrated in Fig. 2.16, which increases its dimension with time. This phenomenon can be considered as the propagation of a disturb, intended as vertical velocity, within the plane of the structure which takes the name of "transverse wave".

The way in which the energy is stored in the fabric for this impact speed regime is strictly related to the phenomena previously described.
The internal energy is mostly attributed to the primary yarns. The highest values of strains are recorded due to local deformation induced by the projectile [40, 79, 112]. On the other side, both primary and secondary yarns contribute to the impact energy stored under fabric kinetic energy.
The transverse wave spreads the projectile energy within the layer and the whole deflected zone contributes to the energy absorption process.
One last mechanism of energy absorption is friction dissipation. Projectile-fabric, yarn-to-yarn and fiber-to-fiber interactions are some phenomena which can dissipate energy during the impact. The amount of energy dissipated by friction is usually lower compared to the other two and is strictly related to yarns relative movement. The amount of energy dissipated by this mechanism is strictly dependent by a large number of factors which include weaving

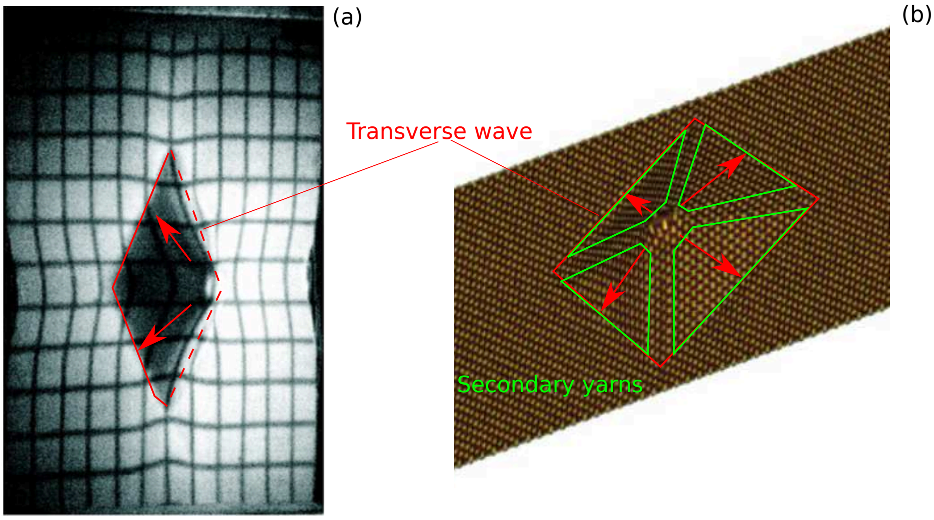

Fig. 2.16 Examples of transverse wave propagation within a fabric during an impact [74, 83].

type, projectile geometry and fabric materials [26, 35, 39].

Low velocity perforating impact

The second zone of the graph is characterized by those impacts which penetrate the structure and present a dynamic similar to that observed for the non penetration cases.
This particular zone is named "low velocity perforation zone" and is characterized by an increasing absorbed energy as a function of the initial velocity, as illustrated by the graph in Fig. 2.14.
The first point of this speed regime is the "Ballistic limit" and it is the first point from which these curves appear distinguishable for different projectile or fabric types.
As for the sub-ballistic limit zone, the propagation of the longitudinal and transverse wave is still observed. Here the strains in the primary yarns are high enough to induce failure, however it is not immediate and the transverse wave have sufficient time to propagate and induce fabric deflection.

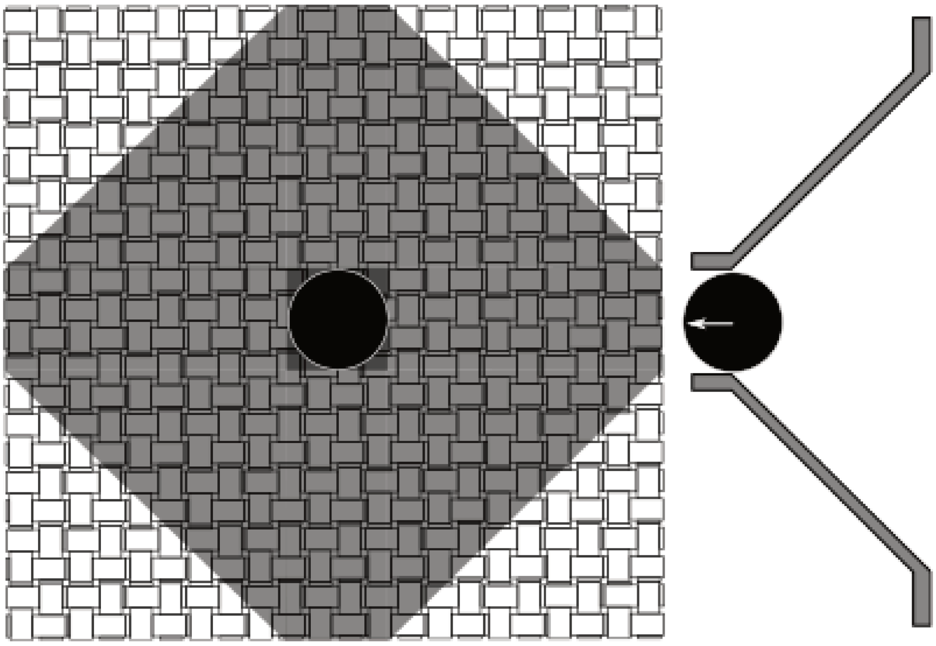

Fig. 2.17 Failure in low velocity penetration regime.

Compared to the non penetration cases, the failure of the primary yarns induce a strong reorganization of the impact zone where relative movement among yarns and projectile brings to important energy dissipation. The penetration mechanic can be very different according to the type of projectile or weaving geometry and generally involves windowing and yarn breaking [73, 79, 107].

High velocity perforating impact

The last speed regime in which an impact can occur is named high-velocity perforation zone and is constituted by those cases were the projectile initial speed is much higher than the fabric ballistic limit.
This specific zone is characterized by a drastic reduction of the absorbed energy compared to the other two with an increasing trend for higher impact speed. The reason for which an instantaneous reduction of the ballistic performance of a fabric is observed relies in the physic of the impact phenomenon.
Here, the initial speed of the projectile is sufficient to induce instantaneous failure of primary yarns and the formation of the deflected zone is not observed [16, 29, 32, 40, 107]. Since the transverse wave has no time to be initialized and propagated, all the kinetic energy of the deflected zone is missing in the energy balance. It results in a drastic reduction of the energy

absorbed by the fabric in the transition between low to high speed regime.

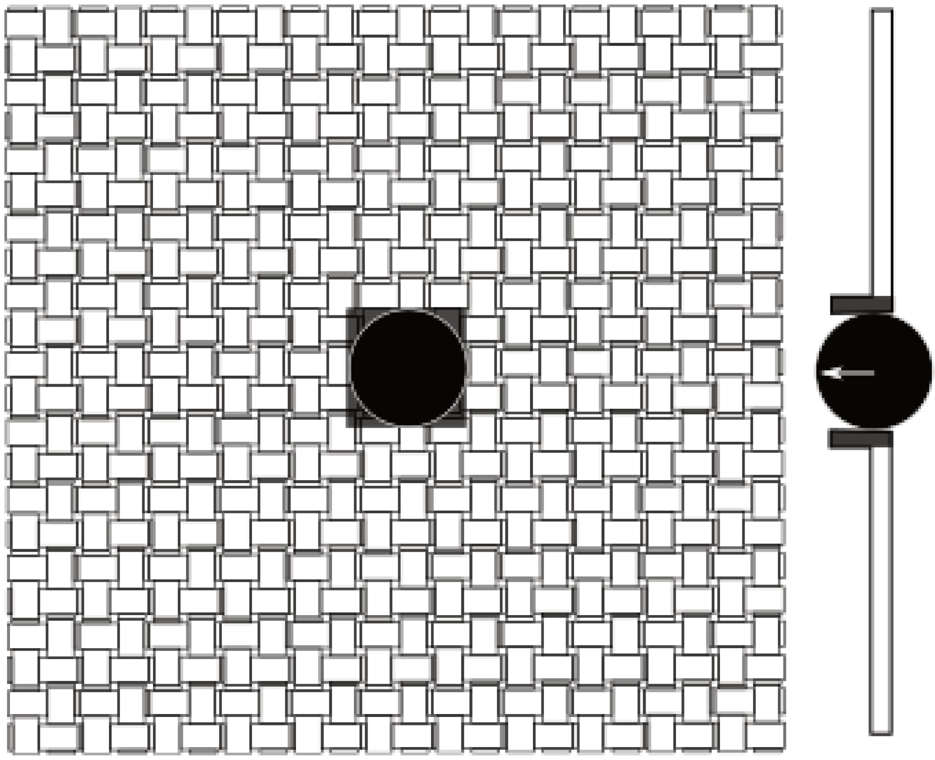

Fig. 2.18 Failure in high velocity penetration regime.

Different authors have remarked the formation of a shear plug during the penetration at this speed regime [32, 42, 86]. From the energetic point of view the formation of the shear plug requires the deformation of the fabric up to the failure point and the acceleration of the material up to a certain speed[16]. For this reason, the energy stored by the fabric at this speed regime can be assumed to be composed of a constant part, the internal energy related to the shear plug formation, and an increasing part, kinetic energy of the plug.
The failure zone appears to be very localized in this case and mostly dominate by yarn breaking. Yarn pull-out and creasing are not observed while the yarns arrangement near the failure point keep its regularity.

The energy absorbed by the fabric at this and the other speed regimes is drastically influenced by a large number of factors. These include, but are not limited to, yarn material, fabric geometry, number of layers. The next part is dedicated to the discussion of how these aspects affect the general fabric ballistic performance.

2.2.3 Ballistic performance: influencing factors

Material properties

The yarn material assumes a primary role in defining the ballistic properties of a fabric. It drastically influence the amount of impact energy stored as internal one and the ability of a fabric to withstand to the impact. Different numerical and experimental studies have been performed to understand how those properties effect the global ballistic performance of these structures.
Generally a materials which present an high sonic speed, ratio among the longitudinal young modulus and the material density, and high toughness perform better than others [25, 30, 87, 93]. These materials are able to propagate faster the energy outside the impact zone which results in lower stresses and wider charged areas.
While experimental observations shown that impacted yarns present extended damaged zone after the failure [13, 54, 107], few works have been performed in order to understand the effect of yarn transverse mechanical behaviour at the level of fabric.
Ha-Minh performed a sensitivity analysis of a Kevlar KM2 fabric ballistic performance to the yarn transverse properties using a finite element model [33]. The effect of Poisson ratios, transverse elastic moduli and shear moduli was investigated using those of a single Kevlar fiber as baseline. No appreciable effects were found with the exception of high shear moduli and low transverse moduli which induce premature failure.
A more detailed investigation about the effect of fibers transverse behaviour on the fabric performance was performed by Grujicic et al. [45]. Here a multifilament model was used to model the yarns as a discrete medium while fibers transverse mechanical properties were taken into account thanks to a user defined contact law. Comparison with experimental results showed non-linear elastic or plastic contact model were required to correctly represents fabric kinematic while a linear elastic approach appeared to be insufficient.

Weaving geometry

The knowledge about yarns material properties is not sufficient to determine the ballistic performance of a fabric. Roylance et al. underlined that yarn material properties and weaving geometry combine together and result in a structural response of the layer [91].
In order to elucidate about the effect of weaving geometry on the fabric impact performance, Yang et al. performed a finite element study of single and multilayer Twaron fabrics submitted to a ballistic impact [112].Single layer results demonstrated the importance of the fabric weaving firmness while plain weave geometry resulted to be the most effective in halting the projectile. The other fabric geometries were characterized by an higher rate of

energy absorption, however their superior yarn mobility induced an earlier penetration due to windowing. This results were coherent with those presented by Chu and Chen where impacts on single layer fabrics have indicated that twill weaves absorbed 70% less energy than the plain weaves with bullet projectiles [24].

A similar study was even performed by Zhou et al. [117]. Following the same numerical approach of Yang here the effect of fabric structure, thread density and linear density were analyzed. As in the previous case, the plain weave fabric resulted to be the most effective in energy absorption due to the high value of interlacing points. The analyses of more exotic geometries as 3D or knitted fabrics were studied by other authors [10, 47, 60], however the general observation is that loosely woven fabrics generally results in lower ballistic performances since windowing and projectile penetration are facilitated.

Friction

The global energy dissipated through friction can be attributed to different phenomena which mainly include yarn-to-yarn interactions, fiber-to-fiber interactions and projectile-to-fiber interactions. The way in which the energy is split among these mechanisms is strictly related to other aspects which influence the structure ballistic phenomena as weaving type and projectile geometry.
The experimental work by Briscoe and Motamedi explored the relation among the frictional characteristic of a fabric and its ballistic performance [11]. Different level of friction were achieved adding and removing surface lubricant from a Kevlar fabric. It was found that a lower level of friction resulted in a lower fabric ballistic limit and higher projectile residual velocity.
A similar observation was performed by Bazhenov [7] and these results were later supported by the numerical work of Duan [39]. Here the effect of yarn-to-yarn and projectile-to-yarn friction on the fabric ballistic properties were investigated thanks to a mesoscopic finite element model. It was found that the energy associated to friction dissipation was negligible up to the fabric failure instant. However the presence of friction modify the configuration of the fabric near the impact zone. In particular more yarns are strained when the friction coefficient is different from zero which results in higher values of kinetic and internal energy absorbed by the fabric. This clearly indicates how complex is the relation among friction and the global ballistic performance.

A second numerical study on the effect of friction over the failure of dry fabric under ballistic impact was performed by Chu [26]. Here different values of static and dynamic friction coefficient for yarn-to-yarn friction were tested and their effect on the primary and secondary yarns stress state analyzed. According to the results inter-yarn friction would significantly affect the ballistic behaviours of fabric. Inter-yarn friction leads to more impact energy shared with secondary yarns, which alleviates the loads in primary one and prolongs their failure initialization. In addition fabric structure is kept much more stable and less slip among primary yarns occurs. Per contra, if inter-yarn friction is too high it can be counterproductive. It will cause the concentrated stresses on primary yarns, resulting in earlier fabric failure. This results was in line with those obtained by Das and Wang [35, 110].

Projectile geometry

The effect of projectile geometry on the ballistic performance of dry fabrics have been investigated by different experimental and numerical works.
It is actually intuitive that some particular projectiles shapes facilitate the penetration of the fabric due to their ability of sliding through the yarns while others are more inclined to make them fail. These facts were confirmed by the experimental work by Tan [107]. Here the author focused on the evaluation of the ballistic properties of a Twaron plain-woven single-ply impacted by different type of projectiles. Four different types of projectile were analyzed, namely hemispherical, flat headed, ogival and conical indenters. When impacted by ogival and conical bullet, fabric presented the lowest absorbed energy and the lowest number of broken yarn. This was simply explained by the fact that sliding through the yarns was much more easy for these shapes. On the other side, hemispherical and flat headed projectiles presented an important number of broken filaments, signs that primary yarns were intensively loaded during the impact. It was even remarked that the rounded bullet induced a longitudinal failure of the yarns while localized shear failure was observed for fabric impacted by the flatted head bullet. Similar results were obtained in the experimental work of Lim [63].

The numerical work by Nilakantan corroborated these experimental results [79]. A mesoscopic finite element model of a Kevlar KM2 fabric was built an the response of the fabric under six different types of projectile geometry. An important dependence of the way in which primary yarns are charged from the projectile geometries resulted from the analyses. Windowing was observed for conical shaped projectile while primary yarns were intensively charged by cylindrical and flat-headed geometries. Spherical projectile resulted in a gradual way of charging the structure, with primary yarns near the impact center more charged compared to the external one. On the other side cylindrical bullet resulted in a more uniform distributed stress among the primary yarns due to its flat surface.

Number of plies

Single fabric layers are never employed as a stand alone components for protective structures but mostly adopted under the form of multilayer systems. The ballistic response of the resultant structure is obviously different from the response of a single layer and it is effected by large number of factors. The way in which the fabric performance changes according to the number of layers adopted for the structure have been the focus of different numerical and experimental studies.

Using a mesoscopic FE model, the ballistic performance of plain, 2/1 twill, 3/1 twill, 5-end satin and 7-end satin weave were studied for a single and multiple UHMWPE layers by Zhou [117]. The whole energy absorbed by the structure results to increase with the number of layers, however the difference in terms of absorbed energy among the different weaving types was enhanced in the multilayer system.
Different results were obtained by Yang who performed a similar study of single and multilayer Twaron fabrics submitted to a ballistic impact [112]. Plain, 2/2 basket, 2/2 will, 4-harness satin weave were considered and for each of these geometries the ballistic performance of a single and of a five-layers fabric were tested. Here, the importance of the weaving pattern was reduced for the multi-layer impact case were all the fabric showed very similar trends in terms of absorbed energy.

Layer to layer interaction was addressed by the experimental work of Cunniff [28]. Here a prediction of the energy absorbed by the fabric as a function of the areal density for Nylon, Kevlar and Spectra multilayer structures was performed using a single layer model. This specific model assumed the different plies of the stacking sequence to behave independently, then the impact was considered as a subsequent series of single ones on the different layers of the structure.
Results showed that the single layer model was not coherent with the experimental values. According to the author, this difference was related to the structural effects and the layer-to-layer interactions which results to have an important influence on the global behavior of the system.

Similar results were obtained by Lim [63]. In his experimental work, the different behaviour of a single and a double-ply Twaron CT 716 fabric to the impact was analyzed. The performance of the two-layers stacking sequence was not equivalent to that resultant from modelling the whole process as two subsequent impacts. The single layer approximation generally resulted in a lower prediction of the system ballistic limit, then importance of layer-to-layer interaction was confirmed even in this case.

The different failure type of the fabric layers during the impact was remarked by Cunniff [29, 31]. In his works, the author cited the inelastic fail of the first plies of multilayer fabric in high speed perforation regime. These layers does not provide any internal energy contribution to the global energy absorption problem due to premature failure [31]. The effect was deeply investigated in a second work where it was found that for high speed regimes the normalized fabric energy is a function of the areal density of the armor system. In other word, two materials which have different mechanical properties but similar weight will perform in the same manner in this speed regime. This effect is attributed to "inelastic" way in which the material fails at these impact speed. The systems with higher areal density were found to be more sensible to this phenomenon

2.2.4 Numerical modelling

In the previous part a general overview of the mechanical behaviour of a fabric under impact loading has been presented.
Due to the highly dynamical nature of the structural problem, the number of information available experimentally are limited and not sufficient to provide a full comprehension of the penetration phenomenon. For this reason numerical models have been used to study this type of problems.

The complicated nature of fabrics make them ideal candidates for mechanical analyses using computer-based methods. This way of proceed is not only able to furnish a quantitative prediction of the parameters of interest, i.e. projectile residual velocity and absorbed energies, but it is even a useful inspection tool to understand the physic behind the fabric penetration and the effect of physical quantities over fabric ballistic performances [78, 99].

Different type of numerical approaches have been developed by the scientific community with the ambitious goal of defining a robust model for textile materials.

The proposed solutions are generally classified according to the smallest scale individually represented within the fabric (Fig. 2.19) and are divided in:

- microscopic Models;
- mesoscopic Models;
- macroscopic Models.

In microscopic models, the whole fabric is represented at the scale of the fibres. Yarn are treated as discrete bodies with none or reduced assumptions on their mechanical behaviour. On the other hand, yarns are assumed as a continuous body in mesoscopic models. The main hypothesis here is related to the yarn constitutive behaviour while the fabric weave geometry is still fully represented. Finally, in macroscopic models the whole fabric is assumed as an homogeneous continuous layer.
Following the previously cited classification, the different modelling strategies adopted for each one of the aforementioned groups are presented with their advantages, drawbacks and typical applications.

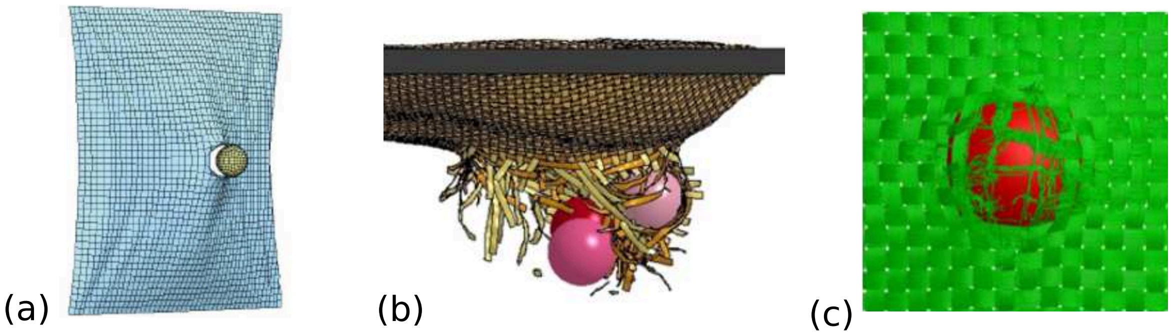

Fig. 2.19 A fabric macroscopic model by Lim [62] (a), a mesoscopic model by Nilakantan [78] (b) and a microscopic model by Wang[110].

Macroscopic models

Macroscale analyses concern most part of textile application as drapping and forming. They deal with the mechanical response of one or multiple layers whose dimensions are much bigger than those of its repetitive unit. In this specific case it is not useful nor recommendable to simulate all yarns, however sometimes it is necessary to implicitly consider their arrangement, geometry and mechanical properties in order to define the global non-linear mechanical response of the equivalent continuous layer.
Different approaches have been proposed in the literature in order to model a fabric as a

continuum body.
The simplest models does not consider the non-linear mechanical response related to the fabric internal microstructure.
In an exploratory work Lim et al modeled a transverse impact on a Twaron fabric using Finite Element Method [62]. The author adopted membrane elements with isotropic elastoplastic material properties to model the fabric layer. Failure criterion and resultant Young Modulus were strain rate dependent, contact was generated by penalty method and bullet-plate friction was even considered. Propagation of the transverse wave and the formation of a conical shape instead of a pyramidal one were observed (Fig. 2.20). The absorbed energy for different impact case was recorded and the typical three impact speed regimes identified but, due to the nature of the model, different phenomena as yarn-to-yarn friction dissipation and yarn ravelling were obliged.

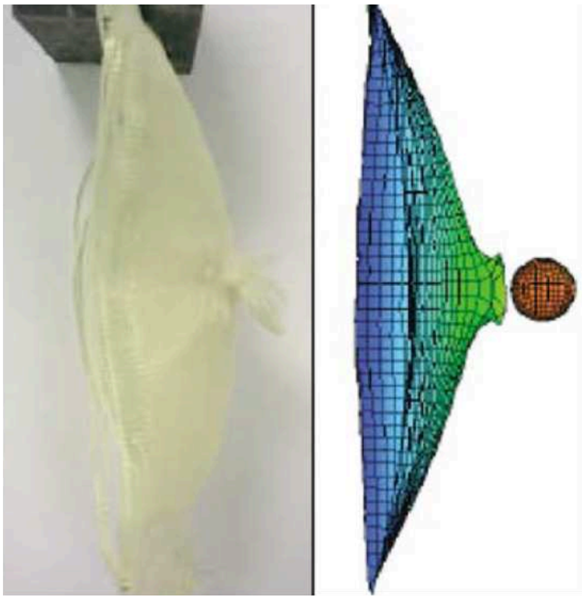

Fig. 2.20 Linear elastic macroscopic model by Lim compared to experimental results[62].

A similar macroscopic model was proposed by Ha-Minh [48, 49] for a ballistic impact on a Kevlar KM2 fabric. Even in this case, the non-linear behaviour of the fabric was not taken into account. The whole layer was considered as a continuum and modeled using 3D shell elements with a linear elastic orthotropic behaviour. The young modulus in the warp and weft direction was considered equal to that of a single yarn while the remaining material parameters were assumed to be very low compared to the other ones. The model results were compared with those obtained using a mesoscopic finite element model. Both of them were able to represent the global phenomenon however projectile speed trend was quite different for the two models. This difference was quite remarkable for low impact speed scenarios where an accurate representation of internal energy storage mechanisms is required.

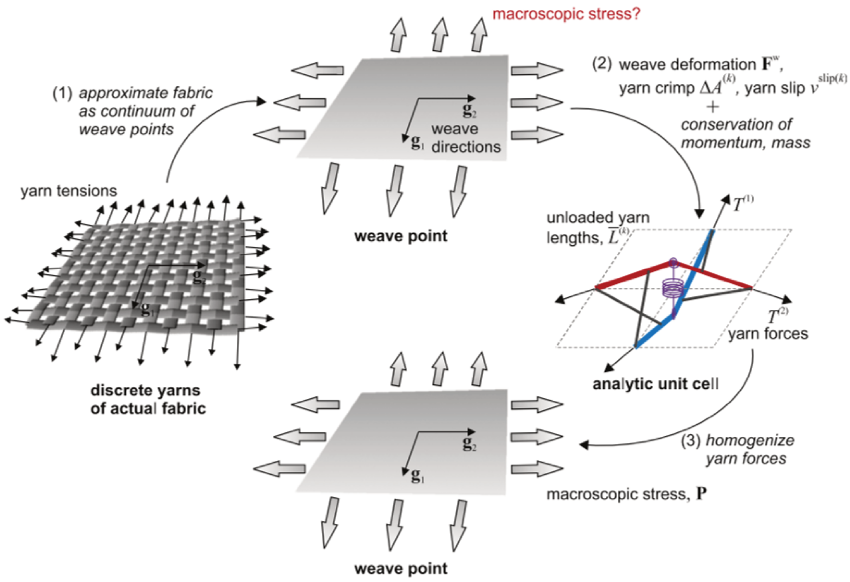

Fig. 2.21 Macroscopic fabric model concept by Parson based on analytical unitary cell response scheme [82].

A more complex approach consists in the formulation of user-defined routine which relate the macroscopic deformation to the global stresses/forces through some analytical relations, Fig. 2.21.
Here the response of the macroscopic homogeneous material in terms of stresses is obtained imposing the global deformation state to a representative unitary cell (RUC) at each time step in each integration point of the continuum. The RUC is usually modeled as a simple system of pin-joined trusses to get a fast-to-compute analytical solution where yarn-to-yarn interaction are simplified. Thanks to this approach the weave geometry is considered even if with some important simplifications. Cross-over point are usually supposed to be rigid with no relative slip among warp and weft while yarn transverse behaviour is hardy taken into account.
An impact application of these models was presented by Ivanov et al. [59] and Shahkarami [92] to predict the ballistic properties of a single and multi-ply Kevlar fabric.

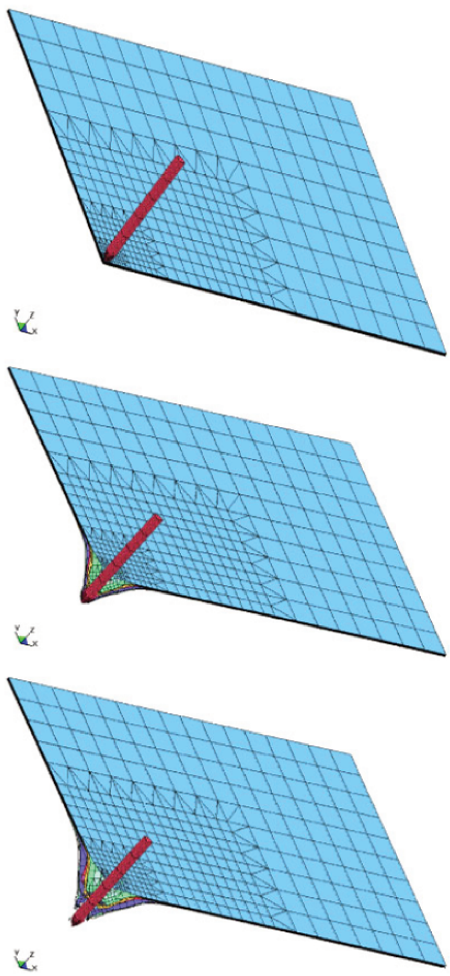

Fig. 2.22 Penetration of a RUC based macroscopic fabric model proposed by Ivanov [59].

An alternative solution adopted by other authors consisted in the determination of the stress-strain relation using numerical or experimental tests. Boisse [50] performed an explicit FE forming simulation where the fabric constitutive behaviour was obtained performing virtual tests at the mesoscale. A similar concept was applied in some successive works where an hyperelastic constitutive model was adopted for a glass plain weave fabric layer [2, 3]. Here the material law parameter were determined by the difference minimization between the experimental and numerical model response to uniaxial strain and shear test.

Mesoscopic models

When the dimension of the analyzed fabric portion is relatively small compared to the repetitive unit or the physical phenomenon is very localized, it is usually possible to model the entire fabric layers as a discrete systems of woven yarns.

In mesoscopic models, the weaving geometry is explicitly considered and phenomena as yarn slipping, ravelling and windowing are naturally taken into account. Yarn-to-yarn interactions are usually treated according to the contact algorithms proposed by the finite element codes. This makes possible the evaluation of the energy dissipation through inter-yarn and fabric-to-projectile friction.

Due to their accuracy, these type of models are not only used to determine the structure ballistic performance but even for parametric studies on physical parameters which affect the fabric response. In this way it is possible to get insight about the physical phenomena behind the impact and get information which can be useful in protective layer design without occurring in the costs associated to the experiments.

Another aspect which makes them a preferable inspection tool compared to the classical experimental facilities is their ability to record a large number of data, i.e. stress, strains, energies. For these reasons they are actually the most popular choice among the researchers and represent a good compromise among computational time and simulation accuracy. Different mesoscopic models have been proposed in the last ten years, however they mostly differentiate among each other for the type of elements adopted.

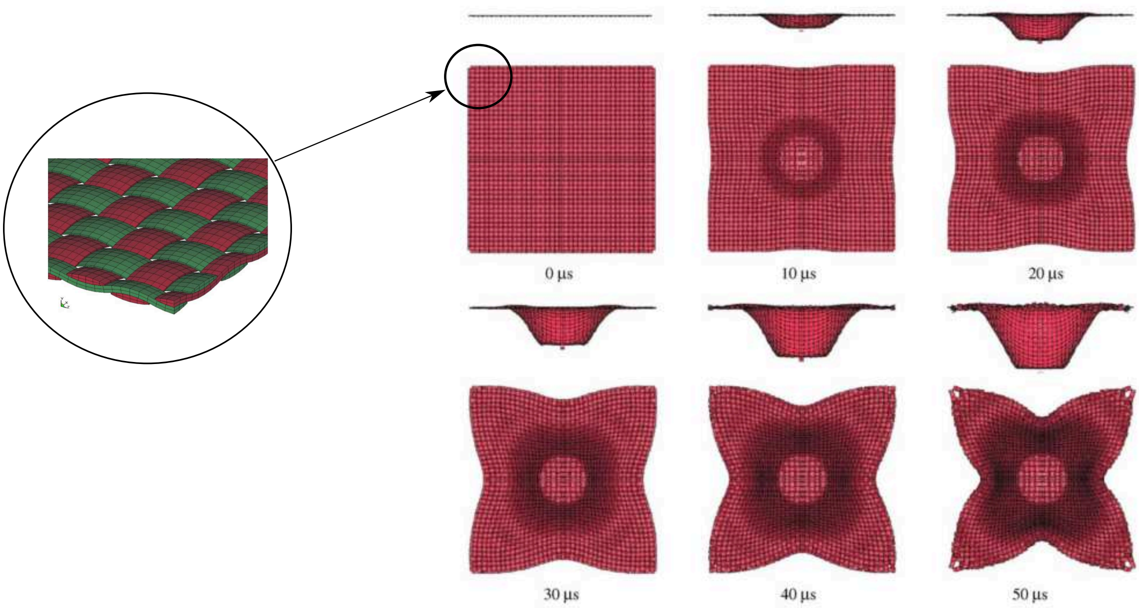

Fig. 2.23 Mesoscopic fabric model using 3D finite elements proposed by Duan [39].

A first mesoscopic finite element model of a fabric was presented by Duan [39, 40] to study the effect of friction and boundary conditions on the ballistic performance of a Kevlar fabric. Here the weaving geometry was fully represented with yarns modeled as a continuum with their cross section defined by a pair of symmetric arcs Fig. 2.23. Twelve

solid elements were adopted to discretize the cross section and a linear orthotropic elastic continuum behaviour as proposed by Gasser [43] was adopted as constitutive law.
The elastic tensile modulus in the fiber direction was obtained by the quasi-static experimental tests, which are probably not representative of the dynamic behaviour of the material, while the other mechanical parameters were assumed to be two orders of magnitude lower than the previous one. Zero Poisson ratios were assumed.
The yarn model was validated using the uniaxial analytical model proposed by Smith. A maximum principal stress[40] and a maximum Von Mises stress [39] were adopted as failure criterion. The author claimed that these choices were equivalent to a maximum tensile strain along the yarn axis due to the low contribution of the stress components related to the transverse direction.
At the fabric level yarn-to-yarn interaction were considered using the contact algorithm implemented in the finite element code while a Coulomb model was assumed for friction.

A similar approach for fabric modelization was adopted by Rao [87]. Even in this case a plain weave Kevlar KM2 fabric was modeled at the mesoscale using finite elements. The same elements, mesh size, material model and failure criterion proposed by Duan were adopted. The only exception was the yarn density which was computed scaling that of the fibers for the yarn volume ratio. Following the work of the previous two authors, Nilakantan developed a mesoscopic finite element model Kevlar S706 fabric. Here, five solid elements within the cross section were adopted to discretize the yarns. The same linear elastic orthotropic constitutive model was adopted with the longitudinal elastic modulus and the yarn density obtained by those of the single fibers scaled by the yarn fiber volume fraction. Maximum principal stress was still adopted as failure criterion. The model was adopted to evaluate the deterministic and probabilistic effect of clamping design [73, 76, 77], projectile characteristics [70, 73, 79], material properties [70, 75] and yarn-to-yarn friction [70, 73] on the fabric ballistic performance.

A different discretization was considered by Chocron for a 10 layer Kevlar 29 745S (3000 denier) fabric model [21]. In order to be able to model each layers explicitly, only two solid elements were used to discretize the yarn cross section. The classical linear elastic orthotropic constitutive behavior was considered for the yarns whose physical values were assumed equal to those of the fibers.
A single yarn model and a single layer model was firstly validated before moving to the whole fabric. The failure criterion here adopted was the classical maximum stress criterion assumed by Rao [87]. Single layer model was validated recording the kinematic of the impact. Pyramidal shape induced by the projectile was measured and compared with the experimental results. Concerning the validation of the full fabric model, a good correlation

with experimental results was found. Numerical prediction of the ballistic limit was in good agreement with the experimental results ,$\approx 400\,\mathrm{m\,s^{-1}}$. Good results were even obtained for the whole fabric kinematic and yarn strain measurement.
Other examples where 3D elements are adopted for the modelization of yarn include the work of Zhou [117], Wang [109] and McKee [60].

A second approach to build mesoscopic fabric finite element models consists in using shell elements instead of bricks to model the fabric yarns (Fig. 2.24). This type of approach was firstly adopted for multiscale analyses [6] and then used for the complete representation of a fabric [46, 47, 49].

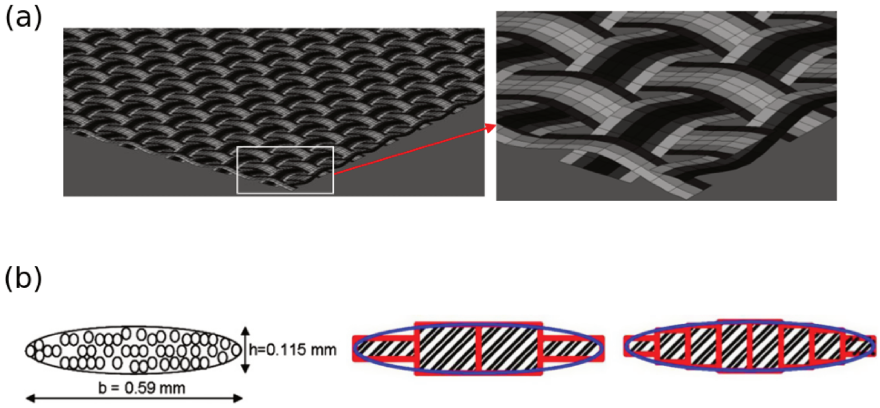

Fig. 2.24 Shell mesoscopic finite element model proposed by Ha-Minh [48].

Ha-Minh performed a numerical study of a 2D Kevlar KM2 plain-woven fabric transversely impacted by a spherical projectile [48] in a non penetration ($60\,\mathrm{m\,s^{-1}}$ and penetration ($245\,\mathrm{m\,s^{-1}}$) impact scenario. The yarns were modeled using 3D shell elements with two integration points along the thicknesses. The number of integration points was justified by the author with the necessity of taking into account the yarn shear resistance in the phenomenon. A linear elastic orthotropic model was adopted for the yarn and the material parameters were assumed to be equal to those of a single fiber [49]. Two different mesh size, 4 and 8 elements per cross section, were tested (Fig. 2.24). It was found that four elements per cross section were sufficient to describe the analyzed impact phenomenon. The same approach was adopted for the investigation of the failure mechanism of a 3D fabrics impacted by a spherical and FSP projectiles [46, 47]. Penetrating and non-penetrating impact scenarios were analyzed and even in this case the global kinematic of the system obtained experimentally was coherent with the simulation results.

The last and more simple way to model a dry fabric at the mesoscale is to represent the yarns using flexible 1D elements (Fig. 2.25). The first examples of these models applied to the impact studies were proposed by Roylance [90] and Shim [93]. Both the authors represented a fabric layer as a yarn assemble interconnected at the crossover point (Fig. 2.25). The yarns were modeled as unidimensional elements whose response in terms of forces was computed starting from the relative distance and speed of the extremities. Failure was then added using a maximum longitudinal strain criterion. In these preliminary models yarn-to-yarn interaction, yarn crimping and friction were not considered. Nevertheless the previous approximations, this approach was able to fairly represent the pyramidal shape induced by the impact and the localized failure at the contact point for different impact speeds. The evolution of the previous approach is represented by those model which make the yarn able to move and slip at the crossover while still using 1D elements for their representation [35, 114]. Here mostly the same approach in terms of constitutive model is adopted where a monodimensional constitutive behaviour is used with a purely longitudinal failure criterion. The difference with the previous ones relies in the adoption of a contact algorithm among the yarn which makes feasible the computation of friction forces, friction energy dissipation.

(a)

(b)

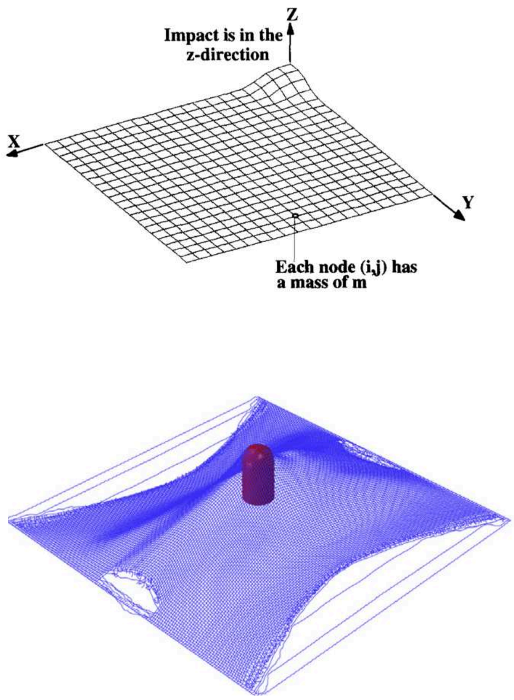

Fig. 2.25 Unidimensional mesoscopic models proposed by Shim (a) [93] and Das (b) [35].

Microscopic models

Most of fabric numerical models deal with a mesoscopic or macroscopic modelization of the system but, more recently, fiber scale modeling of fabrics is gaining popularity. When yarns are considered as a discrete assemble of different fibres interfibre contact phenomena can be explicitly considered and real stress state can be analyzed.

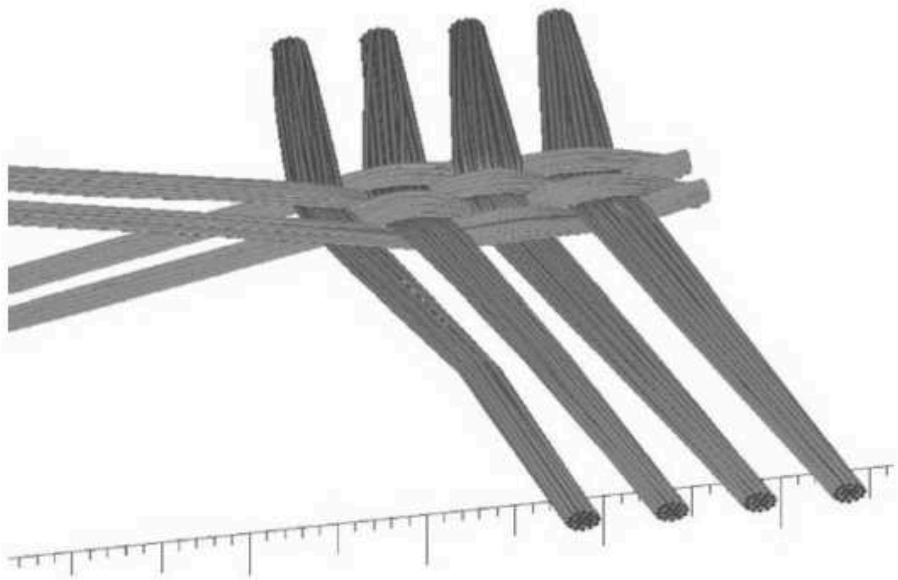

Fig. 2.26 Weaving simulation using Digital Element Method [116].

A first application of the multifibres models was presented by Zhou et al. [116]. In this paper a novel numerical approach for weaving simulation was presented, Fig. 2.26. The basic idea was to develop a numerical method that was able to represented with a good approximation the final geometry of a fabric after the weaving process. This numerical method was named “Digital Element Method”. It consists in a coarse discretization of the yarn into a group of 19-50 macrofibres where each macrofiber was representative of a large number of real scale fibers. Macrofibres were modelled by pin-joint trusses (Fig. 2.27). Since each macrofibre was considered as a parallel system of real scale fibres, evaluation of the longitudinal stiffness was straightforward. Contact algorithm was firstly based on a node-to-node control. Penalty method was used to compute contact reaction and a Coulomb friction model was adopted for dissipative action. Weaving process was considered as a non-linear quasi-static problem. An improved version of the Digital Element Method was presented by Miao et al. [68]. In this work the author developed a new contact algorithm based on a node-to-fibre formulation; sliding and sticking between elements was even implemented.

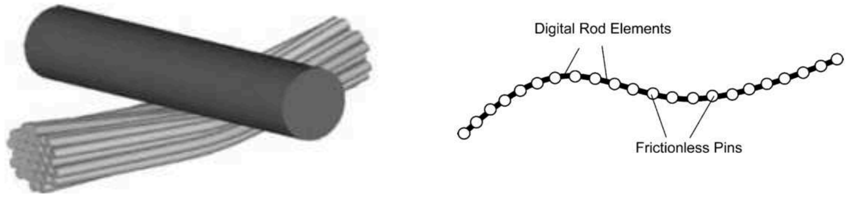

Fig. 2.27 Digital Element fiber discretization [116].

The first application of Digital Element Method to ballistic impact on dry fabrics was performed by Wang et al. [111]. In this optic a new explicit algorithm was formulated for the numerical solution of the problem. Friction was considered and a convergence study on the yarn discretization was performed. It was found that residual velocity of the projectile converged with 19 macrofibres, Fig. 2.28. Stress limit was assumed as failure criterion. In the same work the author mentioned the use of beam elements instead of trusses in order to obtain more accurate results, anyway no more information about the use of these elements have been provided.

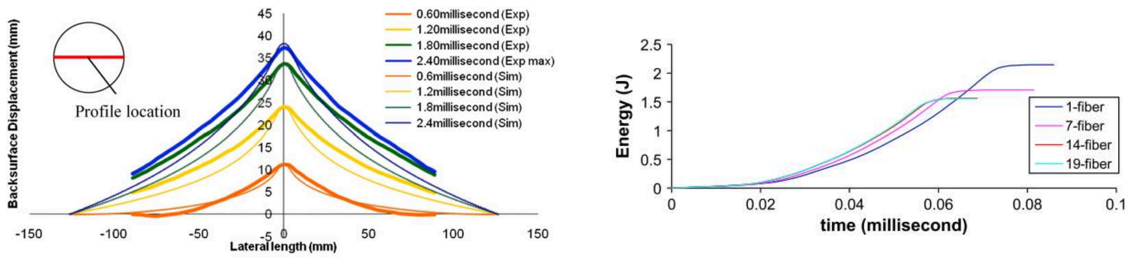

Fig. 2.28 DEM physical convergence study performed by Wang on fabric deflection profile and ballistic performance [111].

In a subsequent work, the Digital Element Method was adopted to understand the effect of interfiber friction on the ballistic performance Kevlar KM2 plain woven fabric [110]. Progressive fiber fragmentation was observed during the impact and failure phenomenon was found to be dependent by fiber-fiber friction coefficient. Windowing and yarn transverse deformation were even captured but numerically evaluated critical velocity resulted to be 25% higher than that obtained by experimental observations (Fig. 2.29).

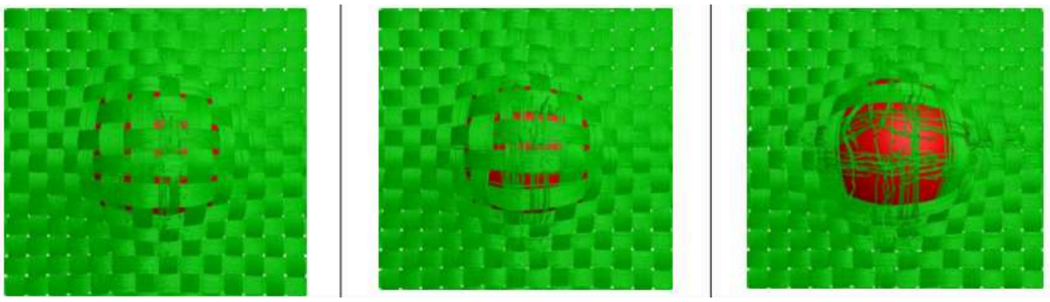

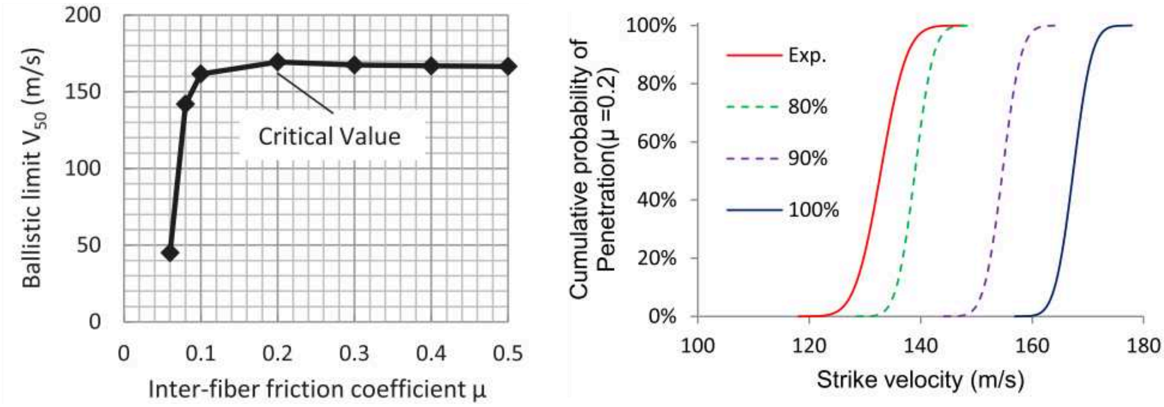

Fig. 2.29 Effect of intrafiber friction over ballistic limit according to the DEM model and comparison with experiments [110].

A second application to ballistic impact of Digital Element Method was performed by Grujicic et al [45]. In this work the author implemented the Digital Element Method in a commercial Finite Element Software. In particular, the effects of the microfiber transverse mechanical behaviour and friction were analysed, Fig. 2.30. It was found that transverse properties of macrofibres largely affect the global behaviour of the fabric under impact. Different models were proposed to the transversal behaviour of macrofibres in order to obtain a global deformation of the fabric close to the experimental data. Stochastic nature of Kevlar stress failure was even considered. It was shown that using stochastic distribution for failure stress, fabric failure appears even outside the impact zone.

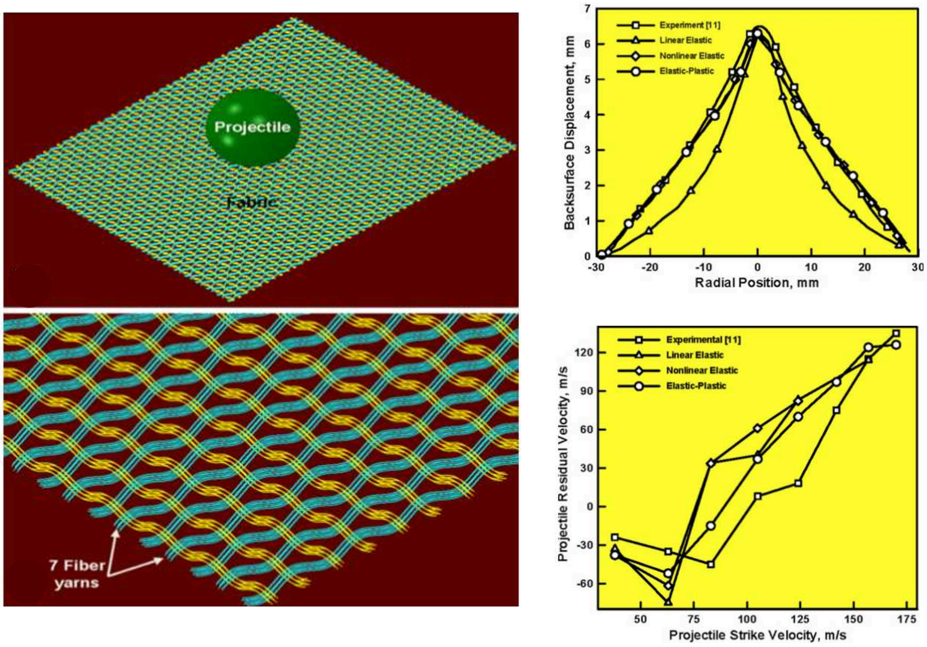

Fig. 2.30 Effect of fiber transverse behaviour over ballistic performance in DEM model [45].

More complex models have been presented since the introduction of the Digital Element Method.

Durville [41] presented a 3D beam model to simulate weaving and quasi-static deformation of fabric. In this work the authors used an enriched beam model to take into account a three dimensional strain field. A novel contact algorithm was developed. It consisted in a definition of those zone who could be potentially in contact followed by the creation of contact element. The model was predisposed for quasi-static implicit analysis. It was used to evaluate mechanical response of classical 2D fabric as plain weave and twill weave.

A significant work on filament-level modelling of dry fabrics have been presented by Nilakantan [69]. In this paper, the author presented a Finite Element model of a single yarn transversely impacted, Fig. 2.31. In this specific frame all the 400 fibres which compose a yarn of Kevlar KM2 were modelled. Each fibre was modelled using nine 3D bricks elements per section. Mechanical behaviour of the material was modelled as transversely isotropic. Using 3D elements, the author was able to consider phenomena as transverse deformation of the fibre section. It was found that elastic response of the system was not affected by friction nor transverse nor torsional stiffness before failure. Since the failure begins, a variation of the behaviour has been founded. Specifically, friction has an important role in determining the final speed of the projectile.

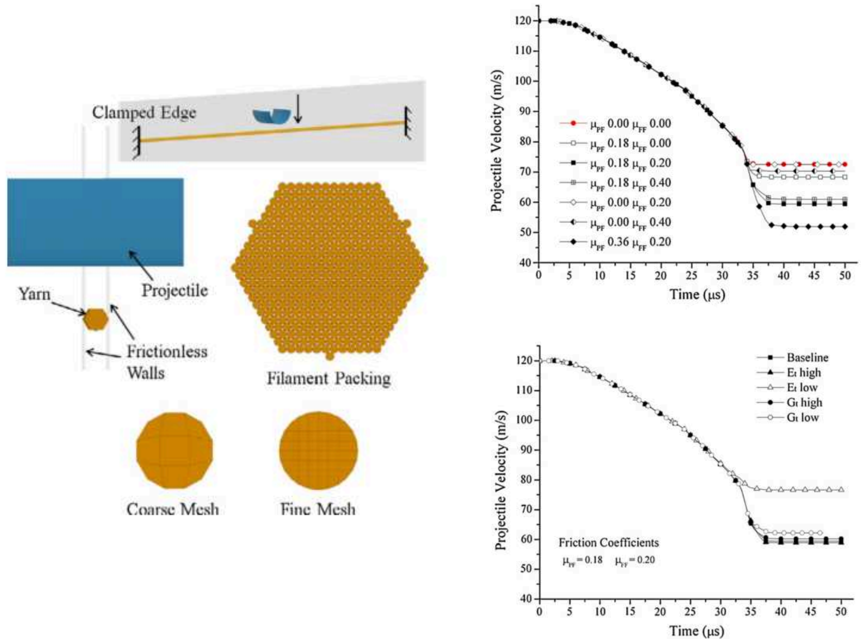

Fig. 2.31 Microscopic model of transversely impact yarn by Nilakantan and its results [69].

Following studies in which a 3D Finite Element microscopic model of yarn was adopted were performed by Sockalingam [98, 100, 101, 103, 104]. In these works the importance of a correct representation of fibers and yarn transverse behaviour in numerical model is continuously remarked.

2.3 Ballistic impact on single yarn

In the previous part the problem and the modelization of a fabric submitted to a transverse impact has been presented and the main aspects which influence the structure ballistic performances have been discussed. As previously stated, the way in which a textile absorbs the energy of a colliding object depends on a large number of factors including weaving geometry, fiber material properties, yarn-to-yarn interactions, fiber-to-fiber interactions, striking speed and projectile shapes. A good design of a protective structure obviously results from the comprehension of those phenomena and their relative interactions.
Due to these reasons, a great effort was dedicated to the study of a single yarn submitted to a transverse impact. This type of problem avoids the complication associated to the weaving type and yarn-to-yarn interaction while focusing on the effect of material choice.

The analytical theory of the longitudinal impact is firstly introduced. This will provide the theoretical bases for the so called "Smith theory". Then, the limit of this analytical approach and the concept of critical velocity are discussed.

2.3.1 Longitudinal impact on a flexible filament

Let us consider a single fiber fixed at one end and whose free end is suddenly subjected to a constant velocity V in the axial direction (Fig. 2.32):

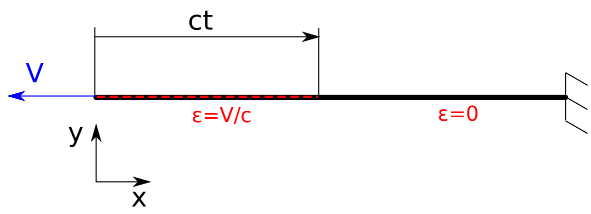

Fig. 2.32 Longitudinal impact on flexible filament.

The equation of motion for the simple monodimensional case is written:

$$\frac{\partial^2 u}{\partial t^2} = \frac{E}{\rho}\frac{\partial^2 u}{\partial x^2}.$$

Where u is the displacement in the axial direction, E is the longitudinal Young modulus of the material and ρ is the material density.
This equation is even known as wave equation and its solution represents a disturbance, or wave, initialized at the free ends which travel along the filament axis toward the clamped one. The velocity of the disturbance is usually indicated by c and is a function of the elastic and inertial properties of the material:

$$c = \sqrt{E/\rho}. \tag{2.1}$$

Concerning the strain state induced within the filaments, the structure can be split in two different parts. Under the hypothesis of free propagation condition, all those points in the wake of the longitudinal wave ($x < ct$) are characterized by a unique strain state $\varepsilon = V/c$ while the remaining part of the system remains unstrained.
It is worth to notice that ,according to this simple analytical model, those materials which quickly propagate the disturbance outer the impact zone induce lower values of longitudinal strains. This is actually an advantage since they will fail for higher value of impact speed, as remarked by Cunniff [30].
The velocity field is obtained by the strain one. The material points velocity v has the only longitudinal component and presents the same direction of that imposed as boundary condition. The value of v is given by the product of the sonic velocity c and the induced strain ε:

$$v = \varepsilon c. \tag{2.2}$$

In this theoretical model the material was assumed as linear elastic, however the theory can be extended to the nonlinear cases [89, 90]

2.3.2 Transverse impact on flexible filaments

The most renowned works concerning the transverse impact on a flexible filaments are attributed to Jack C. Smith and his colleagues [94, 95, 97]. In his series of papers, the author developed an elegant analytical theory which explains the main phenomena that occur when a flexible filament is subjected to this type of loading. This theory is usually named "Smith theory" and here is briefly reported.

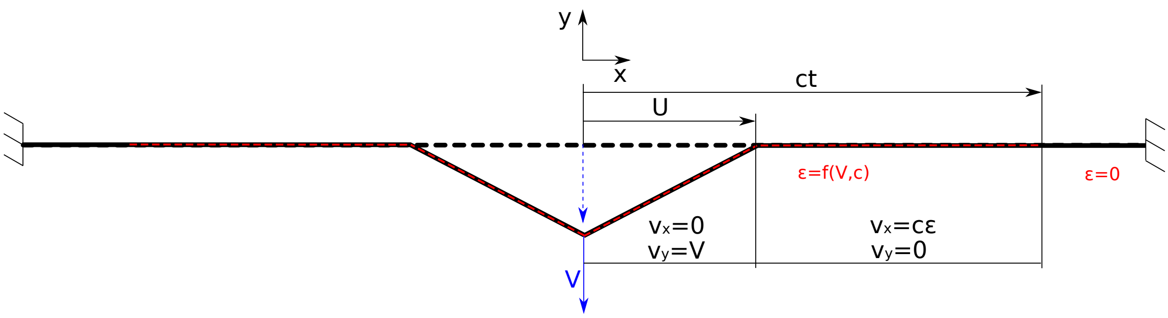

Fig. 2.33 Transverse impact on flexible filament.

The filament is considered as an homogeneous continuous medium, the material is assumed to be linear elastic and the impact is modeled as a constant velocity V imposed at the fiber center (Fig.2.33). Free propagation condition are even assumed in order to avoid complications related to wave reflection.

Starting from the impact point two waves are initialized and propagated along the filament axis. The first wave is the same longitudinal wave observed for the longitudinal impact and it travels with the same velocity c. Behind this wave front, a constant strain state ε is induced while the material points move toward the impact point with a velocity v equal to:

$$v = c\varepsilon. \tag{2.3}$$

The second wave is called "transverse wave". It propagates with a constant velocity U and induces a typical V-shaped zone near the impact. The wave speed U is usually one order of magnitude lower than c and here is reported as an Eulerian measure. Its value is directly related to the yarn material properties and the induced strain state:

$$U = c(\sqrt{\frac{\varepsilon}{1+\varepsilon}} - \varepsilon). \tag{2.4}$$

All those points in the wake of the transverse wave are characterized by a velocity in modulus and direction equal to that imposed as boundary condition while the strain state remains unvaried.

The value of the induced strain state is related to the impact velocity V by the following relation:

$$V = c\sqrt{\varepsilon(2\sqrt{\varepsilon(1+\varepsilon)} - \varepsilon)}. \tag{2.5}$$

Combining this last equation with 2.4-2.3 it is possible to obtain the complete solution of the problem in terms of strains and velocity field.

From an energetic point of view, this classical analytical solution provides a linear trends in time for internal and kinetic energy.
Reminding that a constant strain state ε which travel with a specific velocity c is predicted, the amount of energy stored into filament elongation is written:

$$E_I = \frac{1}{2}\varepsilon^2 EAct. \tag{2.6}$$

Where E is the filament Young Modulus, A the filament cross section and ct the length of the filament under tension at the instant t.
In the same way the filament kinetic energy E_k is given by the contribution of the zone behind the transverse wave front E_{K_u} plus the contribution of the zone between the transverse and longitudinal wave front E_{K_i}:

$$E_k = E_{K_i} + E_{K_u}. \tag{2.7}$$

The zone behind the transverse wave front presents a velocity equal to the impact velocity V imposed as boundary condition:

$$E_{K_u} = \frac{1}{2}\rho AV^2 Ut. \tag{2.8}$$

Where ρ is the filament density.
The second contribution to the filament kinetic energy is equivalent to that computed for the longitudinal impact case and is restricted to the zone among the two wave fronts:

$$E_{K_i} = \frac{1}{2}\rho A(\varepsilon c)^2(c-U)t. \tag{2.9}$$

The most interesting aspect about this theory relies in its ability to predict the strain state from the bullet striking velocity.
This element assumes a fundamental role in the analysis of fibre ballistic performance since, for a given critical longitudinal strain, the minimal impact speed which will penetrate the yarn can be ideally computed. This particular speed is called "critical velocity" and is usually adopted as a preliminary design tool in protection systems. The yarn critical velocity should not be confused with the ballistic limit previously introduced. This new parameter is typical of yarn structure and directly discern from the analytical theory previously proposed.
A material characterized by an higher critical velocity will usually be able to perform better than others once weaved into a fabric form. For this reason is important to correctly determine this value for different yarns and develop prediction tools for its evaluation.

2.3.3 Smith theory limitation

The most important results of the Smith theory are the description of the global kinematic of the impact and the determination of the critical velocity of the filament.
Different experimental works showed how the Smith solution accurately describes the global kinematic of an impacted yarn [22, 56, 96, 105] (Fig. 2.34). The propagation of the transverse and longitudinal waves has been observed during various experiments and the experimental measurements of their speed have been found to be coherent with those provided by Smith [105]. The accuracy in describing the filament kinematic combined with its generality and its closed-form make this analytical model very popular among different authors which used it as a verification of their numerical ones [21, 40].

On the other side, the analytically computed critical velocity is not as accurate as the impact kinematic description. The difference among the experimental and analytical values have been remarked by different authors [8, 22, 56] and the explanation of this discrepancy has been the central topic of different works [8, 55, 102, 108].

The different theories which explain this discrepancy can be generally classified in two categories according to the mechanism at the base of this premature failure:

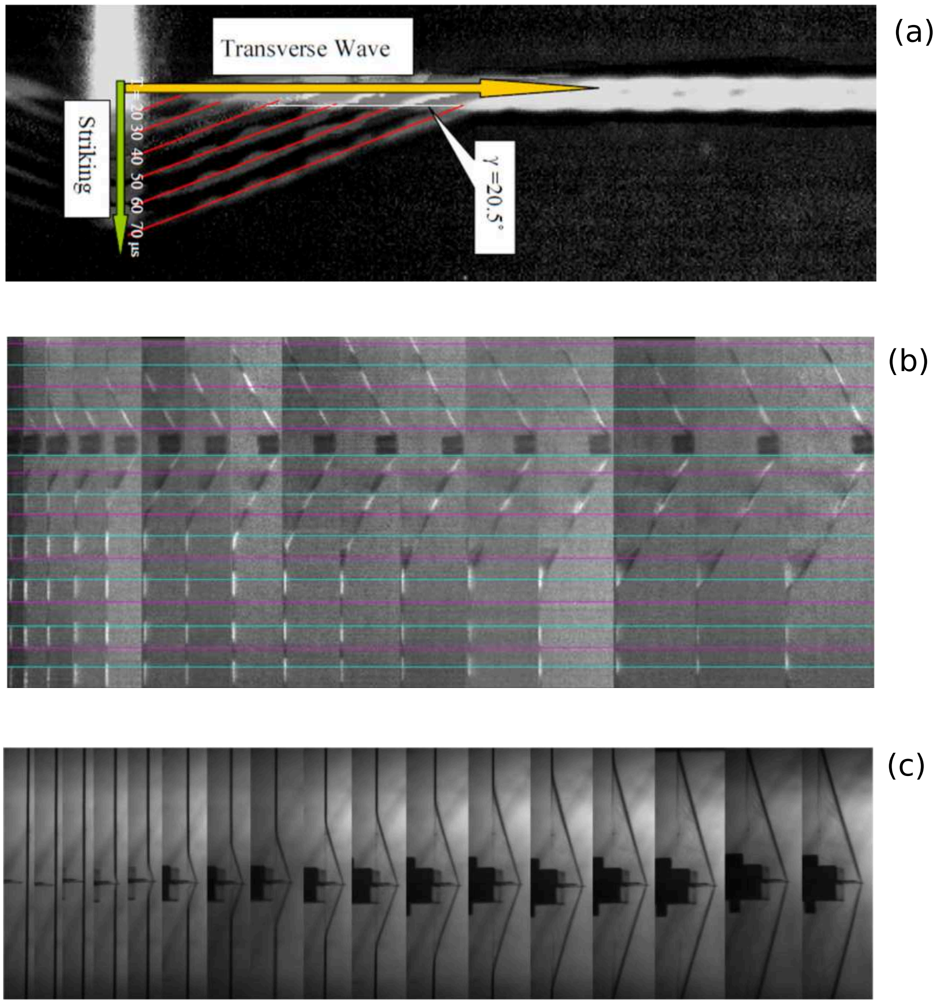

Fig. 2.34 Experimental observation of a transverse impact on flexible filament performed by Song (a)[105], Chocron (b)[22] and Hudspeth (c)[56].

- Structural theories
- Multiaxial stress theories

Structural theories

The first group is composed by those works which justify this difference using structural phenomena but still rely on a purely longitudinal and continuous description of the filament. Different analytical theories have been proposed which takes into account the projectile shape or complex wave propagation schemes [8, 84, 108]. All of them still consider the yarn as a unidimensional continuous medium, neglecting all the contribution associated to its discrete nature, transverse mechanical behaviour and multiaxial stress state.

Bazhenov performed an experimental transverse impact test on an aramid SVM yarn. A spherical projectile launched at 670 m/s was used to test the resistance of the filament. The dynamic of the phenomenon put in evidence the inelastic failure of the system where transverse wave had no time to propagate at this particular striking speed, Fig. 2.35.

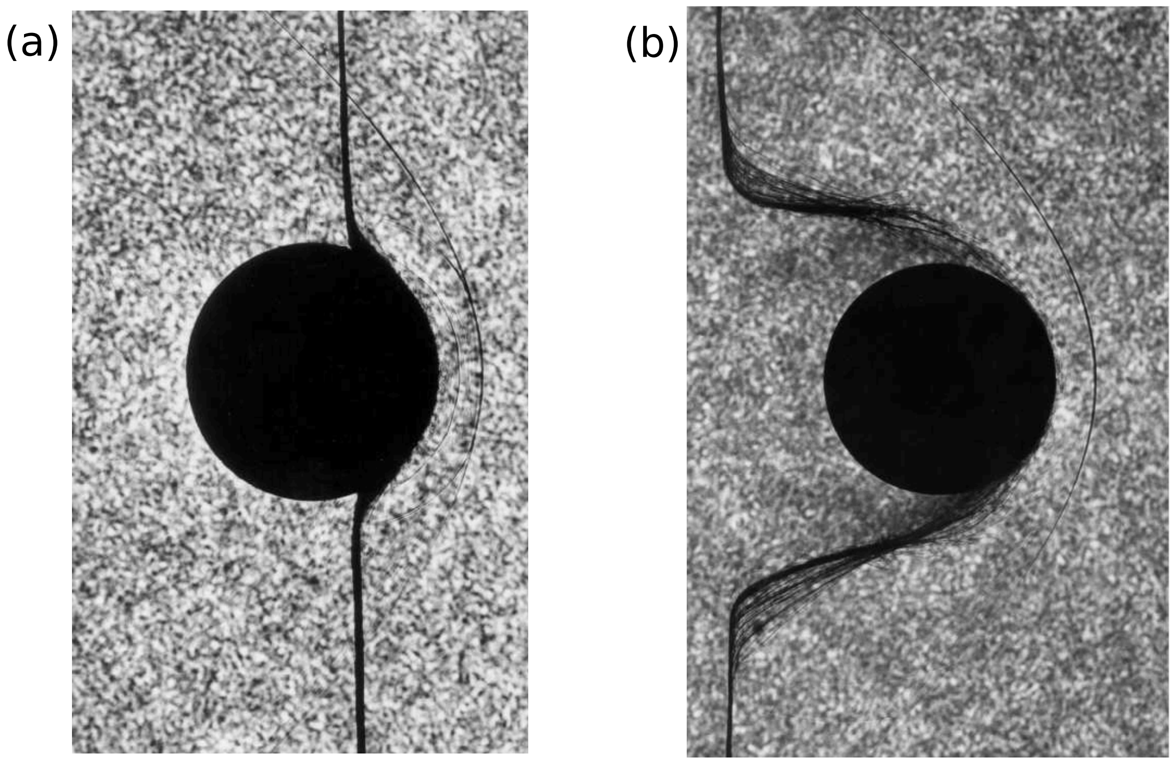

Fig. 2.35 SVM thread impacted by a spherical projectile with a striking speed of 670 $\mathrm{m\,s^{-1}}$ at 15 µs(a) and 64.7 µs(b) [8].

Experimental results shown a critical velocity of 670 m/s while the solution provided by Smith resulted in a critical velocity of 770 m/s. Two different theories were proposed in order to explain this discrepancy.

Firstly the non-linear behaviour of the fibers in their longitudinal direction was considered. Taking into account the material non-linearities the classical wave equation were slightly modified. However the critical speed evaluated taking into account this effect was still far from the experimental observation. The second proposed theory was based on the interaction among the projectile and the yarn. The author proposed a multipoint contact theory for which the longitudinal wave remain confined in the contact zone and can induce strain state levels which are comparable with those required for the material failure.

A second theory of this group was proposed by Walker in 2011 [108]. Even this work remains confined to the unidimensional behaviour of yarns and was developed for the particular case

of an impact with flat-faced projectiles (Cylindrical and FSP). Analyzing some numerical results obtained from a mesoscopic yarn model the author noticed that four different waves were initiated when the yarn bounced off the projectile surface just after the impact.
Two couples of transverse and longitudinal waves were originated from the impact point with one travelling out of the impact zone and the other moving to the yarn centre, Fig. 2.36. This kinematic was assumed as a basis for the analytic solution which results in a relation among the bounce velocity of the yarn, the velocity of the projectile and the strain state induced within the thread.
Two limit cases were analyzed by the author: perfectly inelastic and perfectly elastic collision. For the first case a reduction of the 11% over the classical critical velocity formula was achieved, in the second case the reduction factor raised to 40%. It is interesting to underline that the bounce velocity was a free parameter which is intuitively related to the transverse mechanical behaviour of a yarn.

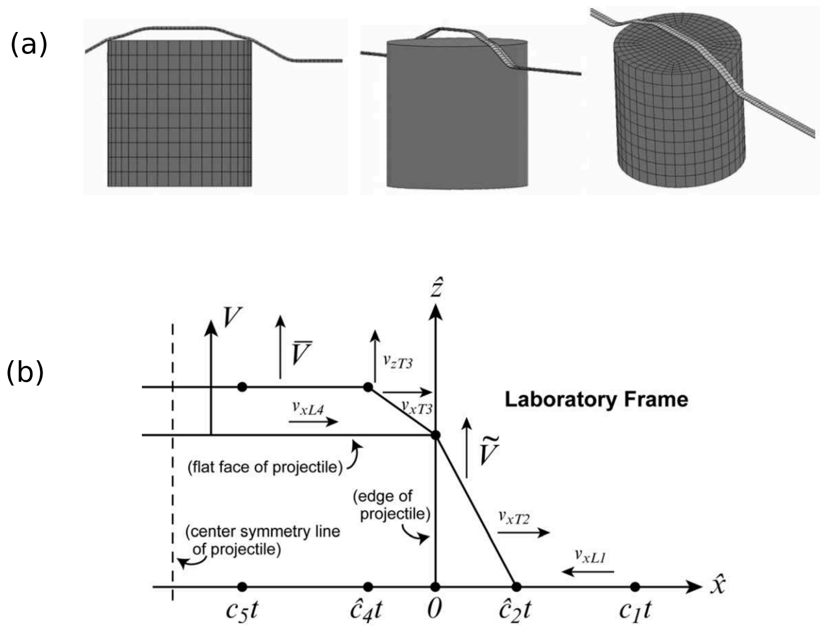

Fig. 2.36 Numerical observation of yarn bouncing off the projectile face under the impact (a) and the deduced kinematic monodimensional scheme (b) by Walker [108].

Multiaxial stress theories

The second group of theory proposes the filament multiaxial stress state as the reason of premature failure of yarns and fibers under transverse impact. Its experimental evidences have been previously presented in the section 2.1.2 where the fiber longitudinal properties degradation due to different load types have been discussed.

More complex investigations

According to the presented theories, both structural effects and multiaxial stress state are a reasonable explanation of the premature failure of yarn and fibers under transverse impact.
The classical Smith theory relies on a large number of hypotheses which are not respected in the reality. Firstly, the projectile has a characteristic shape which is not considered in the original analytical approach but actually influences the local stress state [56, 102]. This effect could be related to different aspects which include complex wave propagation phenomena and multiaxial stress state. Moreover the discrete nature of the yarn should be even considered. Yarns are actually composed of hundreds or thousand of fibers which crush and rearrange under the projectile load [69]. This actually induces a different global behaviour in terms of stresses and kinematic compared to an homogeneous body.
In order to consider all these aspects and their effects on the yarn ballistic performance, Sockalingam performed a full scale microscopic 3D finite element model of a transverserly impactde single kevlar KM2 yarn (Fig. 2.37). According to the results, different phenomena arises during the impact.

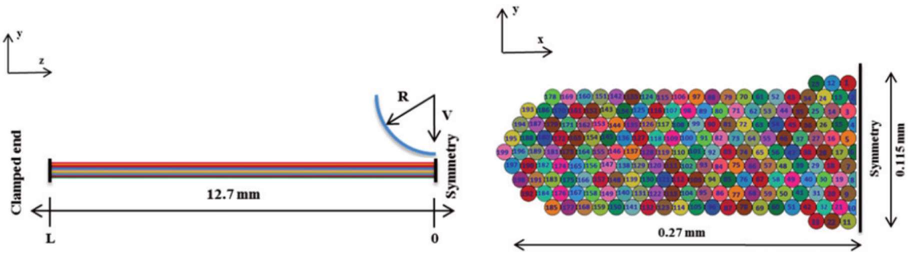

Fig. 2.37 Full 3D microscopic finite element model of a yarn impacted by a cylindrical projectile proposed by Sockalingam [104].

In a first phase fibers undergo under significative transverse compressive deformation due to initial contact with the projectile. Those are actually much higher compared to the longitudinal axial stress induced. In a second phase the development of the transverse and spreading wave with the additional propagation of flexural waves was observed. All the mentioned phenomena induce a multiaxial stress state within the yarn and higher values of longitudinal stress state compared to classical Smith theory, Fig. 2.38.

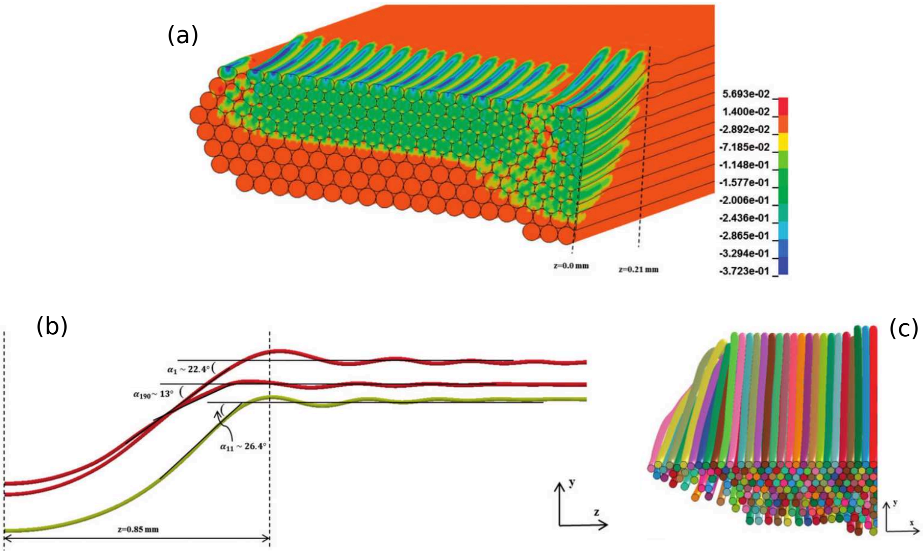

Fig. 2.38 Compression wave propagation (a), flexural waves (b) and spreading wave (c) observed by Sockalingam using a microscopic FE model of a yarn transversely impacted [104].

According to the author, the longitudinal and transverse compressive stresses are sufficient to induce permanent fiber deformations, fibrillation and kinking which could reduce the fiber nominal axial properties.
A sensitivity of the critical velocity to the longitudinal shear modulus value has been even observed, which underline the importance of other material parameters beyond the fiber longitudinal elastic modulus for this type of events.

From this study it is possible to conclude that the premature failure of a yarn compared to a purely longitudinal theory should not be attributed to a singular phenomenon but it is the composition of different factors which include structural effects, wave propagation phenomena and fibers damage.

2.4 Conclusions

In the current chapter, the problem of a dry fabric under high velocity impact and the state of the art of its numerical modelization have been presented.
The dry fabric response to an high velocity colliding object is complex and highly influenced by its multiscale nature. Weaving geometry, number of layers, fibers material, fiber-to-fiber interaction are just some of the elements which affect the global ballistic response.
This level of complexity is reflected by the numerical models where the phenomena which

cannot be explicitly taken into account are implicitly considered in the mechanical behaviour assumed for the structure. As an example, when a fabric is modeled as a continuum layer its non linear behaviour, related to weaving geometry, is taken into account by a non linear constitutive law. The same procedure is valid from yarns where their behaviour as a continuum body should reproduce that of an aligned fibers bundle.
Different numerical models have been presented for dry fabrics under high velocity impact. Macroscopic models are the most efficient from the computational point of view, however they are limited in representation of windowing, creasing and layer failure. Microscopic numerical model are very accurate in the description of the phenomena, but are penalized by an enormous computational cost. Mesoscopic numerical models result to be the most popular choices among the researcher due to their ability of precisely represent impact evolution with a reasonable computational cost.
The current state of the art of mesoscopic modelling of dry fabrics under high velocity impact is summarized by the work of Nilakantan [71]. Here the numerical prediction of the $V_0 - V_{100}$ curve for a Kevlar S760 layer is obtained and resulted to be remarkably close to the experimental data. In the same work the author marks the next numerical challenges in the field, underlining the necessity of physically representing the yarn transverse behaviour and eliminate numerical calibration from yarn continuum modelling.
This aspects plays an important role in multi-layer systems and yarn failure initialization. For these reasons, the aim of this dissertation will be to provide a mesoscopic model of a fabric where the yarn transverse behaviour is physically and correctly modeled.
In a first step, the way in which yarn cross section mechanic influences fabric ballistic performance have to be exploited. To clarify this aspect, the next chapter will be focused on the study of a transverse impact on a single yarn. Thanks to this choice, all the phenomena which affect the fabric ballistic performance but are not directly related to the yarn type will be excluded and the yarn cross effects will be much more evident. The study will be performed using microscopic numerical models of a single yarn, then singular fibers will be explicitly modeled. This choice is related to the natural treatment of the yarn discrete nature and the large number of information that can be obtained.

Chapter 3

Microscale model of a single yarn under high velocity transverse impact

In the previous chapter the problem and the numerical modelling of high velocity impact over a textile structure has been presented.
Mesoscopic models are currently the most popular in this field, since they represent the best compromise among model accuracy and computational costs. Their role is not confined to the prediction of the textile ballistic properties but they have been even adopted to understand the phenomena at the base of the impact.
An existing gap of the current mesoscopic models is the phenomenological linear elastic constitutive law adopted for the yarns. These are assumed as perfectly flexible media which oppose a significant mechanical resistance just along their axes. The problem with this approach is that yarn transverse properties are completely obliged.
Few works in bibliography focused on the role of yarn transverse behaviour over these structure ballistic properties [100, 103, 104].
In order to get insight over this aspect, a yarn microscopic numerical model will be presented and studied under impact.
In the first part of the chapter a novel numerical approach to perform microscopic numerical analyses of yarns and fabrics will be introduced. This is a revisited version of the Discrete Element approach and represents a computationally fair alternative to the classical finite element method.
In the second part, the proposed numerical approach will be adopted to model two impact scenarios.
For both the cases, an impact speed which allows the propagation of the yarn transverse wave without inducing instantaneous failure has been chosen.
In the first one, the yarn response from contact initialization to yarn failure will be analyzed.

The second will focus on the response from contact initialization to the first reflection of the longitudinal wave.
The choice of these scenarios is justified by the relation among these two time scales with fabric behaviour in low and high speed penetration regimes.
It is reasonable to think that the parameters which affect the fabric response in low-speed penetration regime are the same observed for the yarn in its long term response, where failure occurs after transverse wave propagation. On the other side, the penetration of a fabric in high-speed regime is related to phenomena which occurs before the propagation of the transverse and longitudinal wave. These can be easily observed in the second impact scenario, where yarn short time response is considered.

3.1 The Discrete Element Approach

It has been demonstrated that fabric ballistic performances are strongly influenced by parameters involved in contact mechanisms [36, 39, 45, 110], then it should be carefully treated in these numerical models. In order to deal efficiently with contact mechanic, a revisited version of the Discrete Element Method (DEM) inspired by the models developed by Wang [111] hereafter is proposed. Discrete Element Method was firstly developed for simulation of granular media by Cundall [27, 65]. This method consists in using physical particles, usually rigid, named Discrete Elements (DEs) to discretize a granular system.

More recently, the efficiency of different DEM contact search algorithms have led to an extension of this numerical method to continuous media. Examples of these applications were presented by André et al. [4, 5]. In these works the author shows that it is indeed possible to catch a continuous behavior linking the Discrete Elements by mechanical bonds.

In the present application a sequence of equally spaced DEs is used to model each fibre of a yarn. These particles carry out the yarn inertial properties and the numerical treatment of contact mechanic, which involves the fibres transversal behaviour. In order to represent continuous fibres, deformable trusses have been employed to connect Discrete Elements along the fibres axis. This solution provides a continuum linear displacement field along the fibres longitudinal direction.
According to the model, each Discrete Element can be loaded with two different forces: bond forces and contact forces. Spherical DEs are used to discretize the fibres.

Filaments Discretization

Each fibre is discretized as a sequence of bonded DEs (Fig. 3.1). Their diameter is assumed to be constant within the models and equal to those of the fibres (12 µm for Kevlar KM2 fiber [19]). Bonded DEs are initially equally spaced. Their initial reciprocal distance (the bonds length l_0 in the undeformed configuration) is taken equal to the DEs diameter according to convergence analyses over fiber longitudinal properties and contact energy stored. The global mass of a fiber has been equally distributed within the spherical particles. The mass of each DE, denoted m_i, can be evaluated as follow:

$$m_i = \pi \frac{d_{fib}^2}{4} \frac{l}{n_{DEs}} \rho, \tag{3.1}$$

where d_{fib} is the fibre diameter, l is the entire fiber length and n_{DEs} is the total number of Discrete Elements in a fiber.

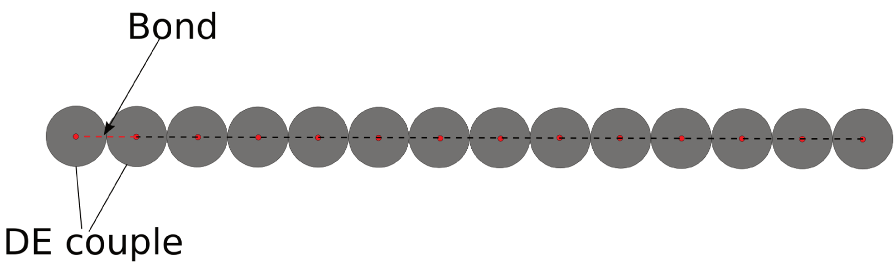

Fig. 3.1 Fibre Discretization.

Bond Constitutive Behavior

Lets consider a general couple of two Discrete Elements in the framework showed in Fig. 3.2.

Properties of the first DE will be referred with the index i while properties of the second DE will be referred with the index j. All bonds of the system are modelled as linear trusses. Bond force $\mathbf{f}_{ij}^b$ applied by the particle j on the particle i at the time t is computed as follow:

$$\mathbf{f}_{ij}^b(t) = k(||\mathbf{r}_{ij}(t)|| - l_0)\hat{\mathbf{r}}_{ij}(t), \tag{3.2}$$

$$\text{with} \quad \mathbf{r}_{ij}(t) = \mathbf{u}_j(t) - \mathbf{u}_i(t) \quad k = \frac{EA_0}{l_0}, \tag{3.3}$$

where $\mathbf{u}$ is the position vector of DEs, $\mathbf{r}$ is their relative position vector, $\hat{\mathbf{r}}$ its unitary vector at time t, E is the Young Modulus of the material in the fibres longitudinal direction, A_0 is the initial area of the fibre section and l_0 is the initial length of the bond.

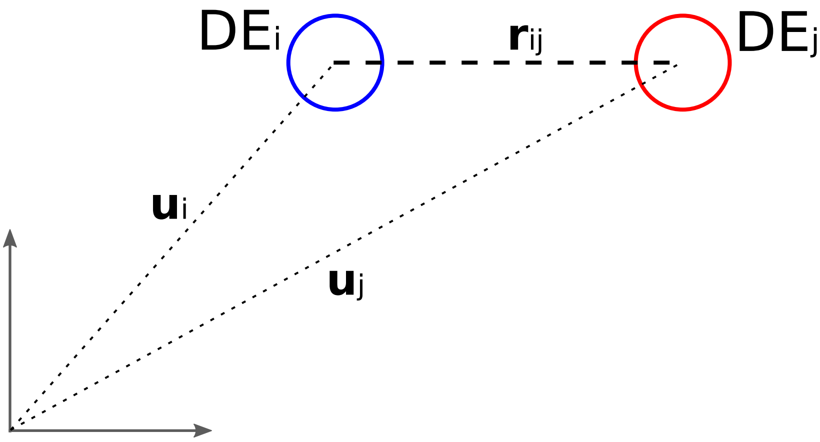

Fig. 3.2 Framework for the couples of DEs.

Failure is modeled using a maximum stress failure criterion, when a bond reaches the failure stress it is deleted by the simulation:

$$if \quad \mathbf{f}^b_{ij} = -\mathbf{f}^b_{ji} \geq ||\mathbf{f}^{lim}|| = A_0\sigma_{lim} \quad \rightarrow \quad \text{the bond is deleted.} \tag{3.4}$$

3.1.1 Contact modelling among the fibers

When two particles get in contact, a repulsive force $\mathbf{f}^c$ dependent on the interpenetration value δ is applied,Fig. 3.3. The value of the contact force from the particle j on the particle i is:

$$\mathbf{f}^c_{ij}(t) = f(\delta)\hat{\mathbf{r}}_{ij}(t), \tag{3.5}$$

where f is a function of the interpenetration δ. The f function have to be negative for all the values assumed by δ and will be defined according to the studied case.
It is important to underline that contact has not been activated between bonded elements before bonding failure.

A Coulombian model has been adopted for friction forces $\mathbf{f}^f$ and gives:

$$\mathbf{f}^f_{ij}(t) = \mu_f||\mathbf{f}^c_{ij}(t)||\hat{\mathbf{v}}^T_{ij}(t), \tag{3.6}$$

where $\hat{\mathbf{v}}^T_{ij}$ is the unitary vector of the relative velocity component in the tangential contact plane $\mathbf{v}^T_{ij}$ (Fig. 3.3) and μ_f, $\mathbf{v}_i(t)$,$\mathbf{v}_j(t)$ are respectively the kinetic friction coefficient, the velocity of the Discrete Element i and j at the time t.

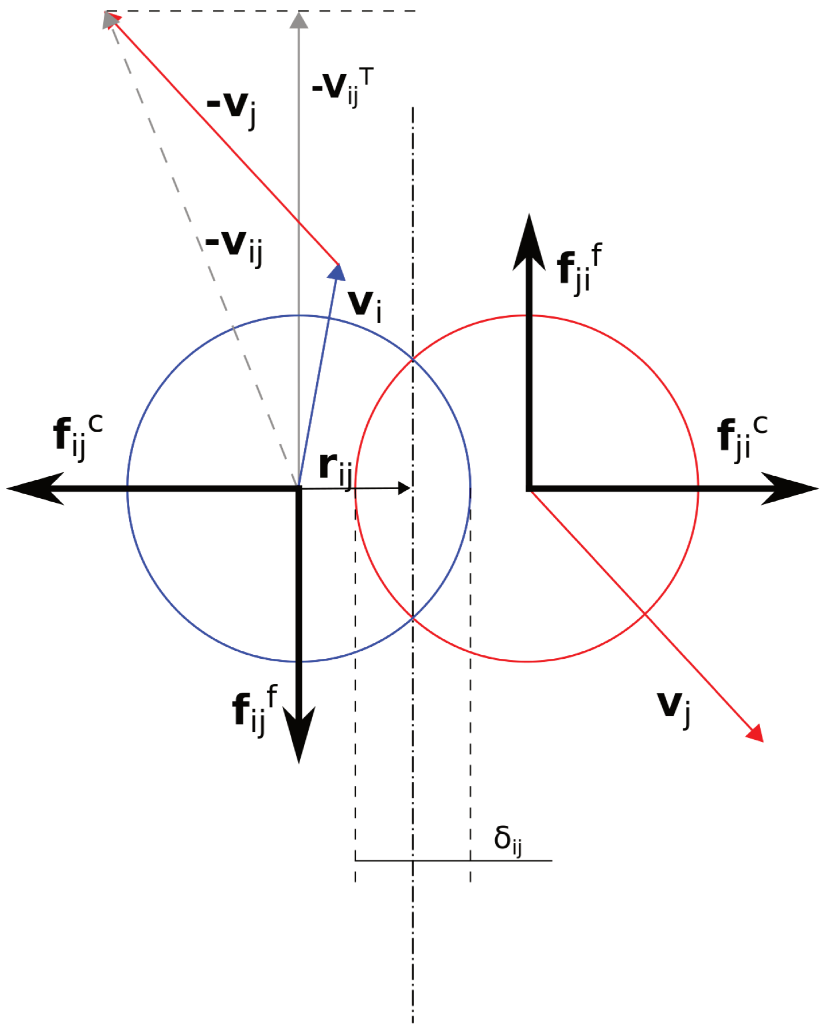

Fig. 3.3 Framework for the couples of two spherical DEs in contact.

3.1.2 Integration Scheme

The discrete element model is solved by an explicit integration scheme based on an adapted version of Verlet Velocity algorithm [4]. Total force on a single discrete element $f_i(t)$ is equal to the sum of all the previously mentioned contributions given by its interaction with the entire DEs domain (equation 3.7):

$$\mathbf{f}_i(t) = \sum_{j=1, j\neq i}^{n_{DEs}} \mathbf{f}_{ij}^b(t) + \mathbf{f}_{ij}^c(t) + \mathbf{f}_{ij}^f(t). \tag{3.7}$$

Considering the step time dt, dynamic equilibrium is driven by equation 3.8 and gives the current acceleration $\mathbf{a}_i(t)$ as a function of the current total force $f_i(t)$:

$$\mathbf{a}_i(t) = \frac{\mathbf{f}_i(t)}{m_i}. \tag{3.8}$$

From Verlet Velocity integration scheme, current velocity and position are finally computed using equations 3.9 and 3.10:

$$\mathbf{v}_i(t) = \mathbf{v}_i(t) + \frac{dt}{2}(\mathbf{a}_i(t) + \mathbf{a}_i(t+dt)), \tag{3.9}$$

$$\mathbf{u}_i(t+dt) = \mathbf{u}_i(t) + dt\mathbf{v}_i(t) + \frac{dt^2}{2}\mathbf{a}_i(t). \tag{3.10}$$

3.2 Single fiber model validation

3.2.1 Impact scenario

Before moving to the yarn impact simulations, the numerical modelization of a single Kevlar KM2 fiber has been validated.

The fundamental hypotheses of the discrete element modelization of a single fiber can be resumed as follow:

- Purely elastic constitutive behaviour;
- Homogeneous continuous body;
- Purely longitudinal behaviour.

These hypotheses are the same of those used by Smith for the formulation of its analytical theory. For this reason it is possible to use this analytical model to validate the proposed approach when the right boundary conditions are applied.
The numerical model adopted for the validation is presented in Fig. 3.4.

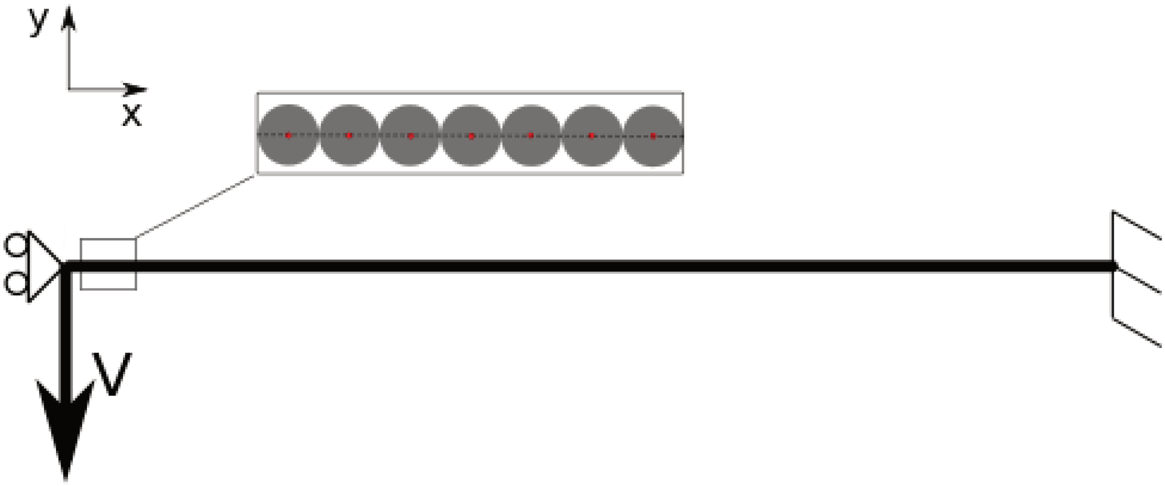

Fig. 3.4 Impact configuration adopted for single fiber validation model.

Half of the fiber has been modeled. Symmetry conditions are applied at the fiber center while fiber end is assumed to be clamped. Impact is modeled imposing a constant vertical velocity at the yarn center as in the original analytical theory. Impact speed is assumed to be equal to $200\,\mathrm{m\,s^{-1}}$.

3.2.2 Material Properties

Kevlar KM2 is notoriously a transversal isotropic material [20, 67]. Since truss elements are used, only longitudinal stiffness here will be considered. Longitudinal Young Modulus E and density ρ are taken equal to 84.62 GPa and $1.44\,\mathrm{g\,cm^{-3}}$ respectively [20, 69].
Maximal longitudinal stress is assumed as failure criterion, with a stress limit σ^{lim} equal to 3.88 GPa.

3.2.3 Results

Fig. 3.5 reports the fiber configuration and the strain field at 0.6 µs.
Transverse and longitudinal wave fronts are immediately evident and indicated with the points "A" and "B" respectively.
The induced strain state ε results of 0.498%, it is constant in the wake of the longitudinal wave front and equal to zero in the other points. Wave speed have been measured using discrete elements position and resulted equal to $7656\,\mathrm{m\,s^{-1}}$ and $505\,\mathrm{m\,s^{-1}}$ for longitudinal and transverse wave respectively.

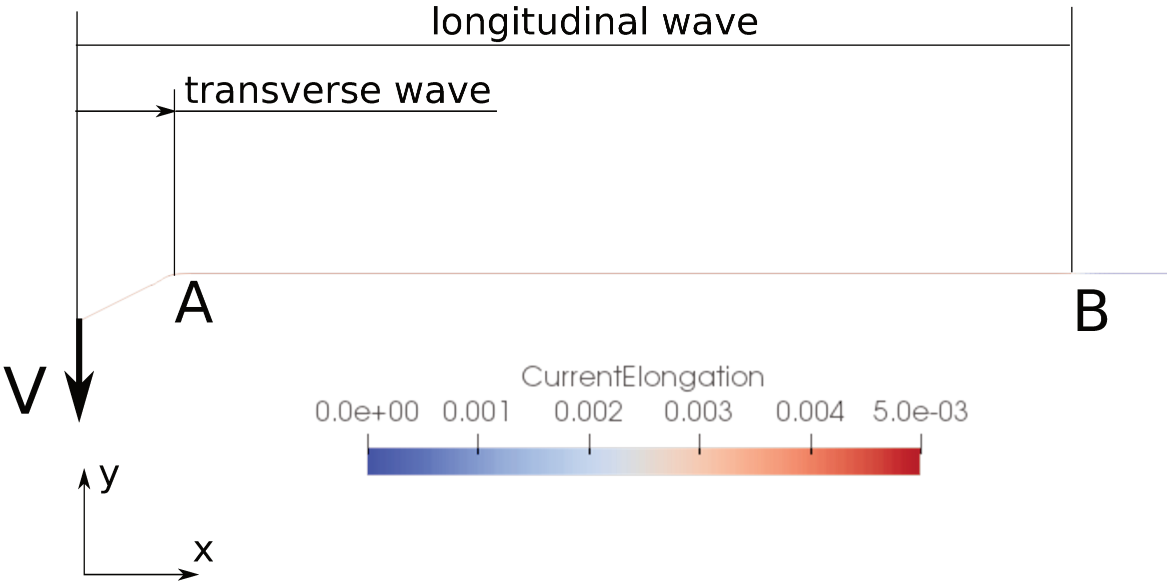

Fig. 3.5 Strain field of single fiber validation model at 0.6 µs.

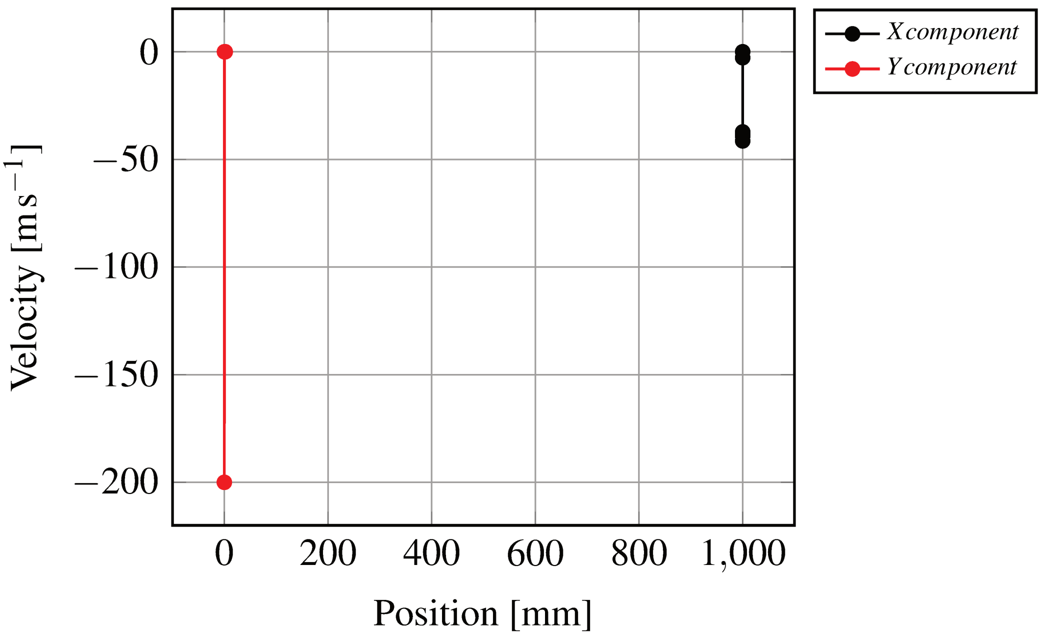

Fig. 3.6 Velocity field in fiber at 0.15 µs.

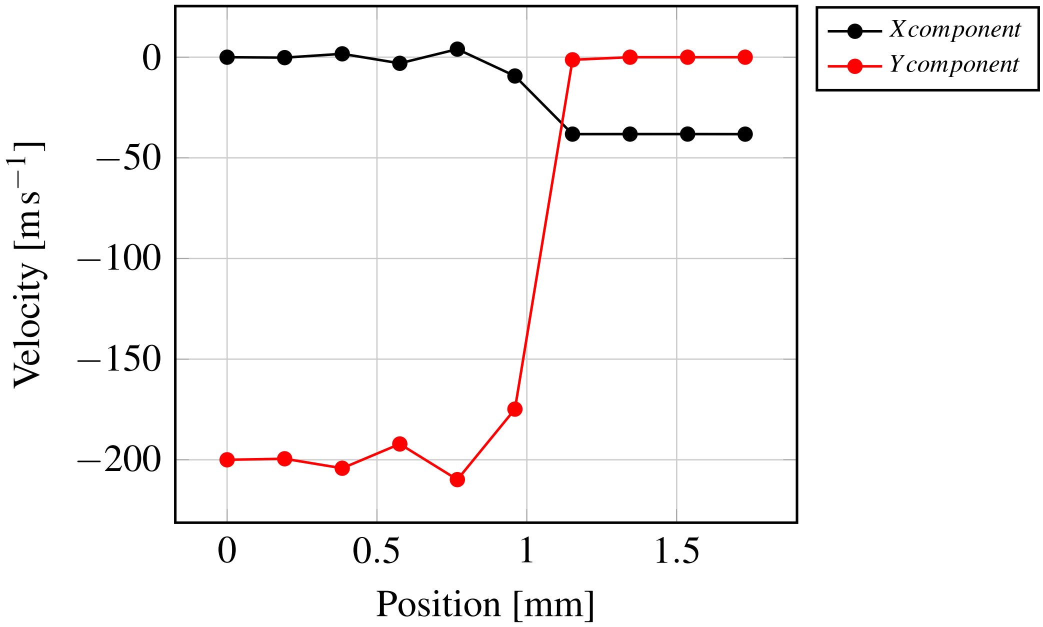

Fig. 3.7 Velocity field in fiber at 2 µs.

Fig. 3.6-3.7 report the velocity field along fiber initial axis at 0.15 µs and 2 µs. In Fig. 3.6 the transverse wave has been just initialized while longitudinal wave is propagated outside the impact zone. In the measured points, the y component of the velocity is different from zero just at the boundary condition. On the other side, the x velocity component is equal to zero at boundary condition, reaches the the value of 38.2 m s^{-1} between the transverse and longitudinal wave front and then goes back to zero, as predicted by Smith.
Propagation of the transverse wave is observed in Fig. 3.7 where the velocity field previously imposed by the longitudinal wave is turned into a velocity equal in modulus and direction to that imposed as boundary condition.

An evaluation of the model critical velocity has even been performed. The same fiber numerical model has been launched different times continuously increasing the imposed velocity V at the fiber centre. The minimum imposed speed for which immediate failure appeared was equal to 1020 m s^{-1} which is close to the theoretical value of 1027 m s^{-1}.

Table 3.1 reports the numerical registered value compared to those computed using the Smith analytical model for different impact speeds. All the obtained values differ from less than 1% then fiber model can be considered to be verified.

Table 3.1 Single fiber validation results.

Imp. Velocity [$m\,s^{-1}$]	200	400	800
Num. Axial Strain	0.498%	1.270%	3.256%
An. Axial Strain	0.498%	1.271%	3.258%
Num. Long. Wave Speed [$km\,s^{-1}$]	7.65	7.65	7.65
An. Long. Wave Speed [$km\,s^{-1}$]	7.66	7.66	7.66
Num. Trans. Wave Speed [$m\,s^{-1}$]	505	774	1162
An. Trans. Wave Speed [$m\,s^{-1}$]	504.2	772	1156

Num. Crit. Velocity [$m\,s^{-1}$]	1020
An. Crit. Velocity [$m\,s^{-1}$]	1027

3.3 Yarn transverse impact: Long period response

3.3.1 Impact scenario

The assumed impact scenario is equal to that proposed in the microscopic 3D finite element study by Nilakantan [69]. It consists in a 25.4 mm length Kevlar KM2 600 single yarn clamped at the extremities (Fig. 3.8) and impacted transversely in the centre by a cylindrical projectile. As in the reference, here all the 400 filaments which compose the yarn are modelled. Fibres are assumed to be straight and circular with an constant diameter equal to 12 µm. A cylindrical projectile with a mass M of 9.91 mg is located in the centre of the yarn with contact condition at the initial time. Its specific dimensions are an height h of 2 mm and a diameter ϕ of 2.2 mm. The impact velocity V is set to 120 $m\,s^{-1}$.Due to the nature of the problem, symmetry conditions are applied. Just half of the yarn is modeled and the original mass of the projectile is divided by two. Moreover, the displacement along the initial yarn axis is imposed to be zero for the yarn centre and for the projectile.
The current work differs from the referenced initial configuration in two details:

- The initial section is supposed to be circular (Fig. 3.9) with a yarn packing density lower than the hexagonal configuration adopted in [69].

- Symmetry conditions are introduced, in order to reduce computational time.

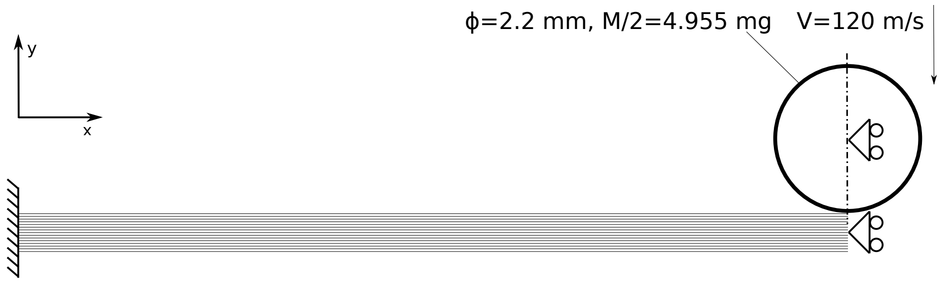

Fig. 3.8 Transverse impact set up.

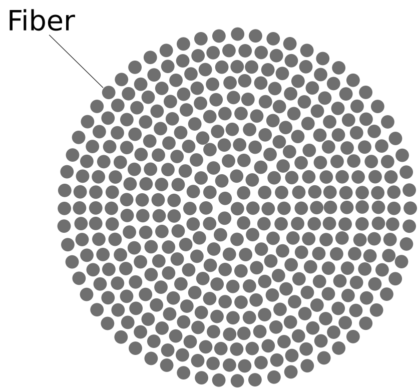

Fig. 3.9 Initial yarn section layout.

Fiber are assumed to be rigid in this first simulation. This assumption is justified by the fact that no significant energy contribution is expected from their transverse deformation at this time scale. A penalty model is used to compute the contact forces among discrete elements with:

$$\mathbf{f}^c_{ij}(t) = f(\delta)\hat{\mathbf{r}}_{ij}(t) = -k_c\delta\hat{\mathbf{r}}_{ij}(t), \tag{3.11}$$

where k_c is assumed equal to $500\,\mathrm{kN\,m^{-1}}$. This value result to be the best compromise between rigid transverse behaviour and numerical stability of the simulation.
Concerning friction coefficients for fibre-fibre and fibre-projectile contact, they have been set respectively to 0.20 and 0.18 [69].

3.3.2 Results

Fig. 3.10 reports the yarn deformed shape at 0 μs(a), 10 μs(b), 25 μs(c) and 40 μs(d).

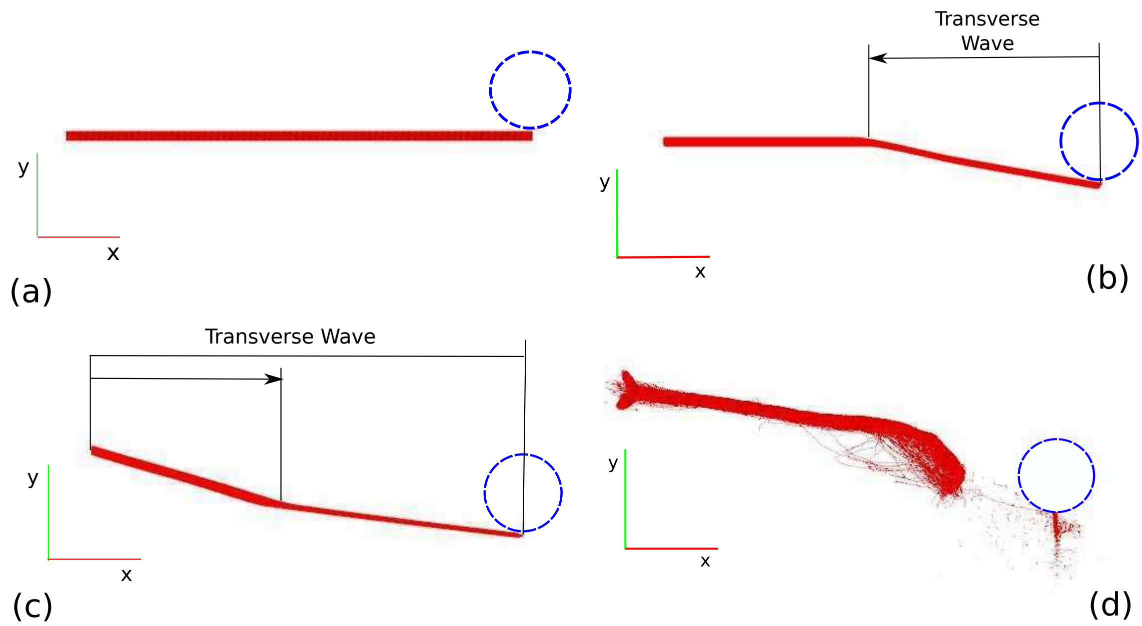

Fig. 3.10 Transverse kinematic of impacted yarn.

Classical transverse wave is clearly observed. It begins to propagate when the cylindrical bullet and yarn get into contact and moves leftwards to the clamped edge in the period between 0 µs and 20 µs. When the wave reaches the boundary conditions it is reflected and moves rightwards to the impact point, 20 µs-30 µs. Finally when it reaches the impact point the yarn fails.

The so called spreading wave is even observed.

This second wave is related to the yarn section rearrangement and is typical of the microscopic analyses [69]. When the yarn gets in contact with the projectile, the different fibres spread under the charge and the yarn section changes into a new configuration. This rearrangement of the section travels in the form of a wave in the same direction of the longitudinal wave, Fig.3.11

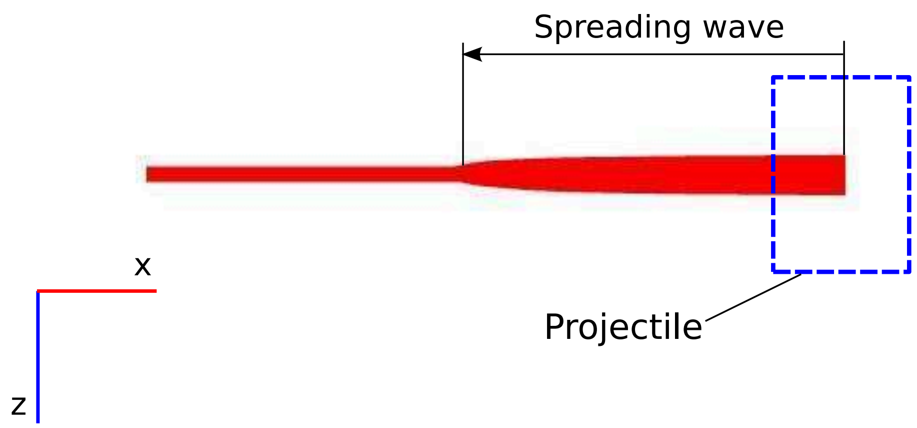

Fig. 3.11 Spreading wave propagation (10 µs).

Energetic analysis

A comparison with the 3D finite element model proposed by Nilakantan has been performed on the elastic energy Fig.3.12. The results of the two models are in good agreement up to the failure initialization. The instant in which the transverse wave is reflected is marked by a dramatic increase of the elastic energy rate. The results are slightly different in the post failure phase. A first difference deals with the shape of elastic energy release. In the current model, it is released more rapidly compared to the 3D FEM. A second difference is in the residual energy. The current model has no residual internal energy after the failure phase while the 3D FEM has a residual one. This could be explained by the lack of bending stiffness of the pin-joined model. After the failure, a large part of internal energy is converted into kinetic one and bending modes become predominant. In this situation, the current model is only able to completely convert the elastic energy in kinetic ones, without restoring it in the bending modes.

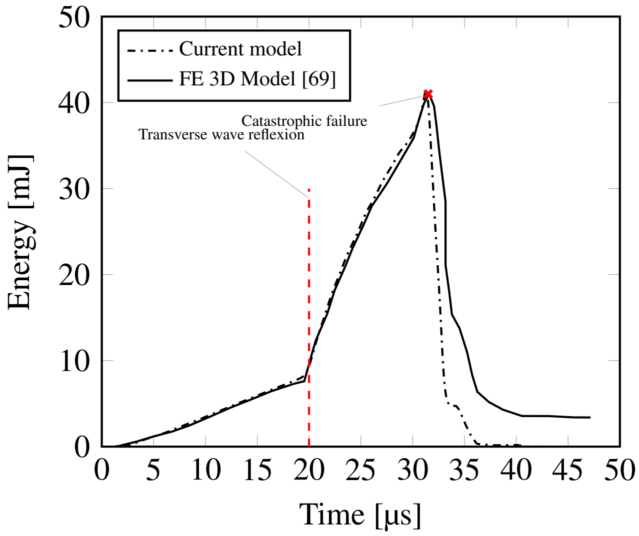

Fig. 3.12 Elastic energy comparison.

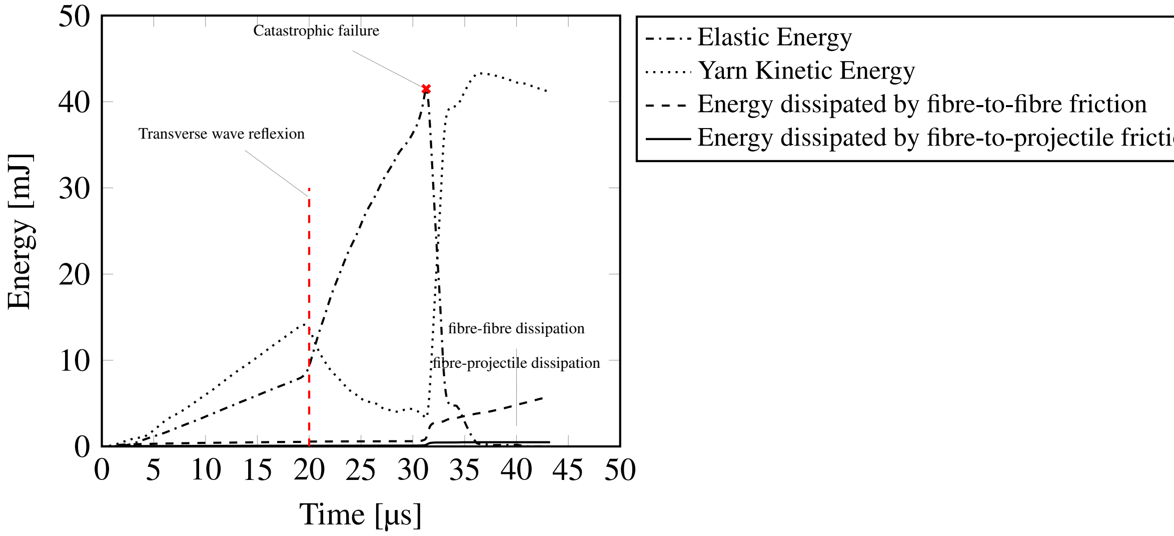

Fig. 3.13 Energy Balance for a transverse impact at $120\,\mathrm{m\,s^{-1}}$.

A complete energetic analysis has also been performed, Fig. 3.13.
Yarn kinetic energy is linearly increasing before the first transverse wave reflection, then a drastic conversion of kinetic energy into elastic energy is observed. Finally, when catastrophic fail occurs, elastic energy within the yarn is fully converted in yarn kinetic energy.

In the current work, friction dissipation has been divided in two different contributions:

- the first is given by the interaction among the projectile and the fibres and will be denoted as external;

- the second is given by the interaction among the fibres and will be denoted as internal.

As it can be seen on Fig. 3.13, friction dissipation doesn't play an important role in energy absorption during the impact while its effects are mostly confined in the post failure phase. This actually means that this form of energy absorption, which is actually related to the cross section evolution, can be neglected at this time scale and impact speed range.

Projectile residual speed

Fig. 3.14 reports the history of the projectile velocity compared to the results obtained in [69]. The curves are in very good agreement up to the failure. The relative difference on the residual velocity between the two models is around $6\,\mathrm{m\,s^{-1}}$, which is closed to 5% compared to the initial speed of $120\,\mathrm{m\,s^{-1}}$.

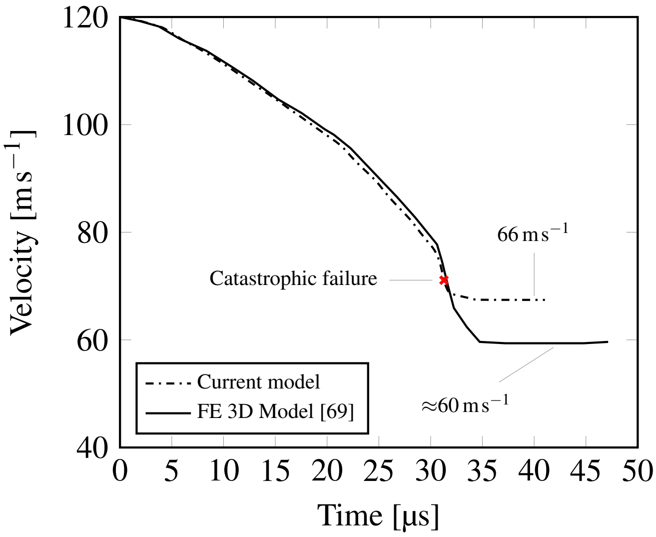

Fig. 3.14 Projectile velocity comparison for a transverse impact at $120\,\mathrm{m\,s^{-1}}$.

Sensitivity Analysis on Friction Coefficients

In order to test the stability of the model and to understand the effect of friction and yarn cross section mechanic on the transverse impact, a sensitivity analysis on friction coefficient has been performed. Three different values for fiber-to-fiber and fiber-to-projectile friction coefficients have been selected [69] for a total of nine different configurations (table 3.2).

Table 3.2 Values for the friction coefficients used for the sensitivity analysis.

fiber-projectile friction coeff.	0.0	0.18	0.36
fiber-fiber friction coeff.	0.0	0.2	0.4

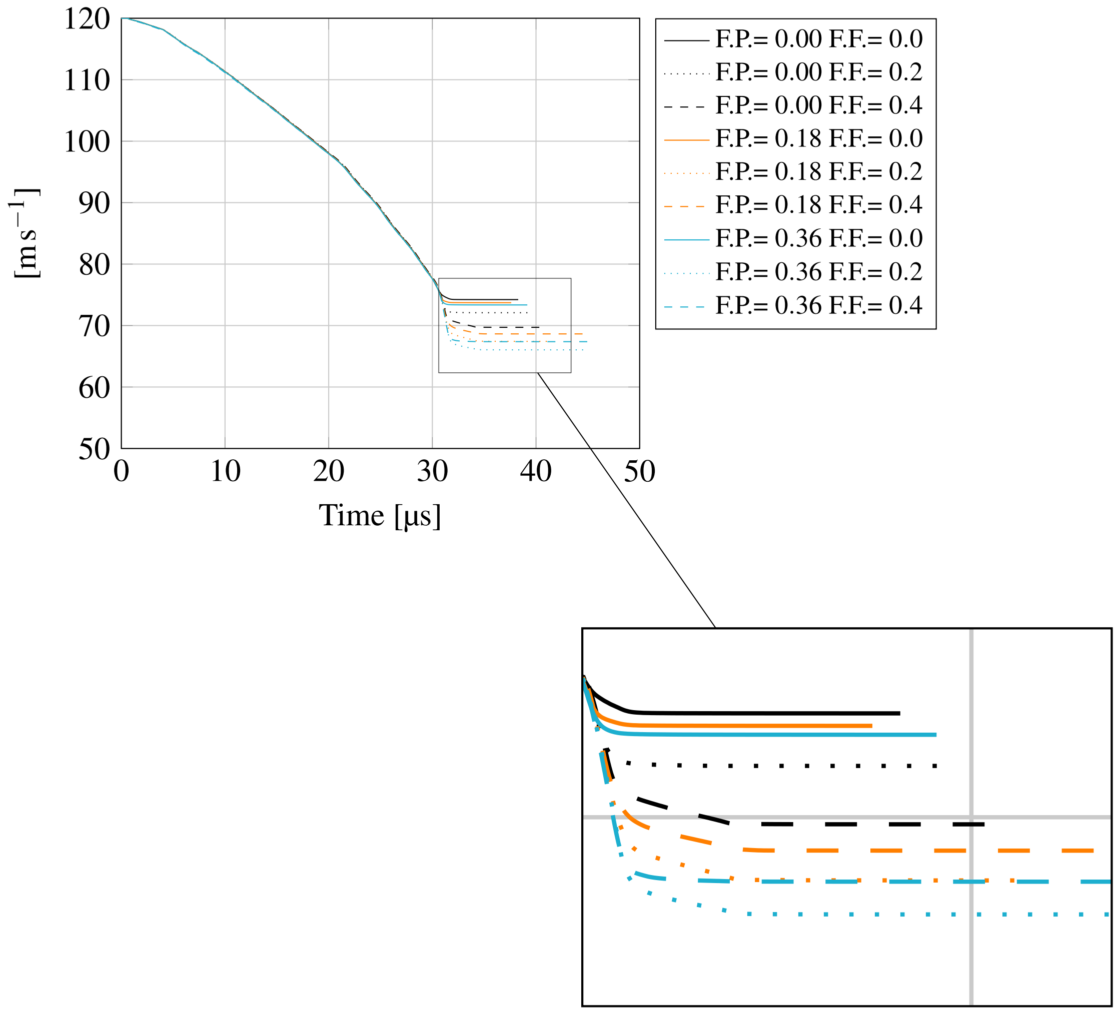

Fig. 3.15 Effects of friction on projectile velocity (*F.P.* and *F.F.* stand for Fiber-Projectile and Fibre-Fibre friction coefficients).

The projectile velocity for the nine different cases is reported in Fig. 3.15. As previously observed by the reference author [69], friction coefficients does not modify the global response of the system but they have a non linear influence on ballistic properties. In particular, fibre-to-projectile friction seems not to have an important effect on the projectile residual speed if no friction among fibres is considered, however a slight increment on fibre-to-fibre friction coefficient leads to some benefits in terms of ballistic performance. It is worth to notice that the lowest residual speed at 66 m s^{-1} has not been obtained using the highest values of both friction coefficient. This clearly shows a reciprocal interaction among these parameters on the final projectile speed and a reciprocal influence on the failure mechanisms of the structure.

In Fig.s 3.16, 3.17 and 3.18, elastic energy and friction dissipation history are reported for the analyzed cases.

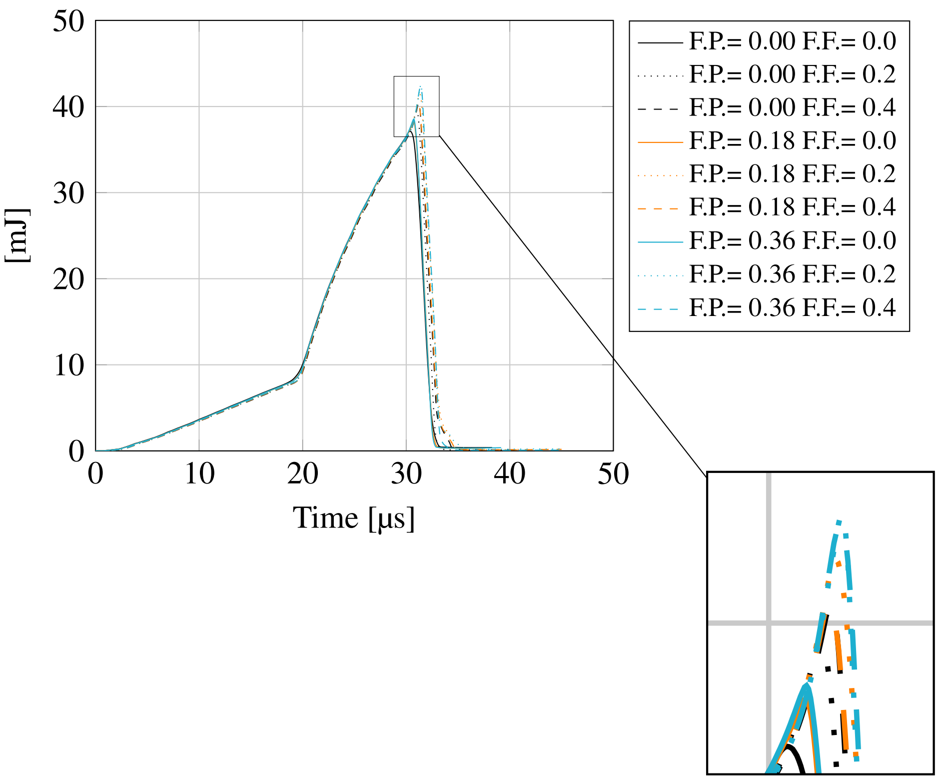

Fig. 3.16 Effect of friction on the elastic energy.

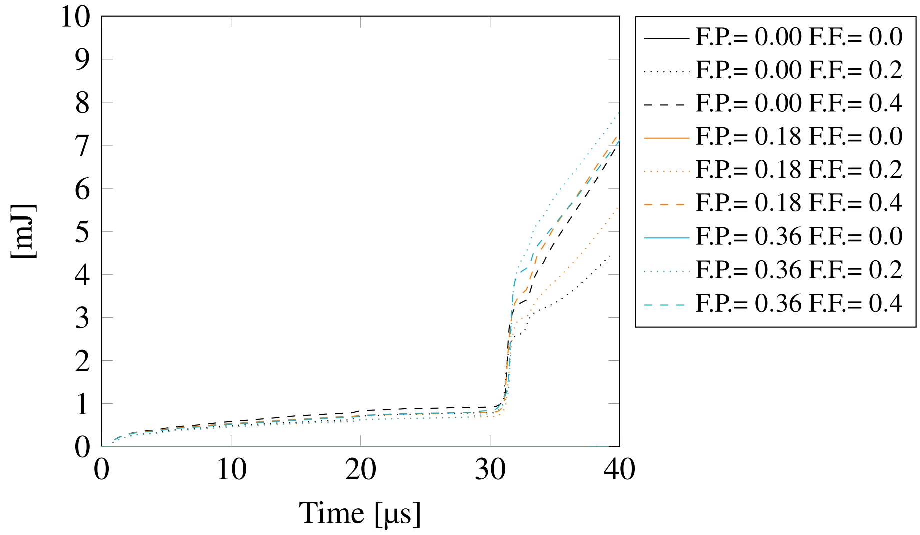

Fig. 3.17 Energy Dissipated by Fiber-Fiber friction.

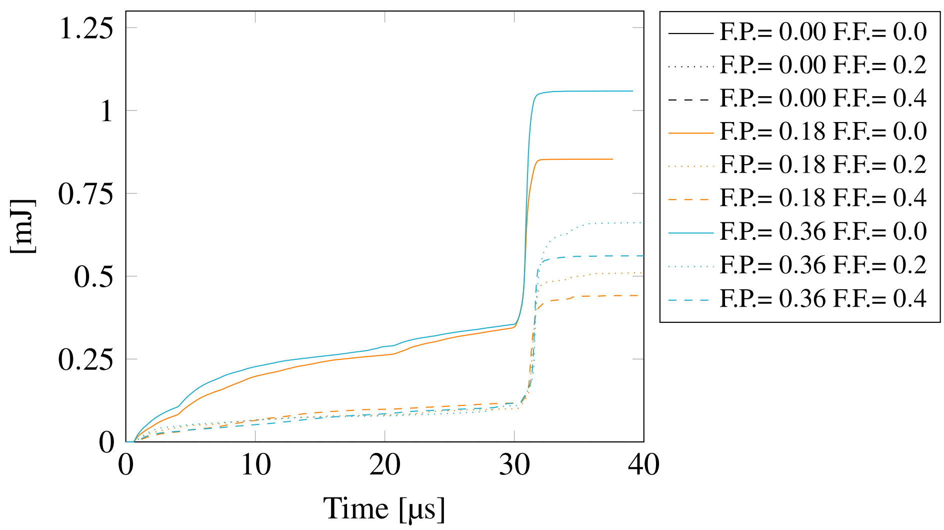

Fig. 3.18 Energy dissipated by Fibers-Projectile friction.

A first statement is that friction, i.e. cross section mechanic, mostly influence failure initialization while it doesn't alter the impact energy asorption process. This effect can be observed by the elastic energy trends, Fig.3.16, in which failure is delayed for those tests which present an higher value of global dissipation. Global friction dissipation is dominated by the fibre-fibre interactions which are one order higher than the fibre-projectile ones (Fig. 3.17 and 3.18). However, friction dissipation remains still negligible compared to the other energy forms.

3.3.3 Discussion

The obtained results show some important aspects which were partially introduced in previous studies [33, 69, 103] and here confirmed.

Firstly, when a yarn is able to withstand the first contact with a projectile a pure longitudinal model for the fibers is sufficient to accurately describe the impact energy absorption process.
The validation of the proposed model, Fig. 3.12-3.14, shows how the energetic contribution of flexural and transverse modes is negligible at this time scale. Then those complication associated to the Nilakatan 3D finite element model are superfluous for this impact scenario if not included into a failure criterion which could anticipate or postpone yarn penetration.

Secondly, here yarn cross section phenomena appears to be negligible from the energetic point of view.
The validation of the proposed model showed how different initial cross section configuration brings to very similar results in terms of energy absorption and projectile speed trends, Fig. 3.12-3.14. Moreover, the same trends resulted to be independent by the friction coefficients before yarn failure occurred, Fig. 3.16-3.15.

The real influence of yarn transverse behaviour is on yarn failure. As observed from sensitivity analysis on friction coefficient, penetration time is regulated by fiber-fiber interaction at this time scale (Fig. 3.15).

It is worth to underline that the observations performed by Nilakantan have been here validated for the first time using a different numerical approach. Then, it is possible to conclude that these observations are related to physical effects rather than numerical one. This means that a consistent mesoscopic finite element model should at least consider yarn cross section behaviour to formulate a physically based failure criterion.

3.4 Yarn transverse impact: short period response

3.4.1 Impact scenario

For the short period analysis, the configuration adopted by Sockalingam in its microscopic finite element study has been considered [104]. The cylindrical bullet diameter Φ as been reduced to 2 mm while the striking speed has been increased to 200 $\mathrm{m\,s^{-1}}$ and kept constant since no remarkable projectile decelleration is expected. Yarn cross section is considered to be elliptical with major and minor axis respectively equal to 0.5337 mm and 0.115 mm while fibers are arranged into an Hexagonal Packing Configuration (HCP) [69, 104], Fig. 3.19.

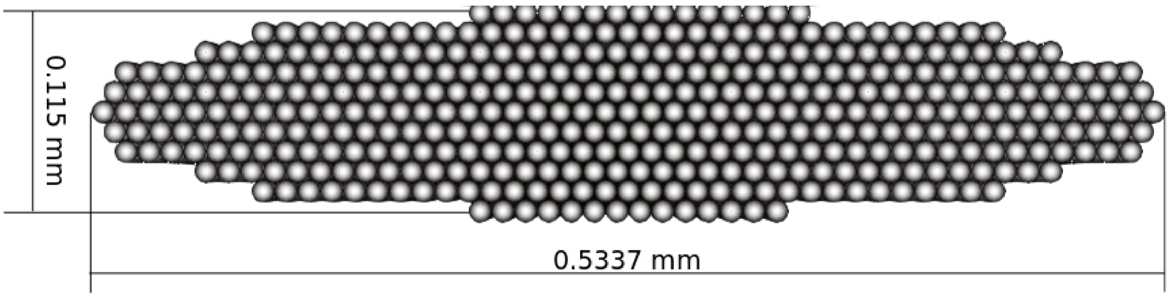

Fig. 3.19 Yarn cross section for short time scale analysis.

The reason of choosing a different yarn cross section relies in the necessity of approaching the yarn configuration scheme observed into Kevlar S706 fabric [69, 103].
Contrariwise to long term analyses, Sockalingam showed how yarn short period response resulted to be affected by parameters related to cross section behaviour [104]. In this previous work, the author showed how particular phenomena as fibers bounce and transverse compressive wave propagation affect the fibers stress state and yarn cross section evolution. For this reason a physical yarn cross section configuration have to be considered and combined with a physical criterion to manage fiber-fiber contact.

3.4.2 Physical contact modelling

The physical basis to the contact model have been provided by the implementation of Cheng results in the contact law.
The contact among two discrete elements have been modeled as the contact between two parallel cylindrical fibers of length l_0 with a constant interpenetration δ_{ij} along their axes, Fig. 3.20. Since all the fibers are composed of the same material, the same deformation is expected at the contact zone and the nominal strain occurring during contact will be given by:

$$\bar{\varepsilon} = \frac{\delta_{ij}}{2\phi}, \tag{3.12}$$

from which

$$\delta = \frac{1}{2}\delta_{ij}. \tag{3.13}$$

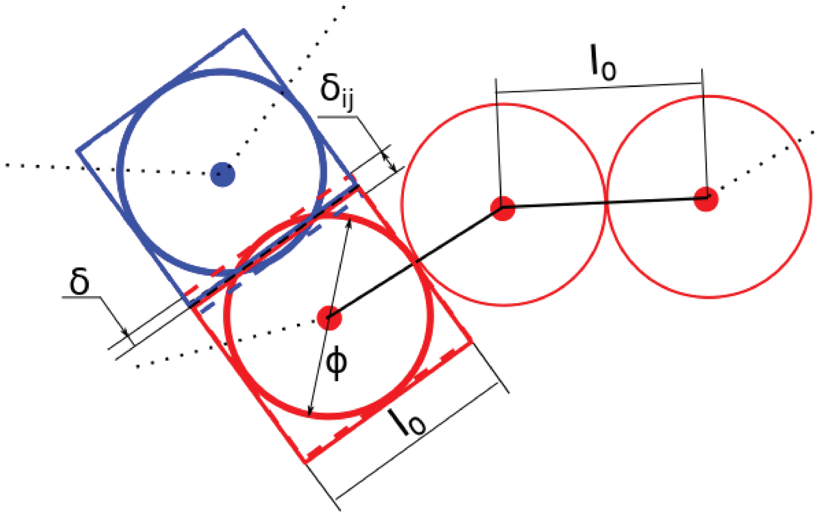

Fig. 3.20 Contact Model in short period analysis.

A non-linear elastic behaviour equivalent to the first load cycle recorded by Cheng has been considered to relate the contact force among discrete elements $\mathbf{f}^c$ with their relative interpenetration δ_{ij}. The experimental $\bar{\sigma} - \bar{\varepsilon}$ curve has been converted into its force-displacement counterpart:

$$||\mathbf{f}_{ij}^c|| = F = \bar{\sigma}\phi l_0, \tag{3.14}$$

$$\delta_{ij} = 2\delta = 2\bar{\varepsilon}\phi. \tag{3.15}$$

This curve have been finally fitted using a third grade polynomial to obtain a closed form relation among the contact force modulus and the discrete element interpenetration:

$$\mathbf{f}_{ij}^c(t) = f(\delta)\hat{\mathbf{r}}_{ij}(t) = -(a_1\delta_{ij} + a_2\delta_{ij}^2 + a_3\delta_{ij}^3)\hat{\mathbf{r}}_{ij}(t). \tag{3.16}$$

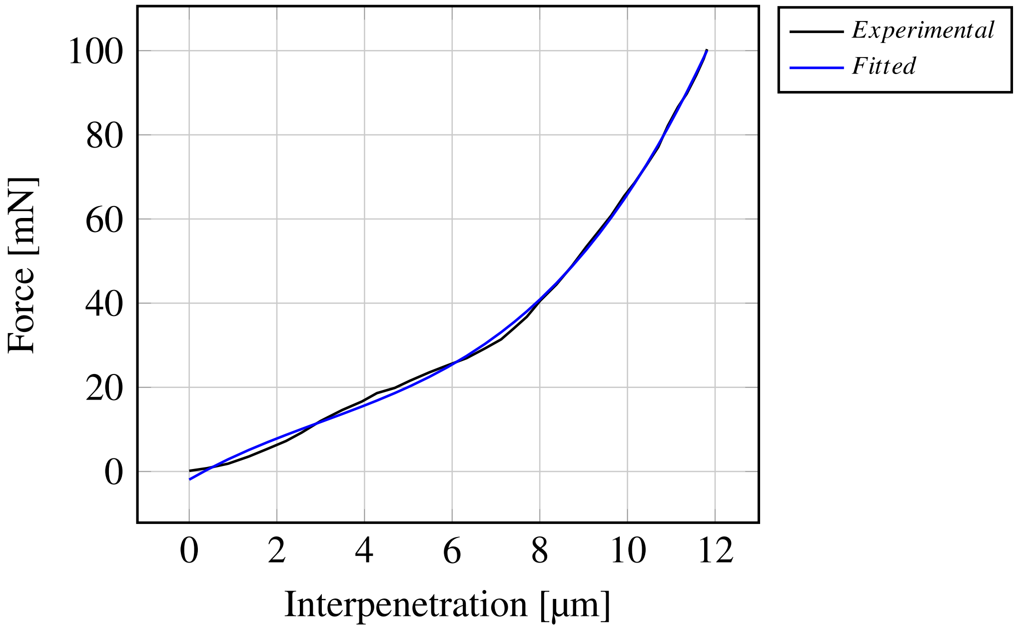

Fig. 3.21 Non-linear contact law adopted for DE interactions.

The polynomial coefficient are reported in Table 3.3 for the case of forces expressed in Newton and interpenetration expressed in meter.

Table 3.3 Non-linear contact law parameter.

a_1 [N m^{-1}]	a_2 [N m^{-1}]	a_3 [N m^{-1}]
6.013e+03	-7.218e+08	7.984e+13

The current contact model relies on different hypotheses which include a uniform contact zone along a length l_0, a purely elastic behaviour and the neglection of stiffening effects related to multiple contacts. Obviously it cannot provides the same accuracy of a 3D finite element model [99] however it dramatically reduce the computational cost and is still able to give some useful information and represents the main phenomena at this time range, as it will be shown later.

The possibility of decouple the internal energy related to the longitudinal extension of the bonds from that associate to the fiber transverse behaviour represents an post processing advantage over microscopic 3D finite element.

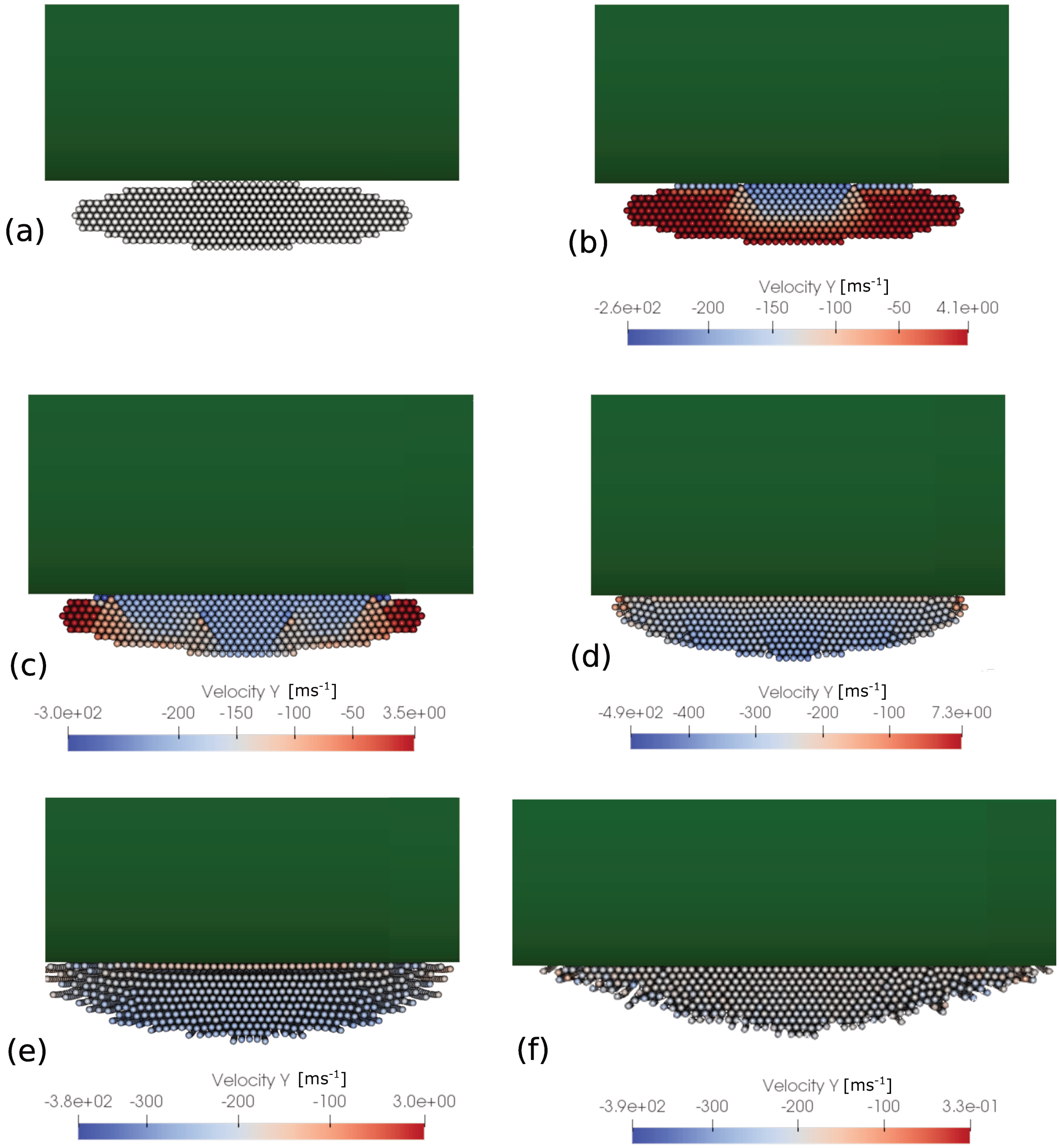

Fig. 3.22 Yarn center cross section at 0 µs (a), 0.0625 µs (b), 0.125 µs (c), 0.25 µs (d), 0.5 µs (e), 1.5 µs (f).

3.4.3 Results

Yarn kinematic and stress state

The yarn center cross section evolution during the impact is presented in Fig. 3.22. At the first time, the projectile get in contact with those fibers at the top of the yarn. These are pushed down the impact direction and, due to relative contact, their motion is transmitted to the adjacent ones. The whole phenomenon results in the propagation of a compressive wave through the yarn cross section, 0 µs - 0.125 µs. This phenomenon was firstly observed in 3D microscopic finite element model proposed by Sockalingam and here the same physic have been represented with a much simpler and computationally effective numerical approach [104]. The impact energy stored in fiber-fiber contact and the relative interpenetration among discrete elements during this impact phase are obviously dependent by the contact law assumed.
When the free boundaries of the cross section are reached by the wave front this is finally reflected, 0.25 µs. Since no mechanical resistance is offered when fibers are pulled apart from each others, those at the yarn bottom "bounce off" the yarn during compressive wave reflection [99, 108]. From this point, fibers spread under the projectile load and a rearrangement of the yarn cross section begins. It is clear from the analysis that the rearrangement propagates from the yarn bottom to the yarn top gradually. During this stage the maximum velocity reached by the single particles is around $400\,\mathrm{m\,s^{-1}}$, which is actually two times higher than the theoretical value of $200\,\mathrm{m\,s^{-1}}$ proposed by the Smith theory.
Once the a stable configuration is assumed by the yarn cross section, the particles velocity reaches the theoretical value of $200\,\mathrm{m\,s^{-1}}$, 1.5 µs.

The fibers elongation at the top and at the bottom of the yarn is reported in Fig. 3.23. When the transverse compressive wave is propagated, the longitudinal wave is initialized. Longitudinal wave front at the yarn top appears slightly further than that at the bottom. This is explained by the fact that longitudinal wave initialization in single yarn fibers appears at different time. Those at the top are immediately strained by the contact with the projectile while those at the bottom are strained just after the reflection of the transverse compressive wave. This difference in wave initialization time makes the longitudinal wave propagates longer in those fibers at the yarn top. A second aspect which is worth to underline is the difference in terms of local fibers strains between the two side of the yarn. Fibers at the bottom appear to be more stressed than those of the top. This effect can be actually related to the fibers bounce phenomenon at its first stage [104, 108]. Fibers at the yarn top mostly present the same vertical velocity, $200\,\mathrm{m\,s^{-1}}$, during the whole impact while those at the yarn

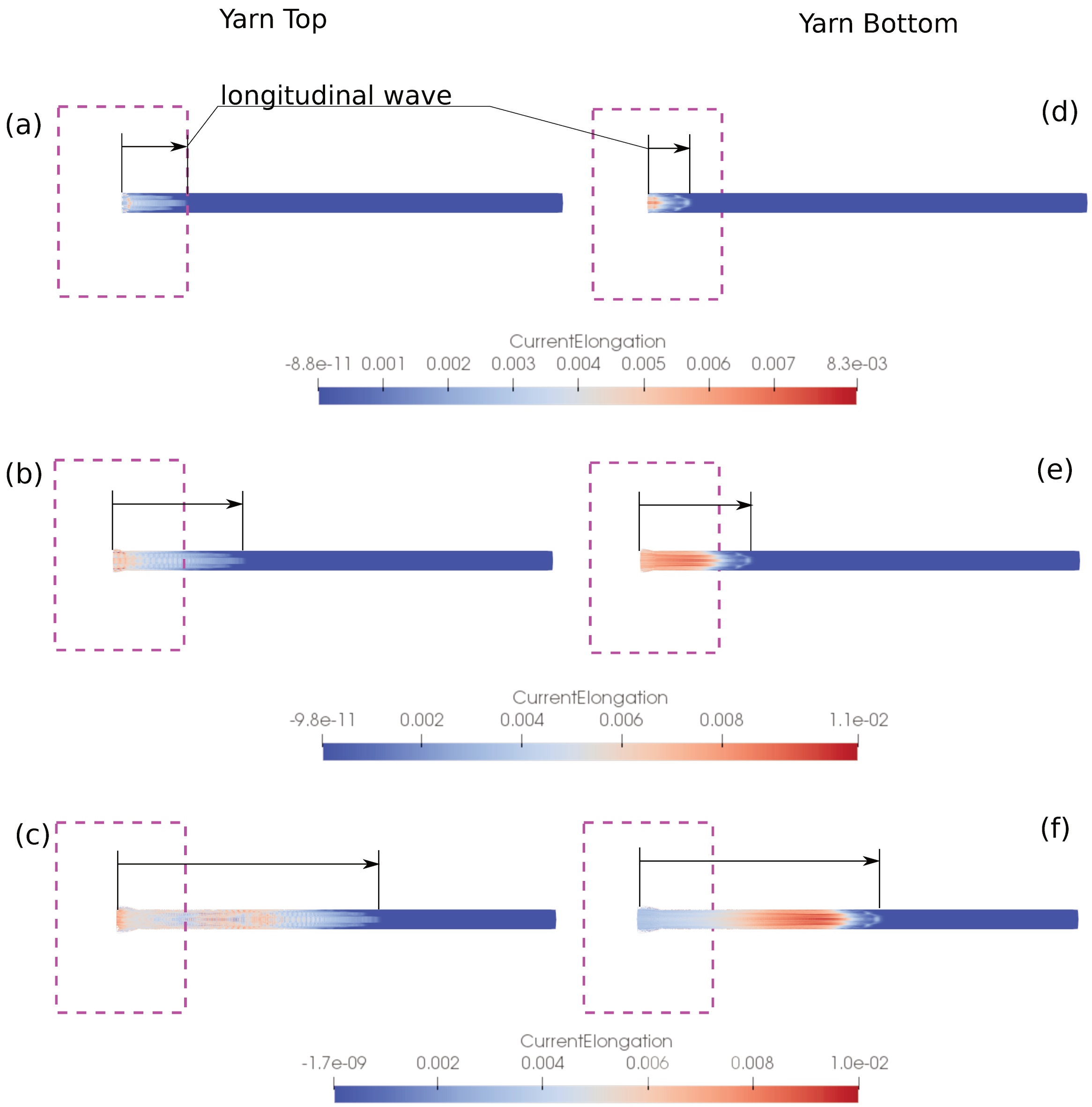

Fig. 3.23 Yarn strain state at 0.25 μs (a-d), 0.5 μs (b-e), 1 μs (c-f).

bottom reach velocities around 400 m s^{-1}. This results into an intensification of the local strains at the yarn bottom. When the fibers bounce is completed a strong intensification of the strains is recorded. Local strains at the yarn bottom reaches a maximum value around 1% while those at the top remains between 0.004% and 0.007%. Assuming the same longitudinal wave speed velocity c for the yarn and its fibers, 7.65 km s^{-1}, the strains evaluated for the same impact using the Smith theory are constant, homogeneous and equal to 0.498%. This theoretical value is reached at the yarn bottom once fibers bounce is terminated while top strains are still around 0.6% near the impact zone.

It is worth to underline how complex appears the yarn strain state after the impact, even for the simple numerical approach proposed. The differences between the single fiber model results, adopted for the validation, and the current ones put a mark on the importance of yarn discrete nature and its transverse behaviour. The longitudinal strains along the yarn are directly related the yarn cross section behaviour and so its failure mechanic.

Energetic analysis

Energetic analysis of the system is presented in Fig. 3.24.

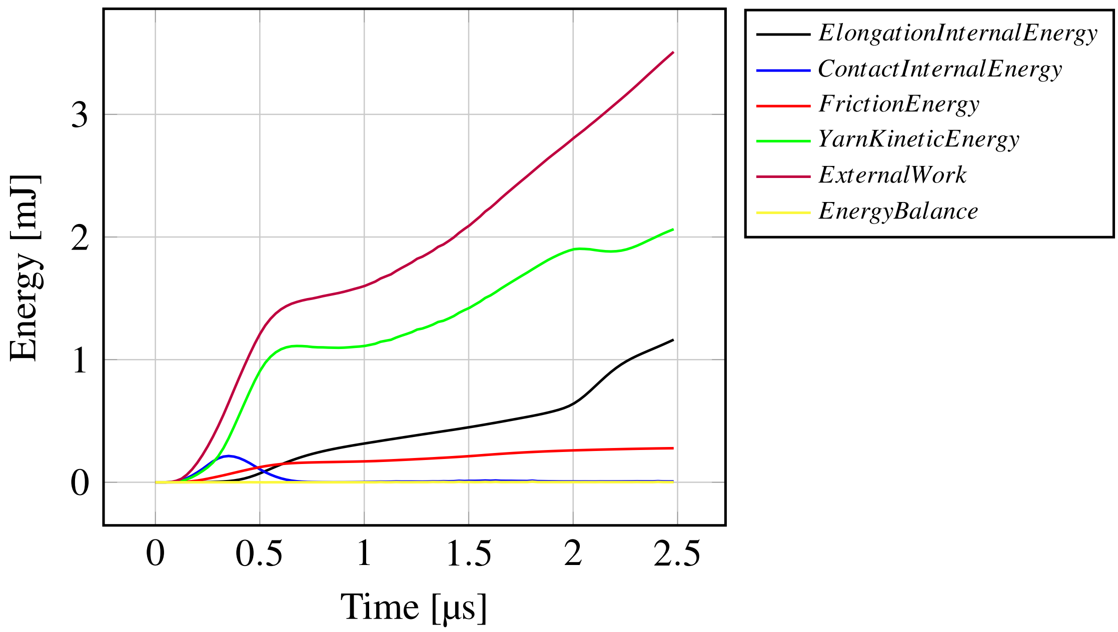

Fig. 3.24 Energetic balance of the impacted yarn in the short time scale.

Initially, an increment of yarn kinetic and internal energy associated to fiber-fiber contact is registered. This actually results from propagation of the compressive wave and fiber-to-fiber contact. At this time, internal energy associated to fiber elongation is actually far lower than the other two and its value appears to be negligible in the global energy balance.
When the compressive wave reach the boundary of the yarn cross section a second phase of the impact begins. The energy stored in fiber-to-fiber contact is released and converted into fiber kinetic energy. The bounce of the yarn fibers and the cross section reorganization put a large number of fibers under tension. This results into a non-linear increment of the internal

energy term related to fiber elongation. Moreover the large number of fibers collisions during the yarn reorganization process dissipate a considerable amount of energy by friction.
Once the yarn configuration reach its regime state, the longitudinal wave is propagated while the yarn zone under the projectile moves joint with the projectile. This results in a linearly increasing trends of elongation internal and yarn kinetic energy. Fibers are no more interpenetrated, contact energy is almost negligible and no appreciable increments of friction energy dissipation are recorded due to the yarn stable configuration.
This free propagation regime ends when the longitudinal wave is reflected.

3.4.4 Discussion

A 4-phases response

According to the previously presented results, the yarn response between impact initialization and the first reflection of the longitudinal wave , 0 µs - 2.0 µs, can be divided in four phases:

- Contact initialization, 0 µs - 0.25 µs;
- Fibers bounce, 0.25 µs - 0.7 µs;
- Cross section rearrangement, 0.7 µs - 1.0 µs;
- Regime, 1.0 µs - 2.0 µs.

During the first phase, the transverse compressive wave is propagated while few fibers are under tensions. This results in impact energy absorption due to fibers transverse deformation and kinetic energy while internal energy related to fiber elongation resulted to be negligible. During this phase the yarn cross section remains almost unvaried with a regular disposition of the fibers.
The second phase begins once the transverse compressive wave reach the yarn cross section boundaries. At this time the wave is reflected, the energy stored in fiber-fiber contact is released and the fibers on the free boundaries bounce out of the cross section. The bounce effect drastically increases their axial strains and velocity. The whole process results into a strong non linear increment in internal elongation and kinetic energy while contact energy goes to zero. This second phase is obviously characteristic of the initial configuration assumed, perfectly aligned fibers in hexagonal compact packing structure. If a more realistic structure would be considered, lower values of contact energy and bounce induced stresses are expected.
The third phase is characterized by the reorganization of the yarn cross section. Here the

yarn kinetic energy becomes stationary while the elongation internal one starts to linearly increase.
In the final phase a dynamic regime state occurs. Here spreading wave starts to propagate and a linear increment of kinetic and internal elongation energy is reached as expected from the Smith analytical solution.

Yarn cross section contribution

Some observation can be performed about the yarn cross section role at this time scale.
The first observation came from the comparison of the short and long time period energy balance (Fig. 3.24-3.13). While in long time response those energies associated to the yarn cross section behaviour appear to be negligible, in short time response they are relevant.
Yarns and fabrics instantaneous failure is actually related the phenomena occurring before the regime state. Contact initialization phase assumes a paramount importance in the definition of the yarn critical velocity and fabric inelastic failure. It defines the amount of internal energy which is stored in fibers transverse deformation and that will be finally converted in kinetic and internal energy during fiber bounce and section rearrangement phases. In the same way, high stresses induced by fibers bouncing and friction dissipation play a significant role as well. This actually emphasizes the active role of yarn cross section mechanic during the first part of an impact and the importance of their correct representation into a mesoscopic numerical model.

Another aspects which is worth to underline is the evolution of the energies associated to yarn cross section and its discrete nature, Fig. 3.25. Even for the short time response the amount of energy dissipated by interfiber friction is higher compared to the projectile-to-fibers contribution. Moreover this dissipation mechanism is totally internal and contradict the classical hypothesis of a purely elastic yarn material model adopted in mesoscopic analyses.

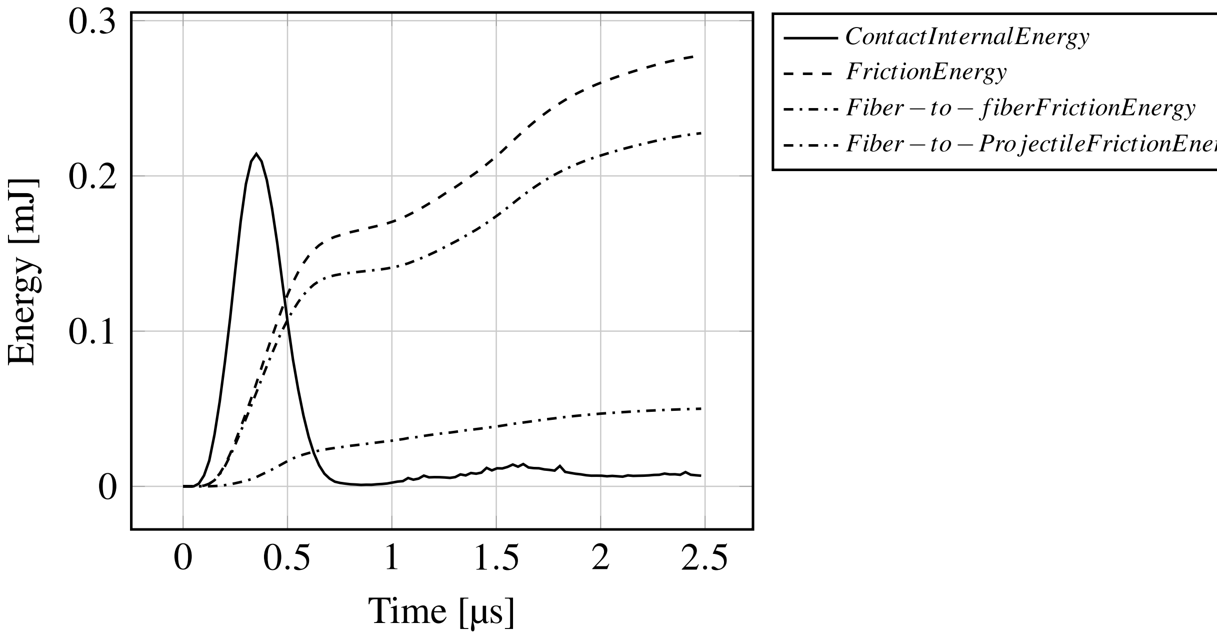

Fig. 3.25 Energies related to yarn cross section evolution.

Yarn critical velocity

The critical impact velocity was introduced by Smith as the lowest impact speed for the which filament fails according to his analytical theory [96]. This particular concept is intrinsically related to the original analytical solution and its fundamental hypotheses.
According to Smith works, the strain state induced by an impact is homogeneous and constant in all those points in the wake of the longitudinal wave front. When the system is under these hypotheses it is intuitive to evaluate the critical velocity and relate it to the ballistic performance of the material. Unfortunately the real impact scenario over a flexible filament is much more complex and when a multitude of fibers are considered the complexity even increases.
As demonstrated in the current and other works [104], the strain state induced in a yarn by an impact is not homogeneous and this brings to a progressive failure of the system [8, 55, 104]. This could be sufficient to revisit the concept of yarn "critical" velocity.
According to the presented results, it is clear that yarns pass through a transitory step before reaching the free propagation conditions. The strains recorded during this period are much higher than those reached at the regime state and could induce partial or total yarn failure. This transitory step is not predicted by the Smith theory as shown in Fig. 3.26, where the yarn energy history provided by the analytical and proposed numerical model are compared. Here, the analytically evaluated energy is that of 400 fibers individually modeled under the

same boundary conditions assumed for the yarn.
The first remarkable difference appears at the contact initialization phase. Here the elongation internal energy predicted by the numerical model is lower than its analytical counterpart. While in the numerical study fibers get in tension after the propagation of the transverse compressive wave, they are immediately stressed in the analytical one. This brings to a longitudinal wave initialisation delay which is evident from the wave reflection time.
A second important difference is found in the fibers bounce phase. Here the fiber bounce predicted by the numerical model results into a strong increment of kinetic energy and high local strains which are not found into the analytical counterpart. All these differences are explained by the hypotheses at the base of the Smith theory. The continuous body, purely longitudinal behaviour assumptions combined with the constant velocity imposed as boundary condition brings to a simplification of the yarn response. This can be acceptable when the time scale assumed for the phenomenon is long enough to make the effect of the yarn cross section mechanic negligible [22, 56, 96, 105], but it is not when a phenomenon occurs in the first phase of the impact. This is actually the case of the critical velocity, where yarn failure appears before the propagation of the longitudinal wave.

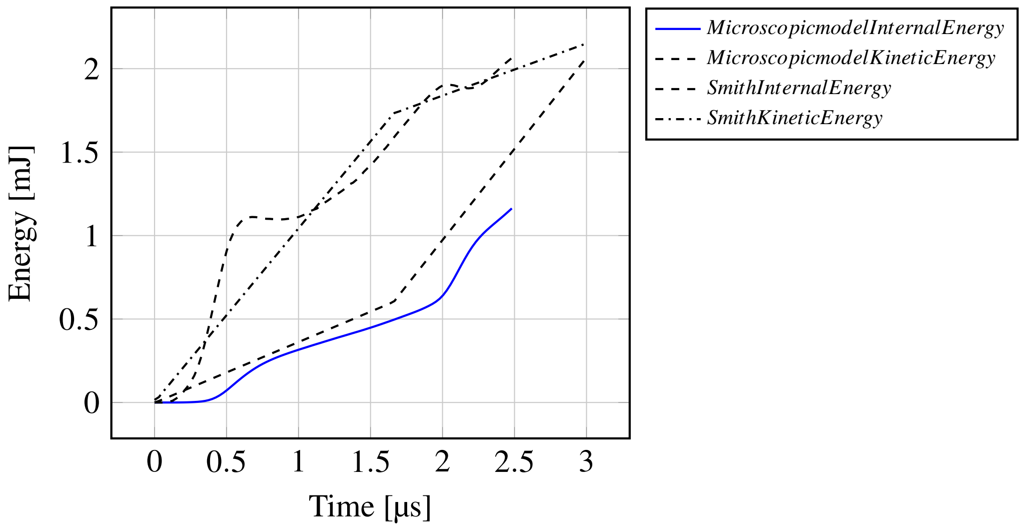

Fig. 3.26 Comparison among energies obtained from numerical and analytical approach.

A novel definition of the yarn critical velocity should include this concept of transition and take into account the partial failure of the yarn. In any case the classical definition by Smith remains a valid tools to evaluate the ballistic performance of a material but should be considered as an indicator more than an absolute value.

3.5 Conclusions

In the present chapter two different microscopic numerical analyses and a novel numerical approach have been presented.
In order to reduce the computational costs, a numerical approach based on the Discrete Element method for yarn and fabric microscopic analyses have been introduced. Here the fibers interaction and inertial properties are treated according to the Discrete element method while their longitudinal behaviour is modeled by springs which connect the different particles. The proposed numerical approach has been validate at the fiber scale using the Smith theory and at the yarn level using preexistent numerical results.
Two different numerical simulations of a Kevlar KM2 600 transversely impacted yarn have been performed using the presented numerical approach. The goal of the investigation was to exploit the role of the yarn cross section mechanic during an impact and how it effects the yarn ballistic behaviour.
The first simulation was focused on the investigation of the phenomena which occurs once the longitudinal and tranverse wave have been propagated. Here a pure longitudinal model was sufficient to accurately describe the impact energy absorption process while failure initialization depends on yarn cross section mechanic. The effect of yarn transverse section mechanic was even observed from the kinematic point of view with the propagation of the spreading wave.
The second simulation was oriented to the investigation and comprehension of those phenomena which take place when the contact among the projectile and the yarn is initialized. In this case yarn cross section plays an active role in both energies trend, yarn strain state and kinematic.
Four different phases have been identified during this impact. Yarn cross section effects are evident during the first, second and third one where high strain values are induced by yarn fibers bounce. According to these microscopic observation, the concept of critical velocity introduced by Smith should be revisited nor used as a predictive tool.
For the previous mentioned reasons, the inclusion of yarn transverse mechanical behaviour into a yarn mesoscopic model appears to be mandatory. It will leads to a correct representation of the impact phenomenon at both the time scales and physical formulation of the yarn failure.

Chapter 4

Mesoscale hyperelastic model of a single yarn under high velocity transverse impact

4.1 Introduction

In the previous chapter a yarn microscopic model has been adopted to evaluate those phenomena related to cross section mechanic which can influence the ballistic properties of a fabric. Results showed how the cross section mechanic influence the yarn response under impact, especially in the first phase of the contact. This justify the effort required to include this behaviour into a yarn mesoscopic model.
In this third chapter the modellisation of a single yarn as an homogeneous continuous body will be treated. Firstly, the universally adopted linear elastic constitutive model will be presented and discussed, with its different advantages and drawbacks. Secondly, a novel hyperelastic constitutive model for yarn structures is presented.
A preliminary theoretical introduction to the model is followed by the identification of the free energy parameters. This has been performed thanks to a novel multiscale strategy in which numerical and analytical solutions are combined to relate fiber level properties to those of the yarn.

The discussion continues with the application and validation of the hyperelastic constitutive model to the study of the transverse impact on a single yarn.
Results are compared with those obtained using the linear elastic approach and fiber-level models. The possibility of capture the yarn transverse kinematic, decouple the different

modes of energy absorption and other advantages over the traditional linear elastic model are remarked. Moreover, a novel physical based multiaxial failure approach is proposed.

4.2 State of the art in yarn mesoscopic modelling

Gasser et al.[43] shown that an orthotropic elastic continuum has yarn behavior if its Poisson's ratios are zero and its shear and transverse elastic moduli are very small compared to the longitudinal elastic one. This constitutive model is written:

$$\sigma^J = \mathbf{C} : \mathbf{D}, \tag{4.1}$$

with

$$\mathbf{C} = \begin{bmatrix} C_{11} & 0 & 0 & 0 & 0 & 0 \\ 0 & C_{22} & 0 & 0 & 0 & 0 \\ 0 & 0 & C_{33} & 0 & 0 & 0 \\ 0 & 0 & 0 & C_{44} & 0 & 0 \\ 0 & 0 & 0 & 0 & C_{55} & 0 \\ 0 & 0 & 0 & 0 & 0 & C_{66} \end{bmatrix}$$

$$where \quad C_{11} = E_{11}, \quad C_{22} = C_{33} = E_{22} << E_{11}, \quad C_{44} = C_{55} = C_{66} << E_{11}.$$

Where σ^J is the objective Jaumman derivative of the Cauchy stress, **C** the Hook tensor and **D** the strain rate.

The direction "1" is identified as the yarn longitudinal axis along fibers are oriented, while the directions 2 and 3 are the transverse ones, Fig. 4.1.

This way of modelling was firstly adopted in impact application by Duan to study the energy absorption process and the effect of yarn to yarn friction on the ballistic limit [39, 40]. After this first work, the material law remained substantially unvaried while applied by other authors to different type of meshes and elements[21, 49, 75].

The key aspect which made the linear elastic orthotropic model a standard is the correct representation of the yarn longitudinal behaviour [21, 40].

The downside of this approach relies in the transverse yarn behaviour which is not physically treated while numerically adjusted. This have two important consequences:

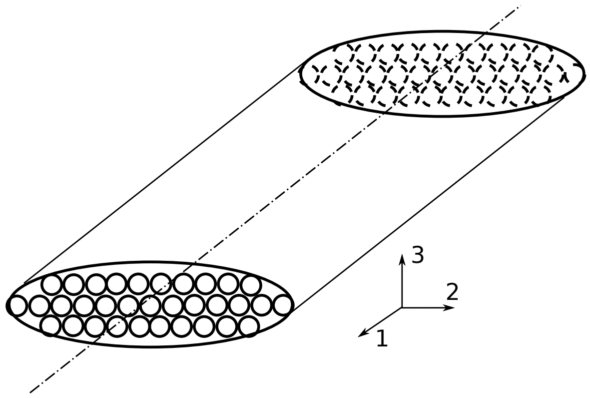

Fig. 4.1 Yarn as an orthotropic body.

- Firstly, the transverse kinematic of the yarn observed using microscopic simulation is not respected [69, 103, 110].
  Since zero Poisson's ratios are assumed, it is not possible for this material to compensate a transverse compression with an expansion in the directions orthogonal to the load [71]. Then, phenomena which could have a certain influence in fabric energy dissipation mechanisms, as yarn section rearrangement or spreading wave, cannot be observed.

- Secondly, the uniaxial nature of the constitutive model and the lack of a physical identification strategy for the off axis elastic parameters do not confer any physical meaning to those quantities measured out of the yarn axis. As an example, those principal stresses which are not related to the longitudinal direction cannot be used to formulate three-dimensional failure criteria due to their non-physical nature. This is in contrast with previous microscopic results which underline the importance of the yarn cross section mechanic for the correct modellisation of the yarn failure .

In order to overcome the limit of the linear elastic model, the approach proposed by Charmetant [14] will be adopted to build an hyperelastic model for yarn structure. The advantage of the proposed model can be resumed as follow:

- The hyperelastic formulation is naturally adapted to the treatment of the large deformation observed in yarn cross section during the impact;

- The identification of the material parameters for the hyperelastic approach can be performed in terms of energy. This approach appears to be more convenient compared to those based on the stress-strain relation. The concept of stress and strains are complex to define for a discrete medium and an energetic approach appears to be more physical.

An introduction to the theory of hyperelasticity for transversely isotropic solids will be presented at first. The theoretical aspects discussed are the essential basis of the following discussions, then it is worth to treat them briefly before moving to the applications.

4.3 Theory

4.3.1 General notions of transverse isotropic hyperelasticity

The total mechanical energy per unitary volume of a body is a composed by the kinetic energy K and the potential energy W. The value assumed by W is a measure of the energy stored in the material as a result of a deformation process and it is even referred as strain energy density. For an hyperelastic material, the relation between the second Piola-Kirchoff stress tensor $\mathbf{S}$ and the right Cauchy-Green tensor $\mathbf{C}$ is defined by the form of the strain energy W. It is assumed that the strain energy is a scalar-valued tensor function of the only deformation state and that the stress tensor $\mathbf{S}$ is directly given by the differentiation of W by $\mathbf{C}$:

$$\mathbf{S} = 2\frac{\delta W(\mathbf{C})}{\delta \mathbf{C}}. \tag{4.2}$$

In order to be physical, a strain energy function have to respect some specific conditions [Holzapfel].
Among them, the fact that a material microstructure could be unaltered in observation under a certain type of orthogonal transformations should be taken into account by the form of W. This means that the energy stored in a materials after a generic deformation have to be unvaried if, before imposing the deformation, the material is rotated in a way to present the same initial microstructure orientation.
Some materials, as rubber or glass, present the same observed microstructure whatever they are oriented, while others ,as wood or composite laminates, show some preferential directions in the space. The first group is called isotropic, while the second is called anisotropic.

This condition on W is mathematically traduced as follow:

$$W(\mathbf{C}) = W(\mathbf{Q}^T\mathbf{C}\mathbf{Q})\forall\mathbf{Q} \in G. \tag{4.3}$$

Where G is the symmetry group of the material.
For isotropic materials the symmetry group G is the group of isometries in R_3, while for

anisotropic material it is a subset of this one.

An alternative form of this relation can be obtained applying the Principle of Isotropy of Space and Representation Theorem [115].
According to the Principle of Isotropy of Space, the anisotropic function $W(\mathbf{C})$ can be written as an isotropic function $\tilde{W}$ of $\mathbf{C}$ and structural tensors $\mathbf{A}_1, \mathbf{A}_2, ..., \mathbf{A}_n$ as additional agencies:

$$W(\mathbf{C}) = \bar{W}(\mathbf{C}, \mathbf{A}_1, \mathbf{A}_2, ..., \mathbf{A}_n). \tag{4.4}$$

The number and type of structural tensors depends on the form of anisotropy.
At this point the Representation Theorem can be applied.
This assures that the isotropic tensor function $\tilde{W}$ can be written as an isotropic scalar function $\breve{W}$ of different invariants $I_1, I_2, ..., I_n$ of $\mathbf{C}$ and $\mathbf{A}_1, \mathbf{A}_2, ..., \mathbf{A}_n$:

$$\bar{W}(\mathbf{C}, \mathbf{A}_1, \mathbf{A}_2, ..., \mathbf{A}_n) = \breve{W}(I_1, I_2, ..., I_n). \tag{4.5}$$

Thanks to the combination of these, it is possible to write an anisotropic scalar-valued tensor function as an isotropic scalar-valued function of some specific invariants $I_1, I_2, ..., I_n$.

Since yarn microstructure is composed by a large number of slightly twisted fibers all oriented in a preferential direction, a transverse isotropic constitutive behaviour will be assumed.
For this particular case the function $\breve{W}$ depends on five invariants.

$$\begin{aligned}
W(\mathbf{C}) = \quad & \breve{W}(I_1, I_2, I_3, I_4, I_5), \\
\\
with: \\
\\
I_1 &= trc(\mathbf{C}), \\
I_2 &= \frac{1}{2}(trc(\mathbf{C})^2 - trc(\mathbf{C}^2)), \\
I_3 &= det(\mathbf{C}), \\
I_4 &= \mathbf{C} : \mathbf{M}, \\
I_5 &= \mathbf{C}^2 : \mathbf{M}.
\end{aligned}$$

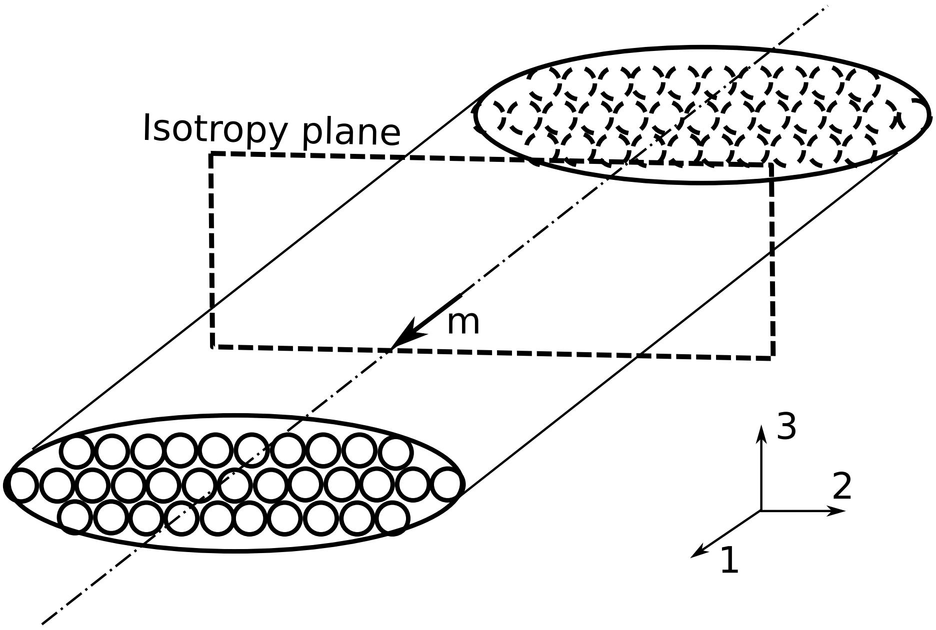

Fig. 4.2 Yarn as an transverse isotropic medium.

The tensor $\mathbf{M} = \mathbf{m} \otimes \mathbf{m}$ is the structural tensor associated to the transverse isotropy symmetry group. The unitary vector $\mathbf{m}$ specifies the fiber orientation in the initial configuration and is orthogonal to the isotropy plane, Fig. 4.2.
The transversely isotropic behaviour of the material is automatically respected if a function of these five invariants is used for the constitutive law. Finally the strain tensor $\mathbf{S}$ assumes the following form:

$$\mathbf{S} = 2\frac{\delta W(\mathbf{C})}{\delta \mathbf{C}} = 2(\frac{\delta \breve{W}}{\delta I_1}\frac{\delta I_1}{\delta \mathbf{C}} + \frac{\delta \breve{W}}{\delta I_2}\frac{\delta I_2}{\delta \mathbf{C}} + \frac{\delta \breve{W}}{\delta I_3}\frac{\delta I_3}{\delta \mathbf{C}} + \frac{\delta \breve{W}}{\delta I_4}\frac{\delta I_4}{\delta \mathbf{C}} + \frac{\delta \breve{W}}{\delta I_5}\frac{\delta I_5}{\delta \mathbf{C}}). \tag{4.6}$$

4.3.2 The notion of physical invariants

The problem of formulating an hyperelastic constitutive law for yarn structure has been reduced to the formulation of a scalar-valued function, named strain energy, of a set of five scalar mathematical invariants. The advantage of using the mathematical invariants for the formulation of the strain energy function relies in the fact that the desired form of anisotropy is automatically obtained. On the other side, this type of entities have no direct physical counterpart for the material and are difficult to relate with results of experimental tests.
An alternative set of invariants for hyperelastic transverserly isotropic material was recently proposed by Charmetant [14].
Following the previous work of Criscione et al.[12], the deformation gradient $\mathbf{F}$ in each point

of an transverse isotropic deformed body can be written into a particular orthonormal basis $B = \{\mathbf{m}, \mathbf{n}_1, \mathbf{n}_2\}$ where it assumes the following form:

$$\mathbf{F} = \begin{bmatrix} f_m & f_{m1} & f_{m2} \\ 0 & f_{11} & 0 \\ 0 & 0 & f_{22} \end{bmatrix}. \tag{4.7}$$

With the tensor in this form, the following multiplicative decomposition can be applied:

$$\mathbf{F} = \mathbf{F}_{el} \cdot \mathbf{F}_{tc} \cdot \mathbf{F}_{td} \cdot \mathbf{F}_{ld}, \tag{4.8}$$

$$\mathbf{F}_{el} = \begin{bmatrix} f_m & 0 & 0 \\ 0 & 1 & 0 \\ 0 & 0 & 1 \end{bmatrix}, \qquad \mathbf{F}_{tc} = \begin{bmatrix} 1 & 0 & 0 \\ 0 & \sqrt{f_{11} f_{22}} & 0 \\ 0 & 0 & \sqrt{f_{11} f_{22}} \end{bmatrix},$$

$$\mathbf{F}_{td} = \begin{bmatrix} 1 & 0 & 0 \\ 0 & \sqrt{\frac{f_{11}}{f_{22}}} & 0 \\ 0 & 0 & \sqrt{\frac{f_{22}}{f_{11}}} \end{bmatrix}, \qquad \mathbf{F}_{ld} = \begin{bmatrix} 1 & \frac{f_{m1}}{f_m} & \frac{f_{m2}}{f_m} \\ 0 & 1 & 0 \\ 0 & 0 & 1 \end{bmatrix}.$$

The important point about this representation relies in the physical meaning behind the decomposition. The global deformation is seen as a combination of four elementary deformation modes namely represented by the four tensorial terms $\mathbf{F}_{el}, \mathbf{F}_{tc}, \mathbf{F}_{td}, \mathbf{F}_{ld}$, Fig. 4.3. More specifically:

- $\mathbf{F}_{el}$ represents an elongation along the fibre direction;
- $\mathbf{F}_{tc}$ represents a transverse section variation in terms of area, i.e. fiber crushing and section rearrangement;
- $\mathbf{F}_{td}$ represents a transverse section variation in terms of shape, i.e. fiber crushing and section rearrangement;
- $\mathbf{F}_{ld}$ represents a shear deformation along the fibres direction, i.e. fiber-fiber slippage.

Each tensor of the decomposition, then each deformation mode, is represented by a single scalar with the only exception of longitudinal shear which are characterized by two:

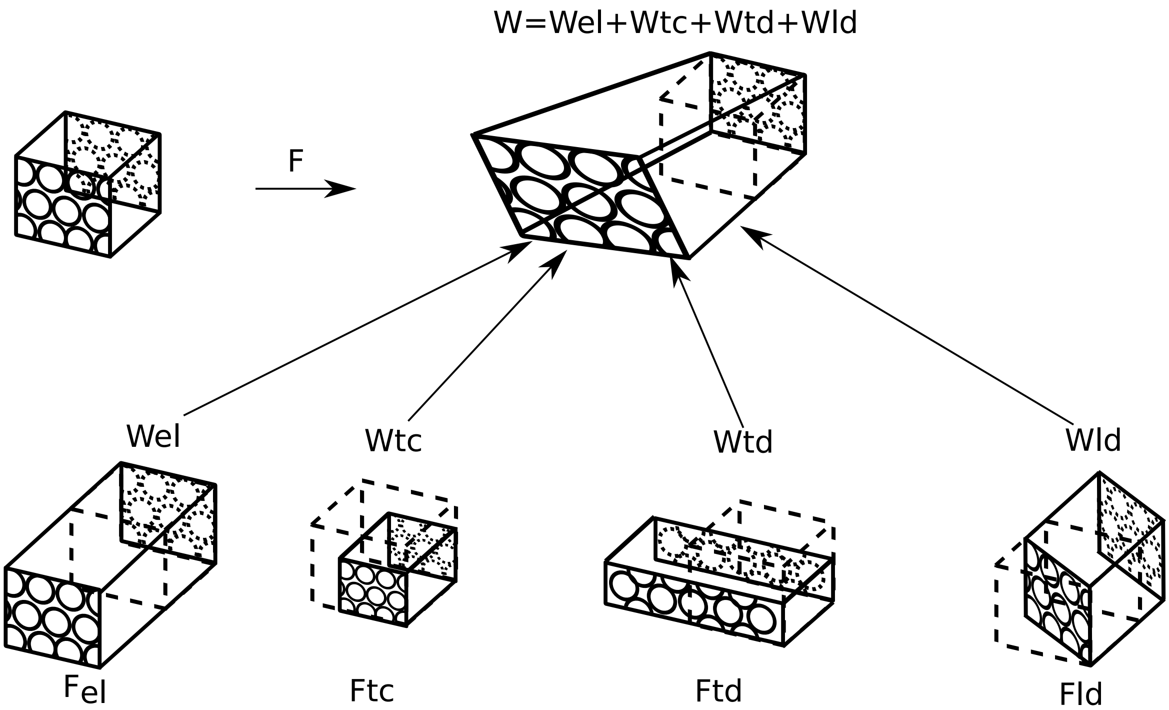

Fig. 4.3 Multiplicative decomposition and Elementary deformation modes

$$\mathbf{F}_{el} = \begin{bmatrix} \alpha_{el} & 0 & 0 \\ 0 & 1 & 0 \\ 0 & 0 & 1 \end{bmatrix}, \quad \mathbf{F}_{tc} = \begin{bmatrix} 1 & 0 & 0 \\ 0 & \alpha_{tc} & 0 \\ 0 & 0 & \alpha_{tc} \end{bmatrix},$$

$$\mathbf{F}_{td} = \begin{bmatrix} 1 & 0 & 0 \\ 0 & \alpha_{td} & 0 \\ 0 & 0 & \frac{1}{\alpha_{td}} \end{bmatrix}, \quad \mathbf{F}_{ld} = \begin{bmatrix} 1 & \alpha_{ld}\alpha_{el}\cos\gamma & \alpha_{ld}\alpha_{el}\sin\gamma \\ 0 & 1 & 0 \\ 0 & 0 & 1 \end{bmatrix}.$$

$$\alpha_{el} = f_m, \quad \alpha_{tc} = \sqrt{f_{11}f_{22}}, \quad \alpha_{td} = \sqrt{\frac{f_{11}}{f_{22}}}, \quad \alpha_{ld} = \sqrt{\frac{f_{m1}^2 + f_{m2}^2}{f_m}}, \quad \tan\gamma = f_{m1}/f_{m2}.$$

The idea at this point is to build a strain energy function taking advantage of these decomposition.

Firstly the longitudinal elongation and longitudinal shear are considered to be uncoupled, in this way α_{ld} is assumed to be fully representative of the longitudinal shear mode. Then a normalization is applied to the scalars in order to make them all zeros in rigid body motions:

$$I_{el} = ln(\alpha_{el}), \quad I_{tc} = ln(\alpha_{tc}), \quad I_{td} = ln(\alpha_{td}), \quad I_{ld} = \alpha_{ld}.$$

These new parameters are usually called physical invariants [12, 14].
Their values are a quantitative description of the contribution of a singular mode to the global deformation of the material and can be directly related to the mathematical invariants with some algebra.

$$I_{el} = \frac{1}{2}ln(I_4), \quad I_{tc} = \frac{1}{4}ln(\frac{I_3}{I_4}), \quad I_{td} = \frac{1}{2}ln(\frac{I_1I_4 - I_5}{2\sqrt{I_3I_4}} + \sqrt{(\frac{I_1I_4 - I_5}{2\sqrt{I_3I_4}})^2 - 1}), \quad I_{ld} = \sqrt{\frac{I_5}{I_4^2} - 1}. \tag{4.9}$$

Finally the global strain energy function is assumed as a linear combination of singular strain energy functions individually associated to each deformation mode:

$$W = W_{el}(I_{el}(I_4)) + W_{tc}(I_{tc}(I_3,I_4)) + W_{td}(I_{td}(I_1,I_3,I_4,I_5)) + W_{ld}(I_{ld}(I_4,I_5)). \tag{4.10}$$

From the physical point of view the strain energy stored within the material is assumed to be a composition of that stored by fiber elongation, W_{el}, by transverse deformation,$W_{tc} + W_{td}$, and by fiber-fiber slipping, W_{ld}.
Finally, the resultant second Piola-Kirchoff stress tensor can be written as:

$$\mathbf{S} = \mathbf{S}_{el} + \mathbf{S}_{tc} + \mathbf{S}_{td} + \mathbf{S}_{ld},$$

$$\begin{aligned}
\mathbf{S}_{el} &= 2\frac{\delta W_{el}}{\delta I_{el}}\frac{\delta I_{el}}{\delta C}, \\
\mathbf{S}_{tc} &= 2\frac{\delta W_{tc}}{\delta I_{tc}}\frac{\delta I_{tc}}{\delta C}, \\
\mathbf{S}_{td} &= 2\frac{\delta W_{td}}{\delta I_{td}}\frac{\delta I_{td}}{\delta C}, \\
\mathbf{S}_{ld} &= 2\frac{\delta W_{ld}}{\delta I_{ld}}\frac{\delta I_{ld}}{\delta C}.
\end{aligned}$$

Where $\mathbf{S}_{el}, \mathbf{S}_{tc}, \mathbf{S}_{td}, \mathbf{S}_{ld}$ are the contribution of the different elementary energies.

4.4 The material model

In the previous section the problem of formulating a strain energy density function for a transversely isotropic hyperelastic material has been reduced to the formulation of four strain energies individually associated to four different deformation modes. In the first part of this section, the mathematical form of these functions will be presented with their relative contribution to the stress tensor $\mathbf{S}$.
The second part will be focused on failure modellisation for this type of materials where a novel approach will be presented.

4.4.1 Strain energy function

Longitudinal elongation

According to the results of the linear elastic mesoscopic model, a linear relation among stress and strain is sufficient to accurately describe the yarn longitudinal behaviour under uniaxial tension. This linear relation results in a quadratic form of the energy for this type of load:

$$W = \frac{1}{2} E \varepsilon^2. \tag{4.11}$$

where E is the yarn longitudinal modulus and ε is the deformation in the longitudinal direction. In the same way W_{el} is assumed as a quadratic function of I_{el}, which is a measurement of the longitudinal deformation in this hyperelastic frame:

$$W_{el} = \frac{1}{2} k_{el} I_{el}^2 \quad for \quad I_{el} > 0,$$
$$W_{el} = 0 \quad for \quad I_{el} < 0.$$

Where k_{el} is a material parameter to determine.
The contribution of this deformation mode to the tensor $\mathbf{S}$ is indicated with $\mathbf{S}_{el}$ and is equal to:

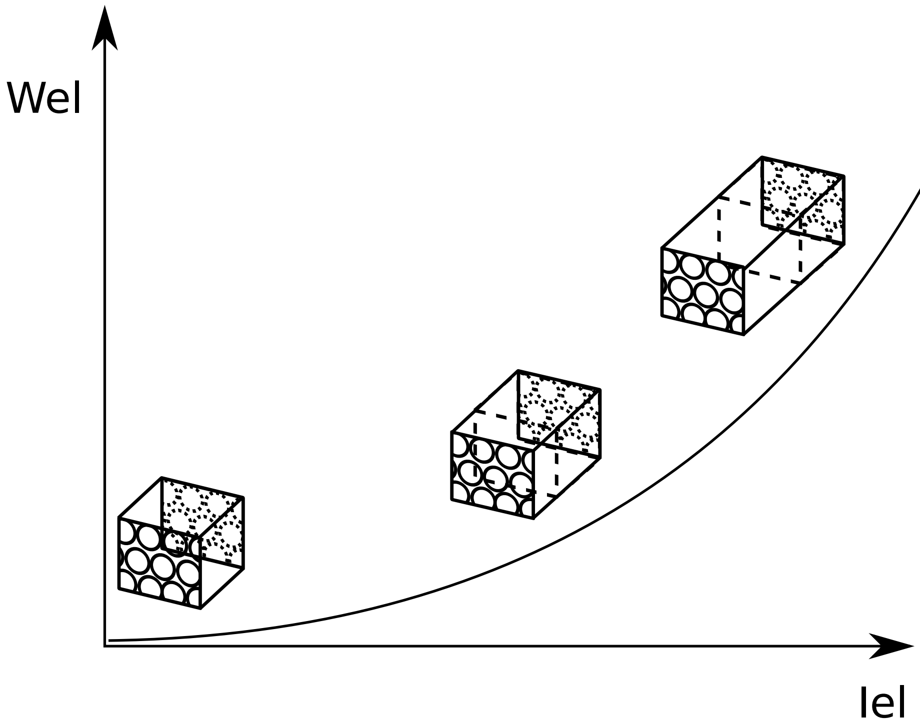

Fig. 4.4 Longitudinal elongation strain energy trend.

$$\mathbf{S}_{el} = \frac{1}{I_4}\mathbf{M}k_{el}I_{el} \quad for \quad I_{el} > 0 \quad else \quad 0.$$

Transverse Compaction

The strain energy function for transverse compaction is presented as the same power based function assumed by Charmetant:

$$W_{tc} = k_{tc}\|I_{tc}\|^p \quad for \quad I_{tc} < 0,$$
$$W_{tc} = 0 \quad for \quad I_{tc} > 0.$$

For this specific mode two parameter have to be identified, k_{tc} and p.
It is worth to notice that zero energy is assumed when the associated invariant I_{tc} is greater then zero. From the physical point of view this is representative of the fact that no energy is

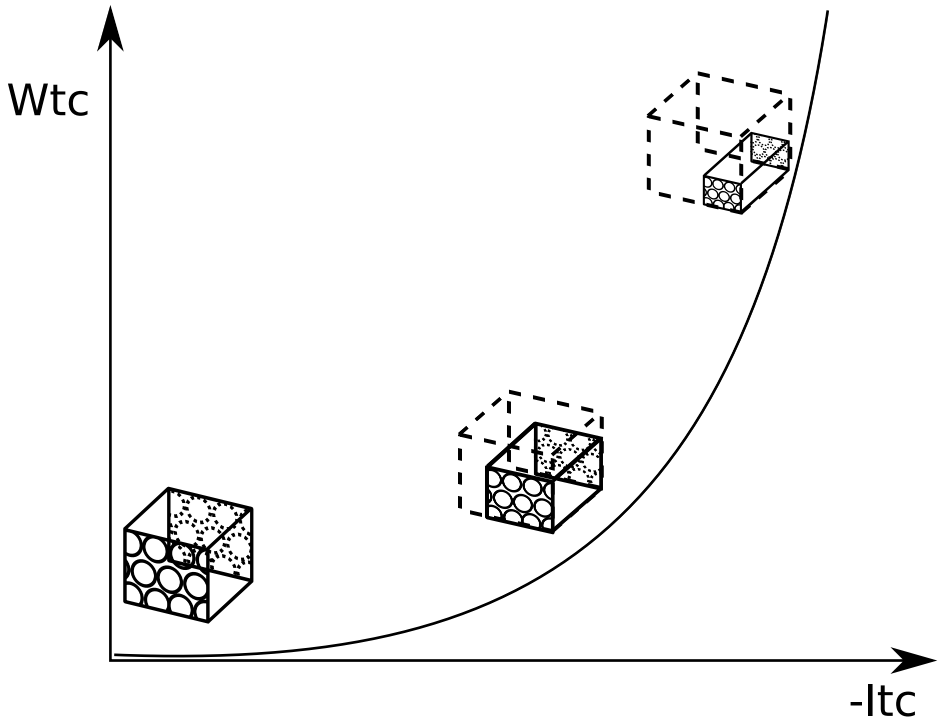

Fig. 4.5 Transverse compaction strain energy trend.

stored in the yarn when fibers are separated from each other. The contribution of transverse compaction to the second Piola-Kirchoff stress tensor is indicated with $\mathbf{S}_{tc}$ and is equal to:

$$\mathbf{S}_{tc} = \frac{-p}{2} k_{tc} \| I_{tc} \|^{p-1} (\mathbf{C}^{-1} - \frac{\mathbf{M}}{I_4}) \quad for \quad I_{tc} < 0 \quad else \quad 0. \tag{4.12}$$

Transverse Distortion

For the transverse distortion strain energy is assumed the same form proposed by Charmetant:

$$W_{td} = \frac{1}{2} k_{td} I_{td}^2. \tag{4.13}$$

where k_{td} is a material parameter which have to be identified
The contribution of this mode to the second Piola-Kirchoff stress tensor is indicated with $\mathbf{S}_{td}$ and is equal to:

$$\mathbf{S}_{td} = 2 k_{td} I_{td} \frac{2 I_4 \mathbf{I} - (I_1 I_4 - I_5) \mathbf{C}^{-1} + (I_1 + \frac{I_5}{I_4}) \mathbf{M} - 2(\mathbf{C} \cdot \mathbf{M} + \mathbf{M} \cdot \mathbf{C})}{4 \sqrt{(I_1 I_4 - I_5)^2 - 4 I_3 I_4}}. \tag{4.14}$$

Where $\mathbf{I}$ is the identity tensor.

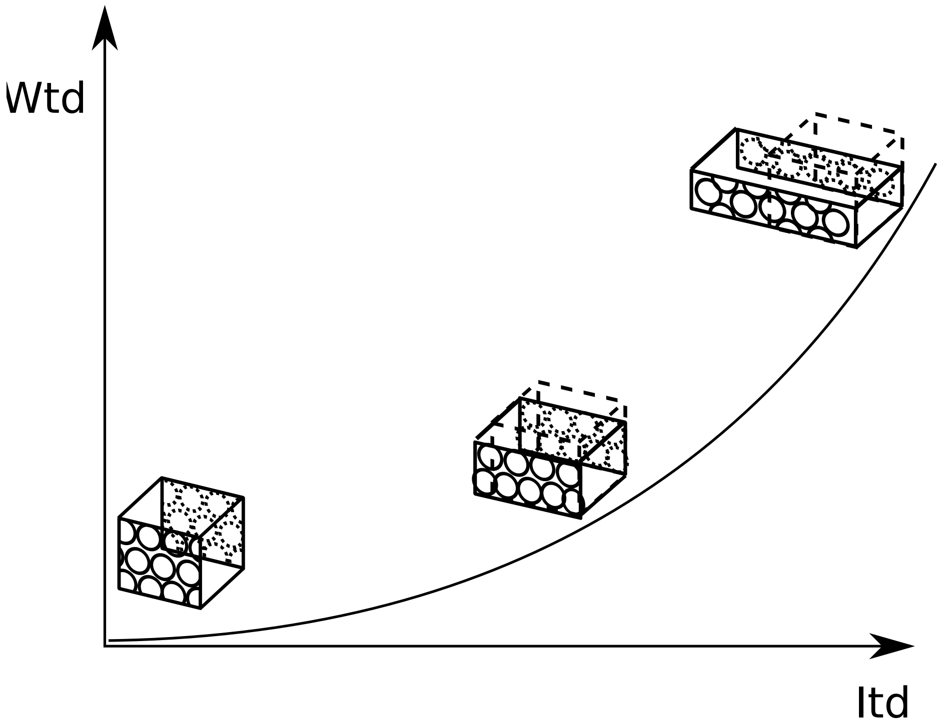

Fig. 4.6 Transverse distortion strain energy trend.

Longitudinal shear

This form of energy is physically representative of the internal energy stored in the yarn while it is sheared in those plane which include its longitudinal axis. It is mostly related to fiber-fiber sliding and is assumed to be negligible compared to the others modes. Due to this assumption, its contribution to the global energy absorption will be neglected:

$$W_{ld} = 0. \tag{4.15}$$

4.4.2 Failure modeling using physical invariants

In this part an invariant based failure criteria equivalent to the maximum longitudinal elastic stress/strain based will be presented. The proposed criterion will be successively enriched with the longitudinal properties degradation effect related to transverse deformation.

Longitudinal elongation failure criterion using physical invariants

The length of the unitary vector $\mathbf{m}$ after the deformation is indicated by λ_m and is equal to:

$$\lambda_m = \sqrt{\mathbf{Cm} \cdot \mathbf{m}} = \sqrt{\mathbf{C} : \mathbf{M}} = \sqrt{I_4}. \tag{4.16}$$

While the longitudinal strain in the fiber direction is defined as:

$$\varepsilon_m = \frac{\lambda_m - ||\mathbf{m}||}{||\mathbf{m}||} = \frac{\lambda_m - 1}{1} = \lambda_m - 1. \tag{4.17}$$

Using the definition of I_{el} we obtain:

$$I_{el} = ln(\varepsilon_m + 1). \tag{4.18}$$

It gives the physical interpretation of the longitudinal elongation invariant which is equal to true strain in the fiber direction.
Writing the previous relation in terms of maximum elongation strain ε_{el}^{lim} it becomes:

$$I_{el}^{lim} = ln(\varepsilon_m^{lim} + 1). \tag{4.19}$$

And the relative purely longitudinal failure criteria is written as:

$$I_{el} < I_{el}^{lim}. \tag{4.20}$$

According to this criterion, the material will fail if the invariants associated to the longitudinal elongation will be greater than the limit true strain along fibers recorded during a uniaxial traction test.
This type of criterion is the invariant counterpart of that normally used in the linear elastic orthotropic model, usually formulated in terms of stress.

Inclusion of transverse effects

Different questions have been posed concerning the necessity of a multiaxial failure criterion for yarn structure. Thanks to the current approach is it possible to include the effect of transverse modes on the material failure.
In this case the following failure criterion is proposed to take into account the damage induced by fibers transverse deformation:

$$\begin{aligned} &I_{el} < I_{el}^{lim}(1 - \alpha\|I_{tc}\| - \beta I_{td}) \quad for \quad I_{tc} < 0, \\ &I_{el} < I_{el}^{lim}(1 - \beta I_{td}) \quad for \quad I_{tc} > 0. \end{aligned}$$

Where I_{el}^{lim} is the limit longitudinal elongation invariant adopted for the uniaxial criterion and α, β are material parameters.
This criterion is equivalent to the uniaxial one if the yarn cross section remains undeformed or expanded, however a reduction of the axial failure properties is considered when yarn transverse compaction and distortion is recorded. This reduction can be physically attributed to fiber damage due to permanent transverse deformations. The parameters α and β regulate the decrease of axial strain limit and have to be identified using experimental or numerical approaches.

4.5 Constitutive law parameters identification

The identification of material parameters which characterize an hyperelastic constitutive behaviour is usually formulated as an inverse problem. This problem consists in the identification of the optimal set of parameters which minimize a defined error among the experimental datas curves and the analytical material response.
This problems can be formulated in term of stresses [81, 88], load-displacement curves [3, 58] or energy [34, 53, 66]. In this work the latest approach will be adopted.

For the proposed constitutive model, the strain energy function is a combination of three independent parts respectively related to three deformation modes. Following this idea, it is ideally possible to identify separately the parameters related to W_{el}, W_{tc} and W_{td}. In order to do this, three set of datas which express the elementary strain energy as a function of its relative invariants are required.
In the present section the strategy adopted for the identification of these data sets is explained and the parameters identified by curve fitting are presented.

4.5.1 Longitudinal elongation mode

The effectiveness of the linear elastic orthotropic model in describing the yarn longitudinal behaviour has been largely assessed, then it is possible to use this model to get the data for the determination of the parameter k_{el}.
Let's induce into a mesoscopic hyperelastic yarn material block a pure homogeneous longitudinal strain state imposing the following boundary condition on the external faces, Fig. 4.7:

$$\mathbf{u} = \mathbf{F}\mathbf{x},$$

$$\mathbf{F} = \begin{bmatrix} \lambda & 0 & 0 \\ 0 & 1 & 0 \\ 0 & 0 & 1 \end{bmatrix}.$$

Where **u** is the displacement vector of the point on the faces, **x** is their position vector in the proposed reference system and **F** is the homogeneous deformation gradient induced written in the proposed reference system.

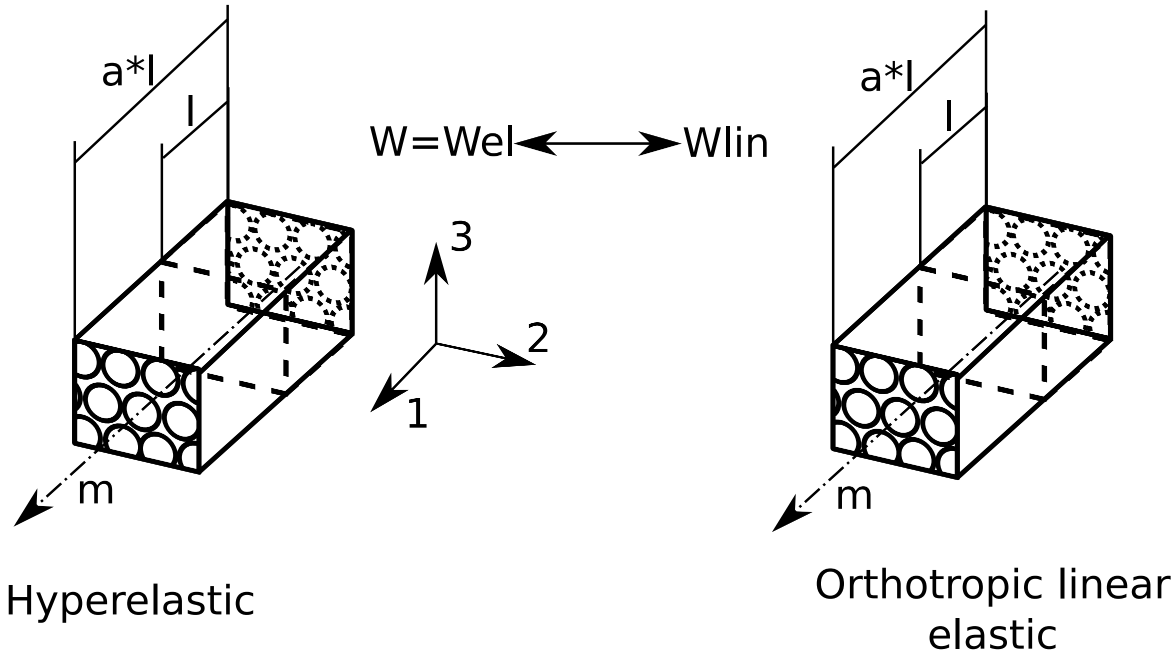

Fig. 4.7 Energetic equivalence for the identification of k_{el}.

Under this condition all the physical invariants are equal to zero with the exception of I_{el}, then the strain energy stored within the block is reduced to the contribution of the longitudinal elongation mode:

$$I_{el} \neq 0 \quad I_{tc} = I_{td} = 0,$$
$$\tilde{W} = \tilde{W}_{el}.$$

For this strain state, the infinitesimal strain tensor ε and the longitudinal elongation invariants are written:

$$\varepsilon = \frac{1}{2}(\mathbf{F}^T + \mathbf{F}) - I = \begin{bmatrix} \varepsilon_f & 0 & 0 \\ 0 & 0 & 0 \\ 0 & 0 & 0 \end{bmatrix},$$

$$I_{el} = ln(\varepsilon_f + 1).$$

Where $\varepsilon_f = \lambda - 1$ is the infinitesimal strain in the fiber direction.

If the Gasser constitutive model would be adopted for the same block under the same boundary conditions, the strain energy function will have the following form:

$$W_{lin} = \frac{1}{2} E_f \nu_f \varepsilon_f^2. \tag{4.21}$$

Where E_f is the young modulus of the fiber in the longitudinal direction and ν_f is the fiber volume fraction of the yarn. These parameters are usually known, then the strain energy associated to a generic ε_f can be easily evaluated
Using Eq. 4.18, the previous relation can be written as a function of the physical invariant I_{el}:

$$W_{lin} = \frac{1}{2} E_f \nu_f (e^{I_{el}} - 1)^2. \tag{4.22}$$

At this point the energetic equivalence among the two models is assumed:

$$\tilde{W}_{el} = W_{lin} = \frac{1}{2} E_f \nu_f (e^{I_{el}} - 1)^2. \tag{4.23}$$

This relation is obviously different from the quadratic form previously assumed, however a good approximation of this function can be obtained with the optimum choice of the parameter k_{el}.

The relation 4.23 has been used to generate a sufficiently large number of couples to provide a good fitting of the hyperelastic model to the linear elastic orthotropic one under pure longitudinal strain condition. Fig. 4.8 reports the results of the curve fitting for a Kevlar KM2 yarn whose properties are listed in Table 4.1 which led to $k_{el} = 82.341$ GPa.
The strain energy $\tilde{W}_{el}$ has been evaluated up to the invariant value for which failure is expected.

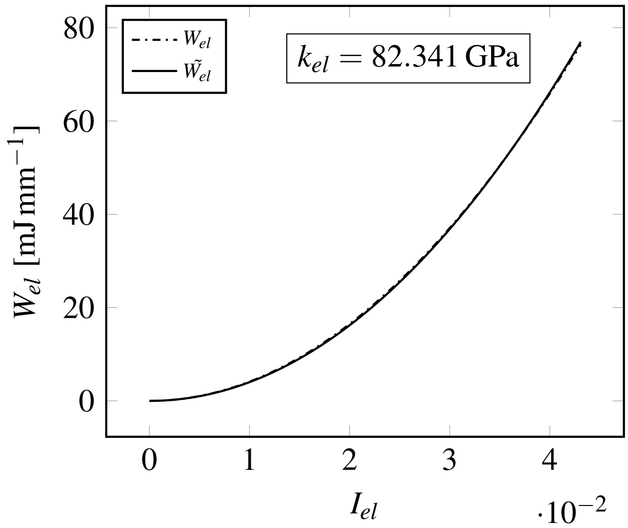

Fig. 4.8 Identification of the parameter k_{el}.

Table 4.1 Longitudinal Properties of Kevlar KM2 yarn.

E_{long} fiber [GPa]	Yarn volume fraction	ε_{max}
84.62	0.9385	4.58%

4.5.2 Transverse compaction mode

For the parameters identification of transverse compaction and transverse distortion the procedure is similar to that adopted for the longitudinal elongation, however here the energetic equivalence is assumed with a numerical yarn RVE.

If a pure transverse compaction mode would be induced within the continuum material block, the following boundary condition should be applied on the six faces:

$$\mathbf{u} = \mathbf{F}\mathbf{x},$$

$$\mathbf{F} = \begin{bmatrix} 1 & 0 & 0 \\ 0 & \lambda & 0 \\ 0 & 0 & \lambda \end{bmatrix},$$

and:

$$I_{tc} = ln(\lambda) \quad I_{el} = I_{td} = 0. \tag{4.24}$$

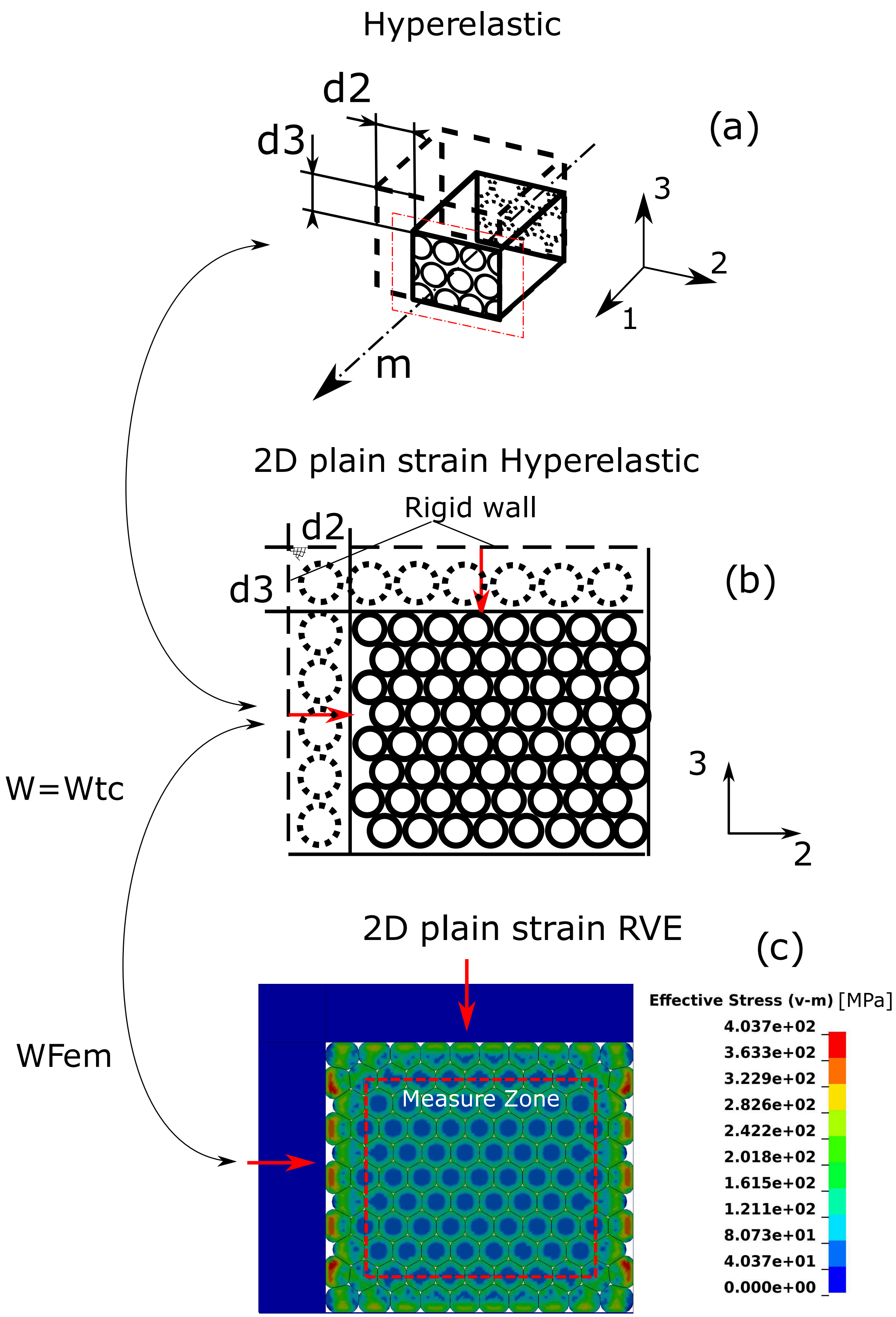

Fig. 4.9 Energetic equivalence for the identification of k_{tc} and p.

Under this condition the strain energy stored within the block is reduced to the contribution of the transverse compaction mode, Fig. 4.9(a):

$$\tilde{W} = \tilde{W}_{tc}. \tag{4.25}$$

From a numerical point of view, the same homogeneous strain state is obtained for a bidimensional plain strain problem where the displacement are applied by four rigid walls in contact with the mesoscopic material, Fig. 4.9(b),

The relation among the displacement δ of the wall i and the scalar λ, representative of the strain state, is given by:

$$L_i - \delta_i = \lambda L_i. \tag{4.26}$$

Where L_i is the length of the relative side.

At this point the energetic equivalent model is introduced.
A group of fibers arranged into an hexagonal close packing configuration has been chosen as the energetic counterpart of the mesoscopic model [69, 100]. A plain strain finite element model of 115 fibres arranged into an HCP configuration subjected to the wall load previously described have been developed.
According to previous results [100], each fiber has been modeled using 108 plain strain four nodes bi-dimensional elements. This mesh density assures a correct representation of the fiber transverse behaviour
For the specific case of Kevlar fibers, a linear elastic transversely isotropic behaviour has been used, Table 4.2. No friction is considered for contact among fibres and walls while a friction coefficient of 0.2 has been assumed for fiber-fiber contact. The model has been implemented in the finite element software LS-Dyna while an implicit integration scheme has been adopted to solve the non-linear static analysis.
Fig. 4.9(c) reports the Von Mises stresses during the simulation. Boundary condition effects are clearly in those fibers directly in contact with the rigid plates. Those present the highest values of stresses while a periodic solution is obtained at the RVE center.
The strain energy has been recorded in the central zone of the numerical specimen where the solution appears to be periodic while the associated invariant has been computed using relation Eq. 4.24 - 4.26 from the wall displacement.

Someone could argue about the consistency among the strain energy here measured and that actually stored in this mode during an impact. Obviously those will differ for a various number of reasons. Non periodicity of the cross section microstructure, dynamic effects and ratio among element and RVE size are some of them.

However the aim of the procedure is not to provide an exact evaluation of the strain energy, but to provide a general physical approach based on fibers mechanic for the determination of the yarn cross section material properties which avoid their numerical calibration.

Fig. 4.10 reports the evolution of the strain energy density stored within the RVE as a function of the transverse compaction invariant and the fitting results from which k_{tc} and p resulted equal to 1.055 GPa and 2.2 respectively.

Table 4.2 Properties of Kevlar KM2 fiber.

Density ($\mathrm{kg\,m^{-1}}$)	E_1 (GPa)	$E_2 = E_3$ (GPa)	ν_{23}	$\nu_{12} = \nu_{13}$	G_{23}(GPa)	$G_{13} = G_{12}$(GPa)
1440	84.62	1.34	0.24	0.6	0.540	24.4

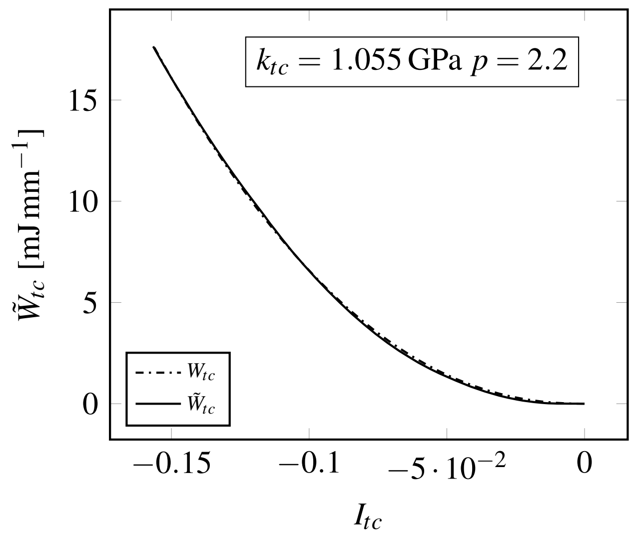

Fig. 4.10 Identification of the parameter k_{tc}, p.

4.5.3 Transverse distortion mode

The strategy adopted for the parameters identification of transverse distortion is based on the same procedure and the same FE model adopted for transverse compaction. The only difference relies in the boundary conditions.

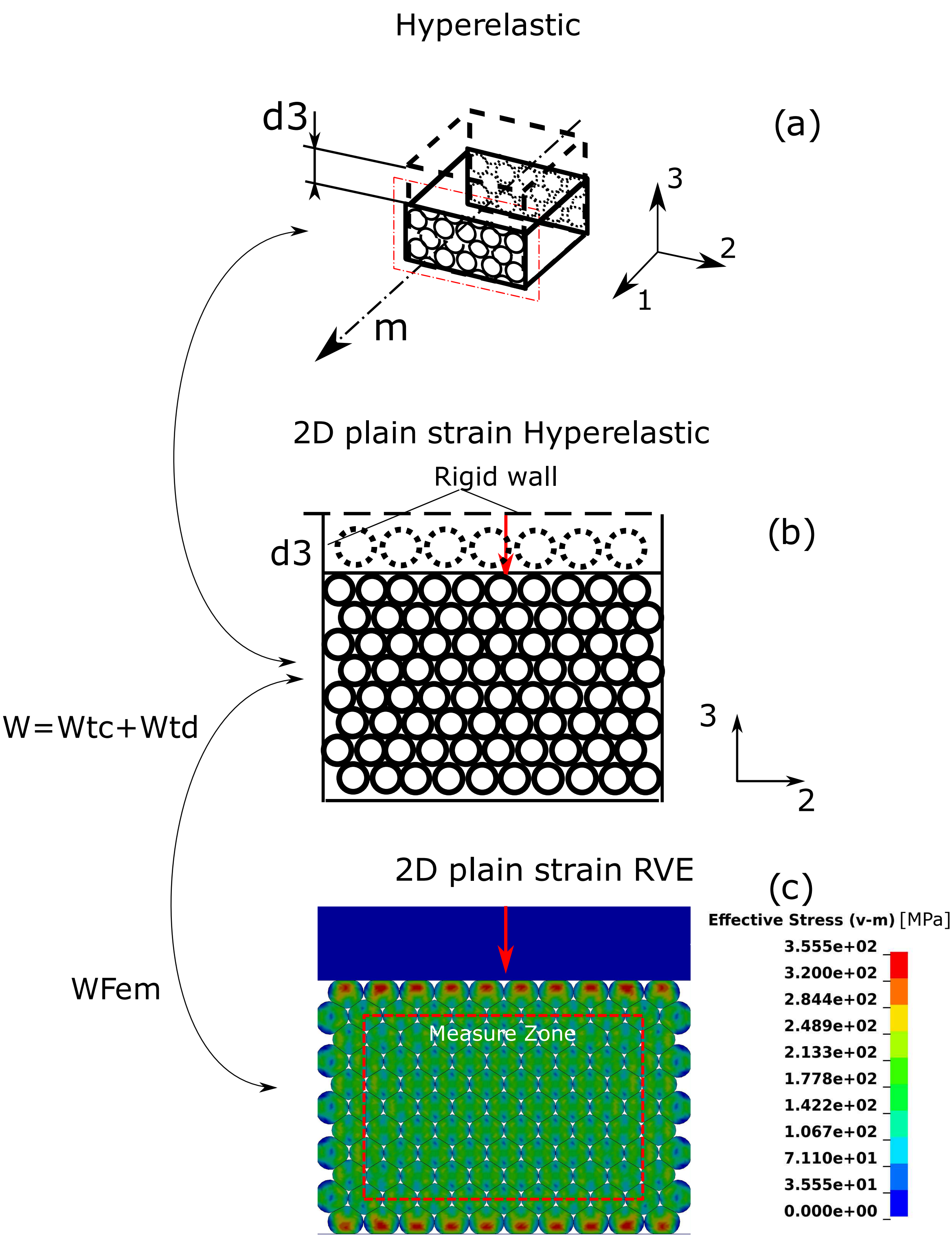

Fig. 4.11 Energetic equivalence for the identification of k_{ld}.

In this specific case a uniaxial compression is applied using wall displacement which induce the following strain state:

$$\mathbf{F} = \begin{bmatrix} 1 & 0 & 0 \\ 0 & 1 & 0 \\ 0 & 0 & \lambda \end{bmatrix}. \tag{4.27}$$

where the relation among the λ and the wall displacement δ is always given by Eq. 4.26. For this strain state two physical invariants are different from zeros:

$$I_{tc} = \sqrt{\lambda}, I_{td} = \sqrt{\frac{1}{\lambda}}. \tag{4.28}$$

and the strain energy function W is given by the combination of two different components W_{tc} and W_{td}.
The values of strain energy associated to the transverse distortion mode can be obtained subtracting the transverse compaction strain energy, evaluated using the parameters previously identified, to the global strain energy density measured in the FE analysis.:

$$\tilde{W}_{td} = \tilde{W} - \tilde{W}_{tc}. \tag{4.29}$$

Fig. 4.12 reports the results of the curve fitting for a Kevlar yarn and the energies recorded during the test. From this procedure k_{td} resulted equal to 0.649 74 GPa.

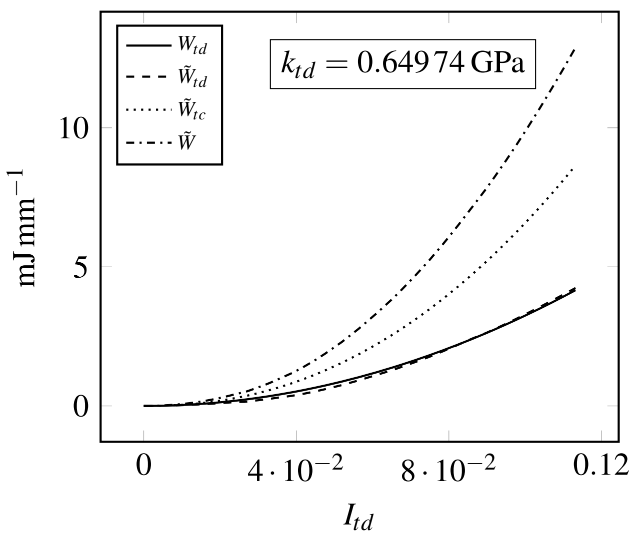

Fig. 4.12 Identification of the parameter k_{td}.

4.6 The single yarn mesoscopic model: Long period response

The current section is dedicated to the study of the transverse impact on a single yarn using a mesoscopic numerical model in the impact scenario presented in 3.3. The proposed constitutive law here is adopted. In the first part, the impact scenario and the relative finite element model will be presented. Then classical results universally attributed to the yarn longitudinal and inertial properties as projectile speed trend or yarn kinematic will be validated using those obtained by linear elastic mesoscopic and microscopic approach. To validate the response of the material, no failure criteria will be implemented in the first part of this study.
Finally, failure criteria will be included in the model. Yarn penetration and projectile residual speed will be compared for the three model while the new opportunities offered by the proposed constitutive law in terms of failure modellisation and postprocessing will be presented.

4.6.1 Impact scenario

In order to validate the hyperelastic constitutive law, the impact scenario is assumed to be identical to that presented in section 3.3 for the microscopic study, Fig. 4.13.

The finite element model has been implemented in the commercial software LS-DYNA. Even in this case the symmetry of the problem has been exploited, then just half of the yarn has been modeled
The yarn cross section is elliptical with major and minor axis respectively equal to 0.5337 mm and 0.115 mm which results into a yarn volume fraction ν of 0.93848.
Twelve elements have been used to discretize the whole cross section [40] which results in 1200 eight-nodes reduced integration hexaedral solid elements for the whole yarn.
Symmetry boundary condition has been imposed to the nodes at the yarn center while those on the extremity have been perfectly clamped.
The proposed transverse isotropic hyperelastic material model has been adopted for the yarn where the material parameters have been identified in the previous section and resumed in Table 4.3.

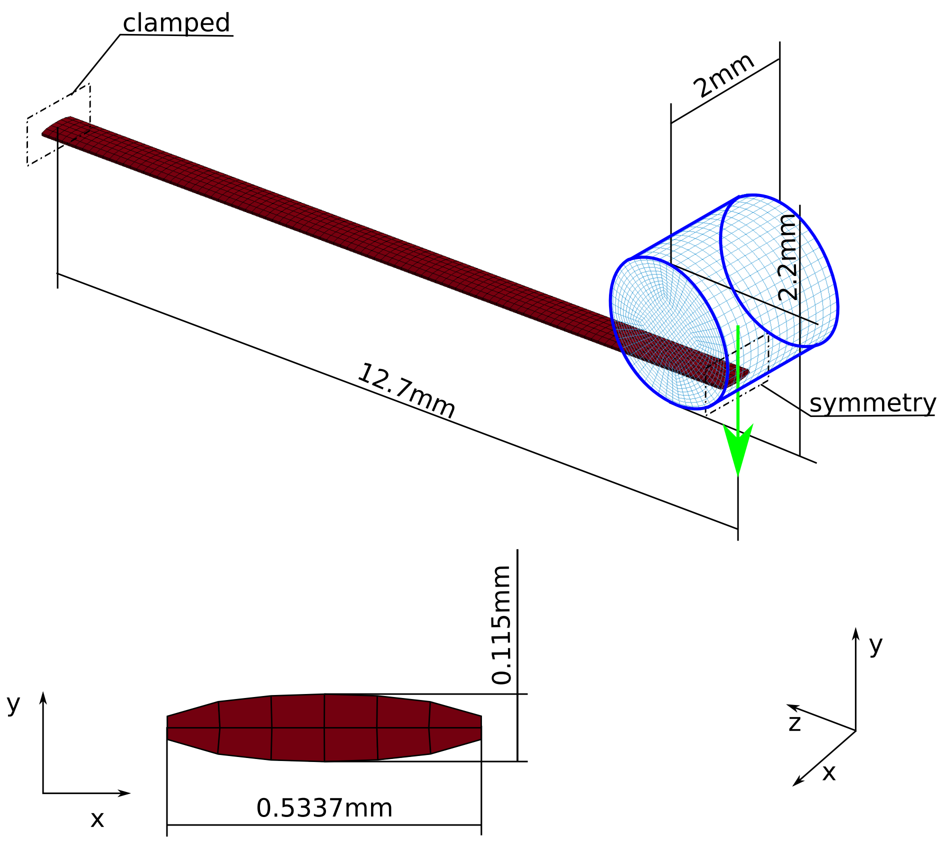

Fig. 4.13 Finite element model.

Table 4.3 Properties of hyperelastic Kevlar KM2 yarn model.

k_{el}(GPa)	k_{tc}(GPa)	p	k_{td}(GPa)
82.341	1.055	2.2	0.649

The density ρ of the yarn is obtained multiplying the density of a fiber ρ_f 1.440 $\mathrm{g\,cm^{-1}}$ for the yarn volume fraction and is equal to 1.351 $\mathrm{g\,cm^{-1}}$.

In order to avoid contact problem between the two parts, the whole projectile has been modeled. Since symmetry conditions are applied, projectile mass has been divided by two and its displacement have been limited to the impact direction. As in the microscopic case, the projectile is assumed to be a rigid.
An automatic surface-to-surface contact has been chosen for the projectile-yarn interaction with a friction coefficient of 0.18.

4.6.2 Results

Yarn kinematic, projectile speed and energy balance: model validation

Here results of the mesoscopic model are reported for the validation of the proposed constitutive law. These results are compared with those presented in the first chapter by the microscopic model and those obtained using the linear elastic approach.
For the second case, the material properties adopted for the yarn are reported in Table 4.4:

Table 4.4 Properties of linear elastic Kevlar KM2 yarn model.

E_1 [GPa]	$E_2 = E_3$ [GPa]	$\nu_{23} = \nu_{12} = \nu_{13}$	$G_{23} = G_{13} = G_{12}$[GPa]
79.414	0.794	0	0.126

The longitudinal elastic modulus has been obtained multiplying the fiber modulus 84.62 GPa for the yarn volume fraction, the transverse moduli have been assumed to order of magnitude lower the longitudinal one and shear moduli have been set according to the work of Duan [39].

Fig. 4.14 reports the yarn kinematic in the impact plane for the proposed mesoscopic model.
The propagation of the transverse wave is observed. This particular wave is directly related to the yarn longitudinal behaviour, inertial properties and strain state along the fiber direction. The transverse wave travels from the impact point toward the extremities of the yarn,

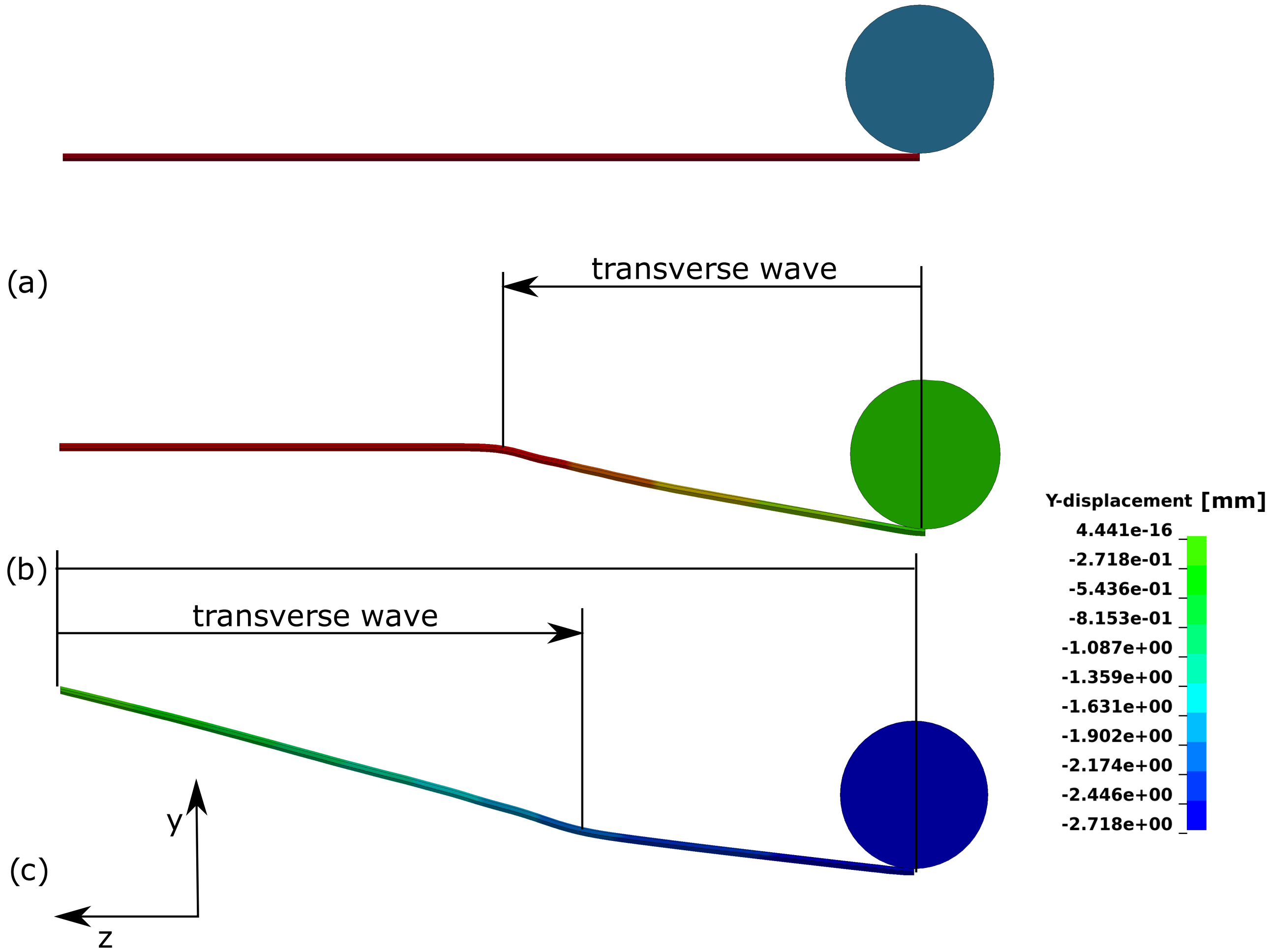

Fig. 4.14 Transverse wave propagation in hyperelastic mesoscopic model at 0 µs(a), 10 µs(b), 25 µs(c).

0 μs-18 μs, it is reflected and then come back to the impact zone, 18 μs-30 μs.
The same kinematic has been obtained by the microscopic and the linear elastic model.
The coherence of the linear elastic model with the microscopic simulation is not a surprise [21, 39]. On the other side, the observation of this same kinematic in the hyperelastic model is a validation of the good representation of the yarn longitudinal and inertial properties, which is the minimum requirement for a correct representation of an impact phenomenon at the fabric level.

Concerning the behaviour in the x-z plane, the three models are not equivalent. Fig. 4.15 reports the yarn configuration in this specific plane during the impact.
The hyperelastic model as the microscopic one presents the propagation of a spreading wave which is not observed in the linear elastic one. It represents the reorganization of the yarn fibers within the cross section which travels outside the impact zone, then its related to yarn transverse mechanical behaviour.
Up to know, this wave was typical of the microscopic approaches and has never been observed in any other yarn continuum model.
It propagates from the impact point up to the yarn extremities 0 μs-18 μs, it is reflected and then come back to the impact zone 18 μs-30 μs.

In order to quantify the propagation of this wave, the displacement along the x direction of the yarn cross section external node have been tracked in four different point along the yarn length during the impact, Fig. 4.16.

The general trend is similar in all the measured points, Fig. 4.17. The displacements are almost negligible up to the time when they are reached by the wave. After that moment a strong increment is measured which is followed by a stabilization period where the displacements are almost constant. This period is finally interrupted from the front of the reflected spreading wave. Contrariwise to microscopic models, here the spreading wave is more progressive and fully develops outside the impact zone. According to the author this type of behaviour is related to the coexistence of transverse distortion and transverse compaction in the same zone. The components of the stresses associated to transverse distortion actually reduce the global x displacement induced by the transverse wave. A different identification strategy for hyperelastic material parameters could solve this particular problems, as presented in the perspectives.

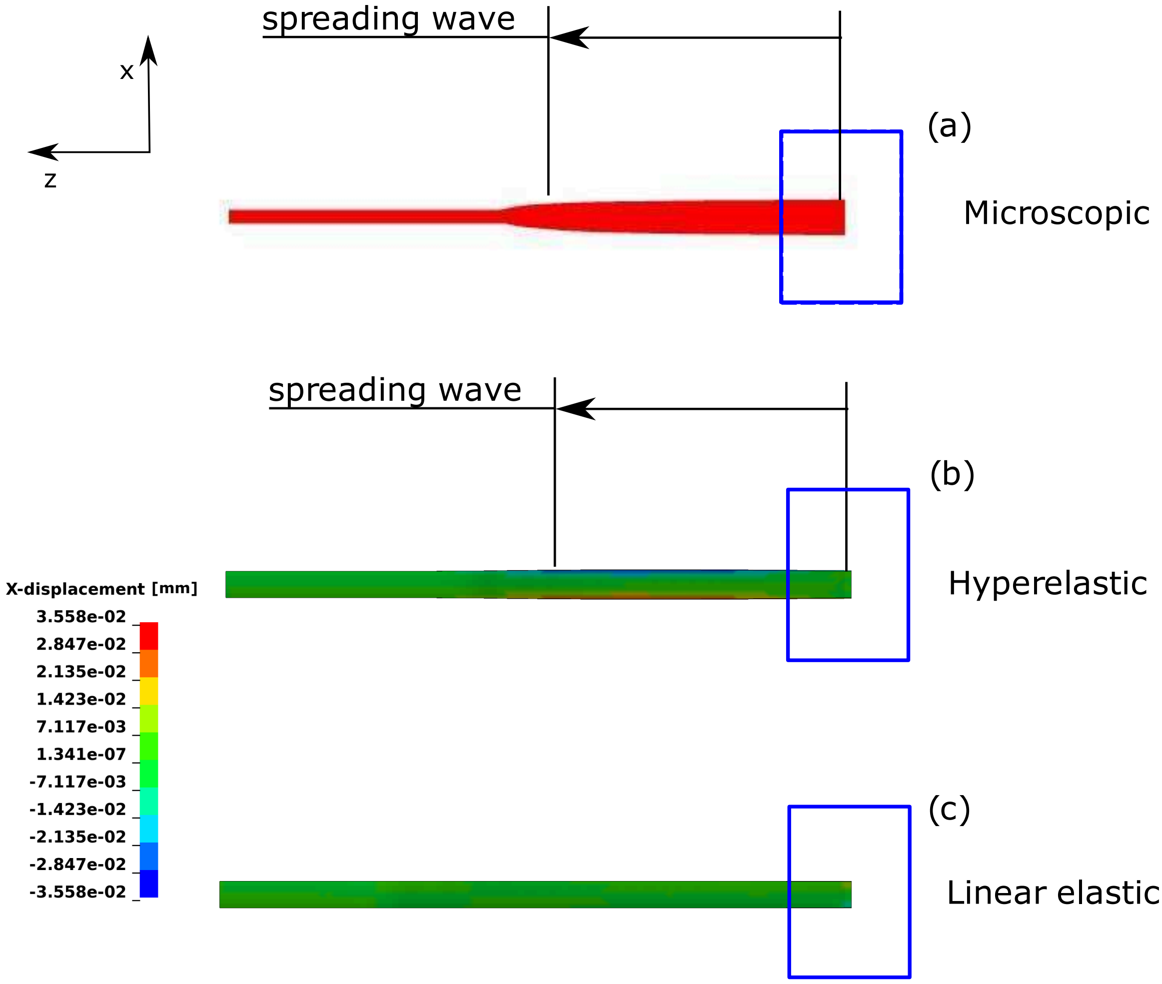

Fig. 4.15 Spreading wave propagation in microscopic and mesoscopic models at 10 µs.

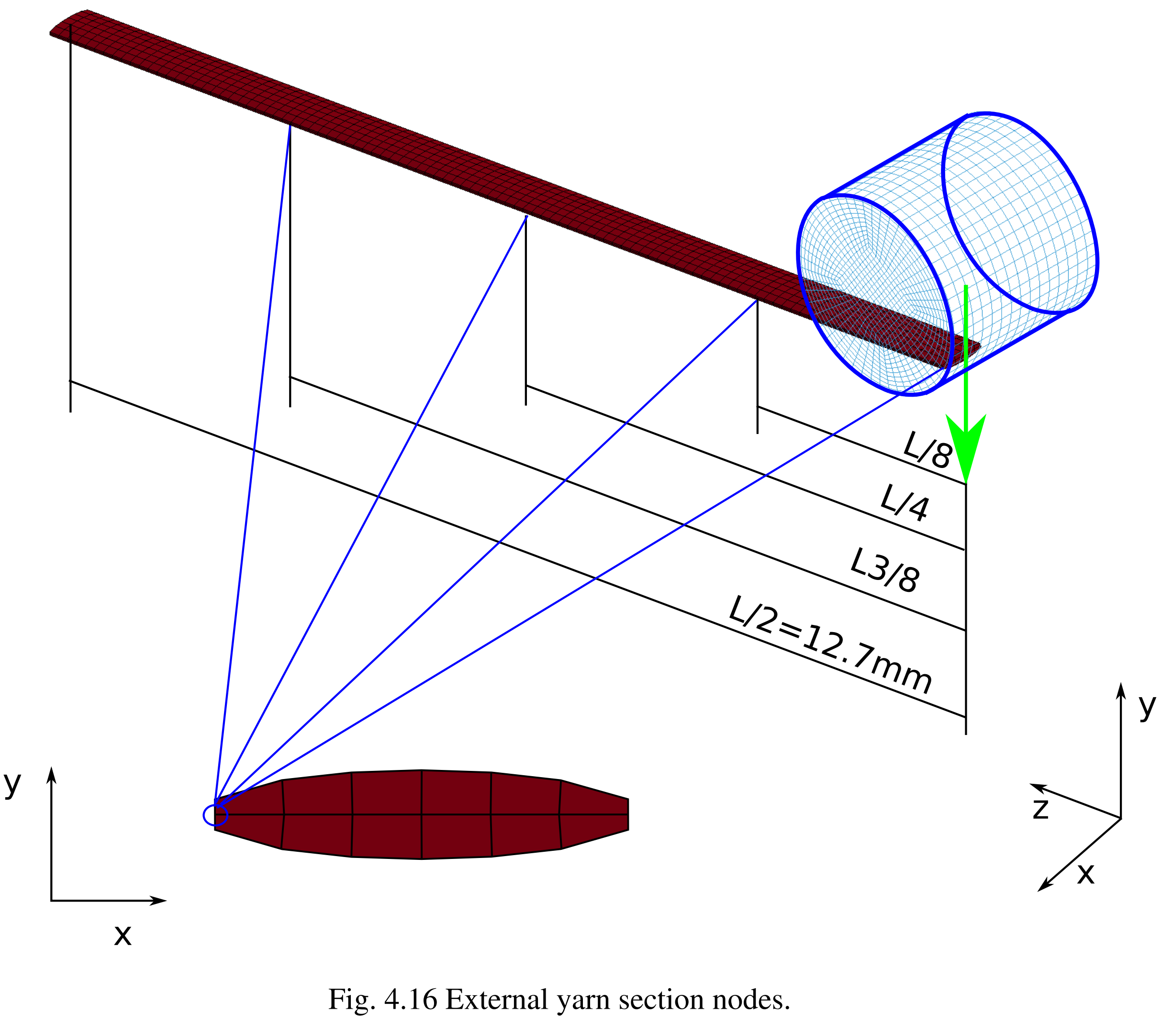

Fig. 4.16 External yarn section nodes.

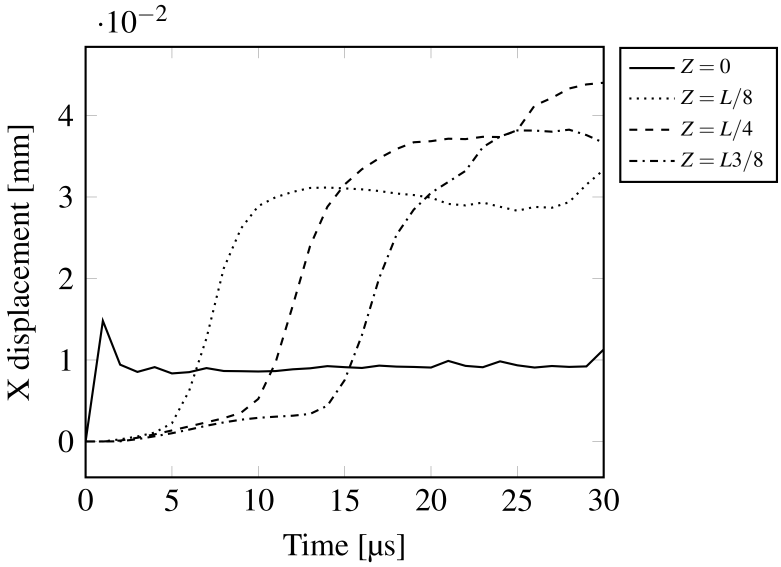

Fig. 4.17 Displacement of the cross section external node for different position along the yarn.

Microscopic observation showed how spreading and transverse waves propagate at the same speed [69]. It is possible to verify this relation checking that the effect induced by the passage of these two waves from a point appears at the same time.
When the transverse wave pass through a point, its displacement along y starts to linearly increase. On the other side, the transition of spreading wave from a point is characterized by a drastic increment of the point displacement along x.
Fig. 4.18 displays the normalized displacement of the points presented in Fig. 4.16 along the x and y directions. For each point, transverse wave and spreading wave effects appear at the same time. This means that the two waves travel at the same speed.

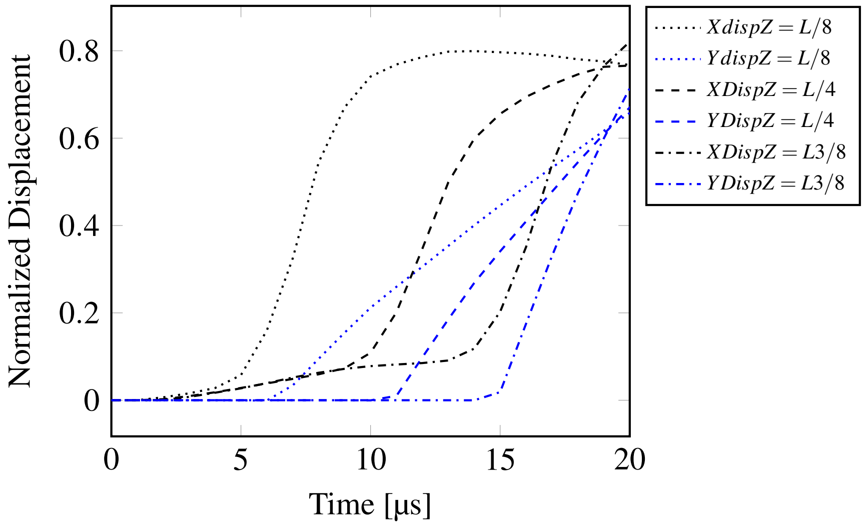

Fig. 4.18 Normalized displacements of the cross section external node for different position along the yarn.

The projectile speed evolution as a function of the time is reported in Fig. 4.19. This trend is particularly important since it gives a macroscopic quantification of the energy absorbed during the impact. It is worth to remind that here failure is not implemented, since we are interested in the validation of the pure constitutive law.

The three models are in very good agreement among each other. This was expected due to impact scenario. Previous results proved that yarn transverse mechanical behaviour have no effect on the absorbed energies at this time scale.

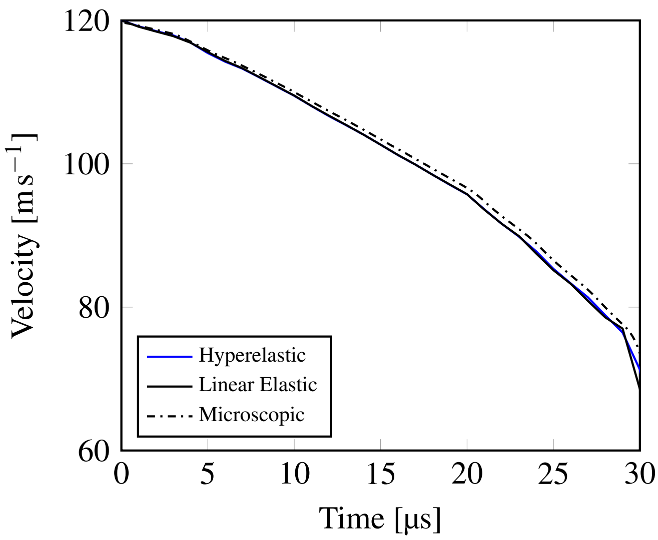

Fig. 4.19 Projectile Speed.

The last step of the validation is the analysis of the internal and kinetic energy stored during the impact. These energies are presented in Fig. 4.20.
Even in this case a good agreement among the models is obtained. The coherence of these trends gives an explicit indication about the correct representation of the mass and the mechanical properties of the system.
Another validation of the global kinematic is given by the time in which the trends of the energies are inverted. Those instant correspond to transverse wave reflection, then they mark the time required by the wave to travel form one side of the yarn to the other. Since those instant are the same for the three models, the wave speed will be equal in all the three cases, which is another prove of the good representation of the yarn kinematic.

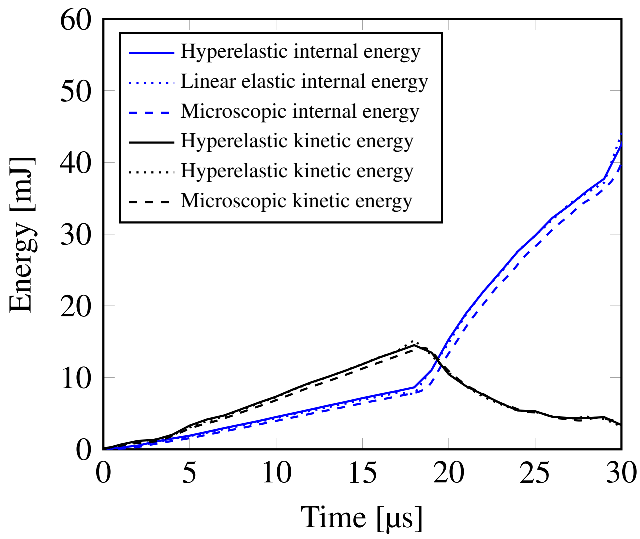

Fig. 4.20 Internal and Kinetic energies.

Local energy trends: An important tool for impact numerical analyses

One of the most interesting aspects of using the hyperelastic constitutive law is the possibility of identify the different elementary strain energies in each integration point of the model. This information can be used to push further the comprehension of impact phenomena. While classical approaches are confined to a global indication of the energy stored within the structure, here the strain energy can be split in its three original components giving a much more revelatory information. Analyzing the strain energy density associated to singular elementary modes, it is possible to understand the mechanisms of energy storage within the fabric, how a zone of the fabric is charged, how the geometry of a textile affects the partitioning of the strain energy among the different modes or what type of projectile is mostly inclined to the solicitation of a particular energy storage.

In this study the trends of the elementary strain energies has been followed during the simulation in order to have some insightful information about the impact.
In Fig. 4.21 is presented the evolution of the elementary strain energy associated to the longitudinal elongation. This strain energy propagates along the yarn axis under the form of a wave which is actually equivalent to the longitudinal wave observed in other analytical and numerical models [94, 95, 97]. The speed of this wave c has been found to be equal to $7559.52\,\mathrm{m\,s^{-1}}$ which is very close to the analytical value $C = \sqrt{\frac{E}{\rho}}$ of $7665.76\,\mathrm{m\,s^{-1}}$.

Once the wave is completely propagated within the yarn, it is continuously reflected between the yarn centre and the clamped zone. During this period, the strain energy density stored in this mode continuously increase up to the end of the simulation, 30 µs, where a maximum and minimum value of $37.42\,\mathrm{mJ\,mm^{-1}}$ and $28.98\,\mathrm{mJ\,mm^{-1}}$ have been recorded. It is worth to notice that after the first longitudinal wave reflection this elementary strain energy is different from zero in the whole yarn.

Concerning the elementary strain energies related to transverse compaction and transverse distortion, they are reported in Fig. 4.22 .

Contrariwise to the case of longitudinal elongation, here the elementary energies remain confined within the contact zone for the whole impact event. Their minimum value is constantly equal to zero outside the impact zone, while their maximum one reach $8.96\,\mathrm{mJ\,mm^{-1}}$ and $6.68\,\mathrm{mJ\,mm^{-1}}$ respectively for transverse compaction and transverse distortion at the interface with the projectile.

This is coherent with the dynamic of the phenomenon, where only those fibers near the impact zone are submitted to important transverse deformations. Interestingly, cross sections outside the impact zone appears to be deformed even if no transverse strain energy is recorded. This type of behaviour is representative of the spreading wave and its related to the zero energy deformation modes assumed in the constitutive law.

Another interesting point concerns the comparison among the different elementary strain energies distribution. From Fig. 4.21 and Fig. 4.22 is evident the reason for which previous sensitivity analyses have found the global internal energy trend to be insensible to the choice of transverse parameters. Since the contribution of the transverse modes is confined to a very small area it is obvious that those of energies do not affect the global energy balance and projectile velocity trends. On the other side, physical phenomena associated to the

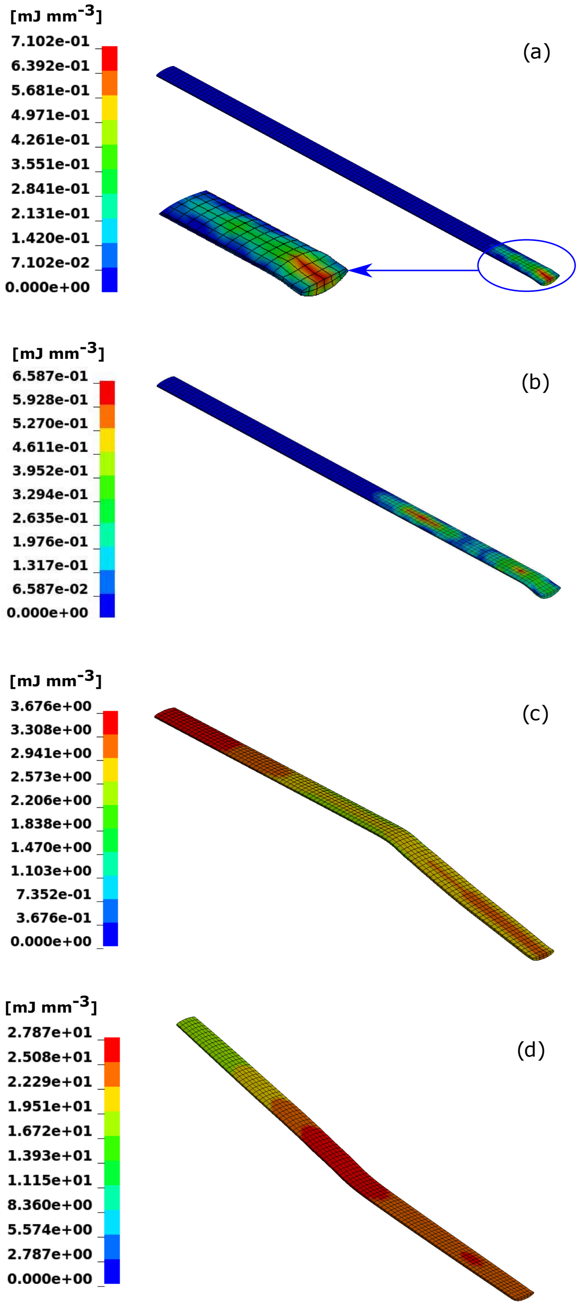

Fig. 4.21 Longitudinal Elongation Strain energy at 0.5 µs(a) 1 µs(b) 10 µs(c) 25 µs(d).

transverse compaction and distortion elementary energies could have an influence on some local phenomenon as failure initialization.

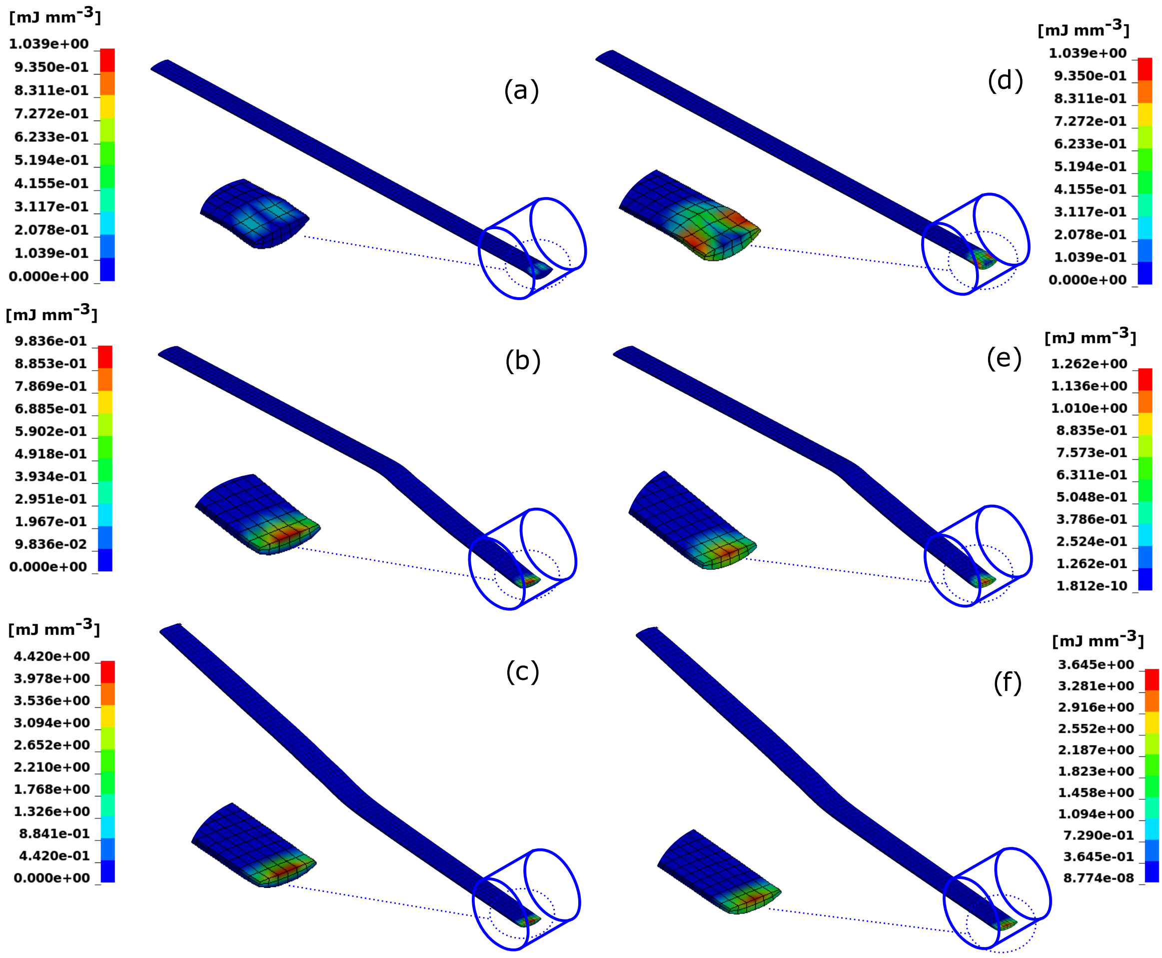

Fig. 4.22 Transverse compaction (a-b-c) and transverse distortion (d-e-f) strain energies at 0.5 µs(a-d) 1 µs(b-e) 10 µs(c-f).

Fig. 4.23 reports the trends of the maximum value of each elementary strain energy recorded within the yarn during the impact. This trend is linear increasing for all the elementary strain energies up to the first reflection of the transverse wave. After this point a strong increment in the longitudinal elastic strain energy is remarked, which is in accordance with the total strain energy trend.

The trends for transverse distortion and compaction energies appear to be very similar. They are generally lower than the longitudinal elongation one, $\approx 24\%$ of its value at 30 µs, but not totally negligible.

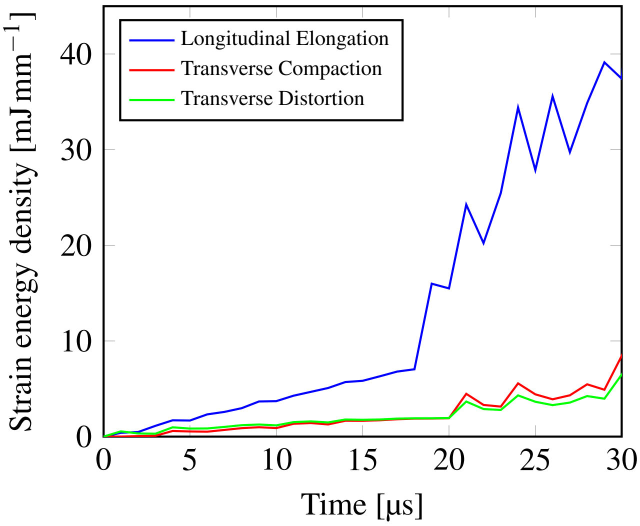

Fig. 4.23 Maximum elementary strain energy value during the impact.

An exception is marked by the elementary strain energy density distribution at 0.5 µs. At this time the longitudinal wave is still far to be propagated and confined to the zone were transverse strain energies are different from zeros. In this case the maximum strain energy density value associated to the longitudinal elongation mode, 0.71 mJ mm^{-1}, is lower than the maximum values recorded for transverse compaction, 1.04 mJ mm^{-1}, and transverse distortion, 1.38 mJ mm^{-1}.

4.6.3 Failure parameters identification

In this final part the choice of the failure criterion for the proposed hyperelastic model is treated.

In the frame of the previously presented impact scenario both the criteria presented in subsection 4.4.2 have been tested and compared with the results obtained using classical mesoscopic and microscopic approach.
In order to be coherent with the microscopic simulation, a the maximum longitudinal strain criterion has been assumed as basic failure criterion for the two mesoscopic models. Maximum strain value ε_{el}^{lim} has been assumed equal to those of the Kevlar fibers, 4.58%, which is equivalent to a maximum longitudinal elongation invariant I_{el}^{lim} of 0.044782.
This criterion has been implemented in the linear elastic model as the classical maximum stress failure criterion. Here the maximum stress σ_{lim} is equal to 3.637 GPa and has been obtain multiplying the yarn longitudinal modulus for the maximum strain in the fiber direction.

Concerning the multiaxial failure criteria, this is obviously implemented just for the hyperelastic case and the parameters α and β have been optimized in order to minimize the discrepancy among the proposed model and the microscopic simulation.

Table 4.5 reports the ballistic limit study for the three different failure criteria, maximum longitudinal strain (mesoscopic hyperelastic, microscopic), maximum stresses (mesoscopic linear elastic), multiaxial (mesoscopic hyperelastic). The cases for which no penetration occurs are indicated by "NP" while no performed cases are indicated by "-".

Table 4.5 Projectile Residual Speed for different models and failure criteria[$\mathrm{m\,s^{-1}}$].

In. Velocity [$\mathrm{m\,s^{-1}}$]	Micro	Meso Lin. El.	Meso Hyp. UF	Meso Hyp. MF $\alpha = 1.8 \beta = 0.0$
80	NP	NP	NP	NP
100	NP	40	NP	NP
120	64	74	NP	64
140	-	-	18	-

According to microscopic results, projectile residual velocity for an impact speeds over $120\,\mathrm{m\,s^{-1}}$ is $64\,\mathrm{m\,s^{-1}}$, while for lower velocities yarn failure doesn't appear[69]. As it possible to see, classical mesoscopic approach predicts yarn failure for an impact speed of $100\,\mathrm{m\,s^{-1}}$ which is inconsistent with results obtained at the microscale where no failure occurs. The proposed model overestimate the yarn resistance if the purely longitudinal criterion is adopted. No penetration is observed for an impact speed of $120\,\mathrm{m\,s^{-1}}$ but penetration occurred for $140\,\mathrm{m\,s^{-1}}$ with a residual speed of $18\,\mathrm{m\,s^{-1}}$. It is interesting to observe how a real uniaxial failure criterion, adopted by the hyperelastic model, differs in the results from a principal stress based criterion. This last criterion sub-estimates the ballistic limit evaluated by the microscopic analysis and this could be related to the effect of some transverse material parameters [33].
On the other side, it is possible to get a very good coherence among the microscopic and mesoscopic response if the multiaxial failure criterion is adopted. This results emphasizes two main points:

- The transverse elementary modes and their parameters are not negligible when local effects, as failure, are considered;

- It is possible to use numerical or experimental data in order to find these parameters and formulate complex failure criteria which take into account the evolution of the yarn cross section and fibers damage induced by transverse elementary modes.

Fig. 4.24 reports the yarn configuration after failure of the hyperelastic and linear elastic model for a $120\,\mathrm{m\,s^{-1}}$ stricking speed. It is evident how the proposed model presents large deformation at the level at the cross section while it remains underformed in the linear elastic one. After failure, the yarn fibers spring-back and buckle resulting into an apparent expansion of the cross section [69]. this kinematic is correctly represented by the hyperelastic model which results in a better description of the yarn kinematic even in the post failure phase.

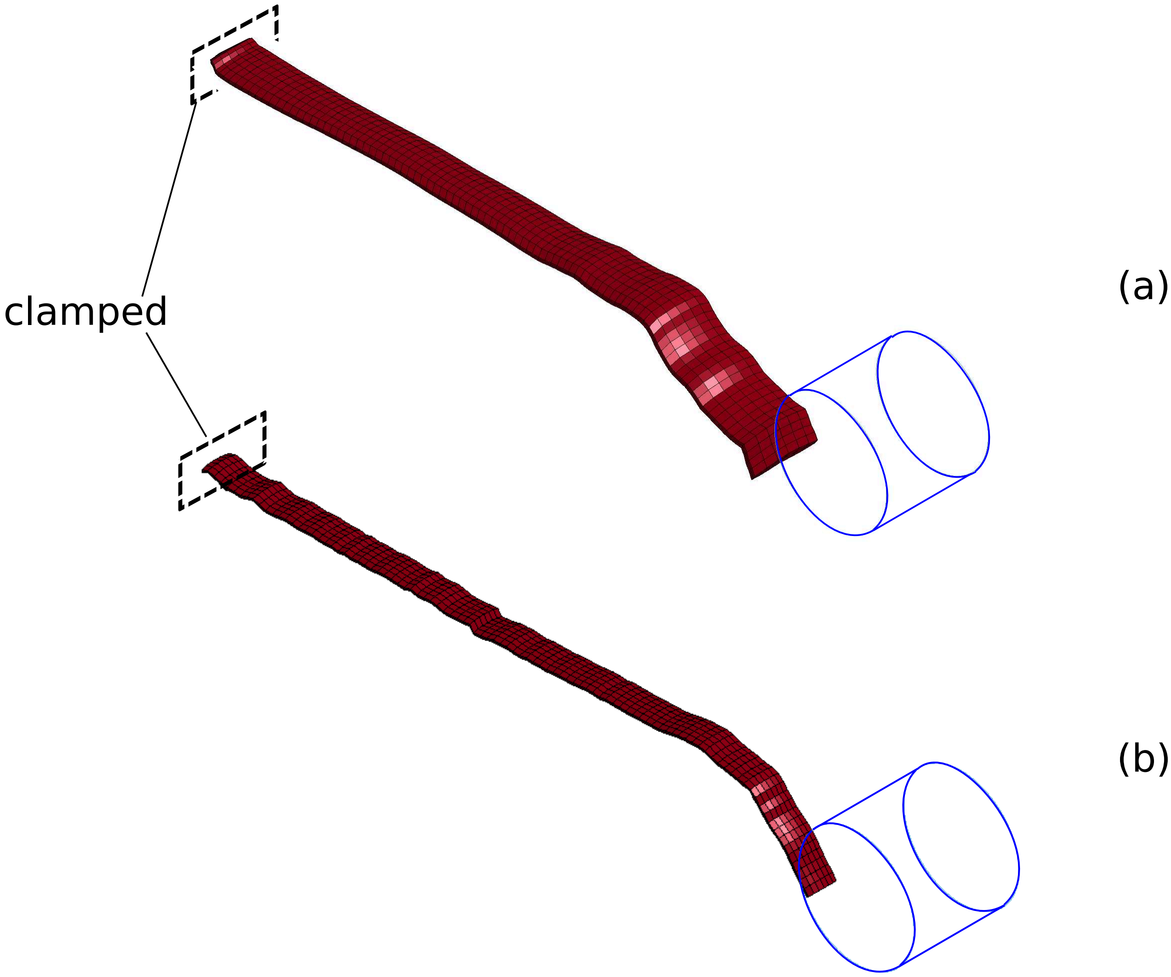

Fig. 4.24 Failure configuration for hyperelastic (a) and linear elastic (b) yarn model for a striking speed equal to $120\,\mathrm{m\,s^{-1}}$.

4.7 The single yarn mesoscopic model: Short period response

In the current section the yarn mesoscopic model response during the first phases of an impact will be analyzed. As previously demonstrated by microscopic numerical analyses, yarn cross section mechanic assumes a fundamental role at this time. Here the energy absorbed by the yarn presents a considerable contribution by fiber transverse deformation, moreover kinetic energy and initial stress state are both affected by the "fibers bounce" phenomenon.
The proposed constitutive law and the classical linear elastic one will be adopted to model the same impact scenario presented in the first chapter for the yarn short period response. The evolution of the yarn cross section provided by the two constitutive law will be discussed and compared with that obtained by the microscopic study. In the same way a global energy balance will be performed for the two mesoscopic models. Here the contact initialization, section rearrangement and regime states will be identified and their energy trends compared with those from the microscopic simulation. In the final part, the trends of elementary strain energy densities from hyperelastic model will be analyzed and discussed.

4.7.1 Impact Scenario

In order to perform a fair comparison with results presented in the first chapter, the same impact scenario of Section 3.4 has been considered. The yarn finite element model as the material parameters adopted for the hyperelastic and linear elastic constitutive law are the same used in the long term response analysis.
The same automatic surface-to-surface contact adopted for the other mesoscopic analyses is assumed for projectile-yarn interaction with a friction coefficient of 0.18.

4.7.2 Yarn kinematic during the impact

According to microscopic results, the yarn response during the first stage of an impact can be divided in four different stages. Contact initialization stage goes from the first contact among the yarn fibers and the projectile up to the reflection of the compressive transverse wave. Here yarn internal energy is mostly associated to fiber transverse deformation while kinetic energy raises regularly due to fibers acceleration. Fibers bounce starts when the compressive wave reach the cross section boundaries and ends once yarn fibers begin their rearrangement. During this stage a strong increment in yarn kinetic energy is recorded. Then fiber rearrangement stage followed by regime state occur and longitudinal, transverse and spreading wave are free to propagate.

The evolution of the cross section at the yarn center for the linear elastic and hyperelastic models have been reported in Fig. 4.25 and compared to the microscopic results. During the contact initialization both linear and hyperelastic yarn models present the same behaviour, 0 µs-0.25 µs. Yarn is compressed on the top while the bottom still appears to be undeformed. Propagation of the transverse compressive wave does not appear in mesoscopic models due to the coarse mesh adopted. During cross section reorganization phase the first differences between the two mesoscopic constitutive models arise,0.5 µs. Higher displacement values are recorded for the hyperelastic yarn while its cross section shape is qualitatively more similar than the linear elastic one to that observed in microscopic simulation.
The previous observations are still valid in the regime phase where higher displacement value are recorded for the hyperelastic model and spreading wave propagation is observed.

4.7.3 Energetic Analysis

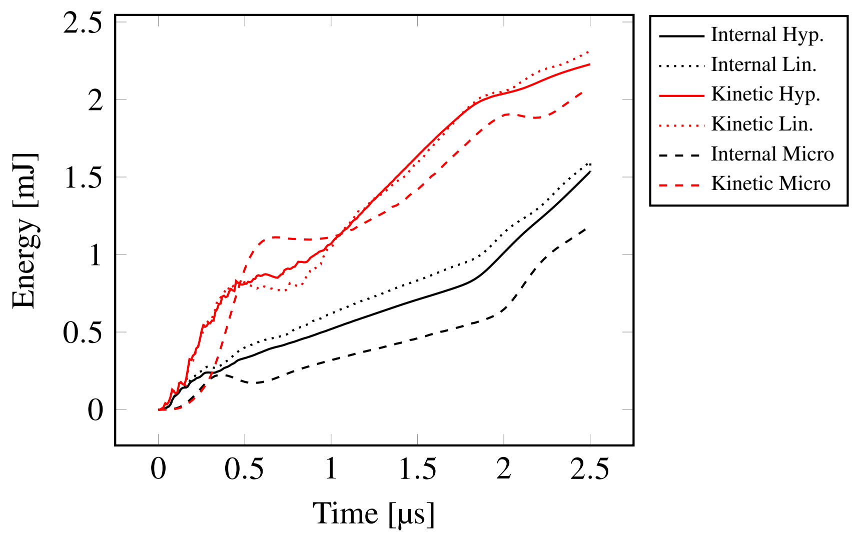

Fig. 4.26 Energy comparison among micro and mesoscopic model for the short time impact response.

Fig. 4.26 reports a comparison among the internal and kinetic energies recorded during the simulations for mesoscopic and microscopic models. Mesoscopic linear elastic and hyperelastic models appear to be in very good agreement for both the energy forms. Internal energy linearly increase for both the models up to the time when longitudinal wave is reflected,

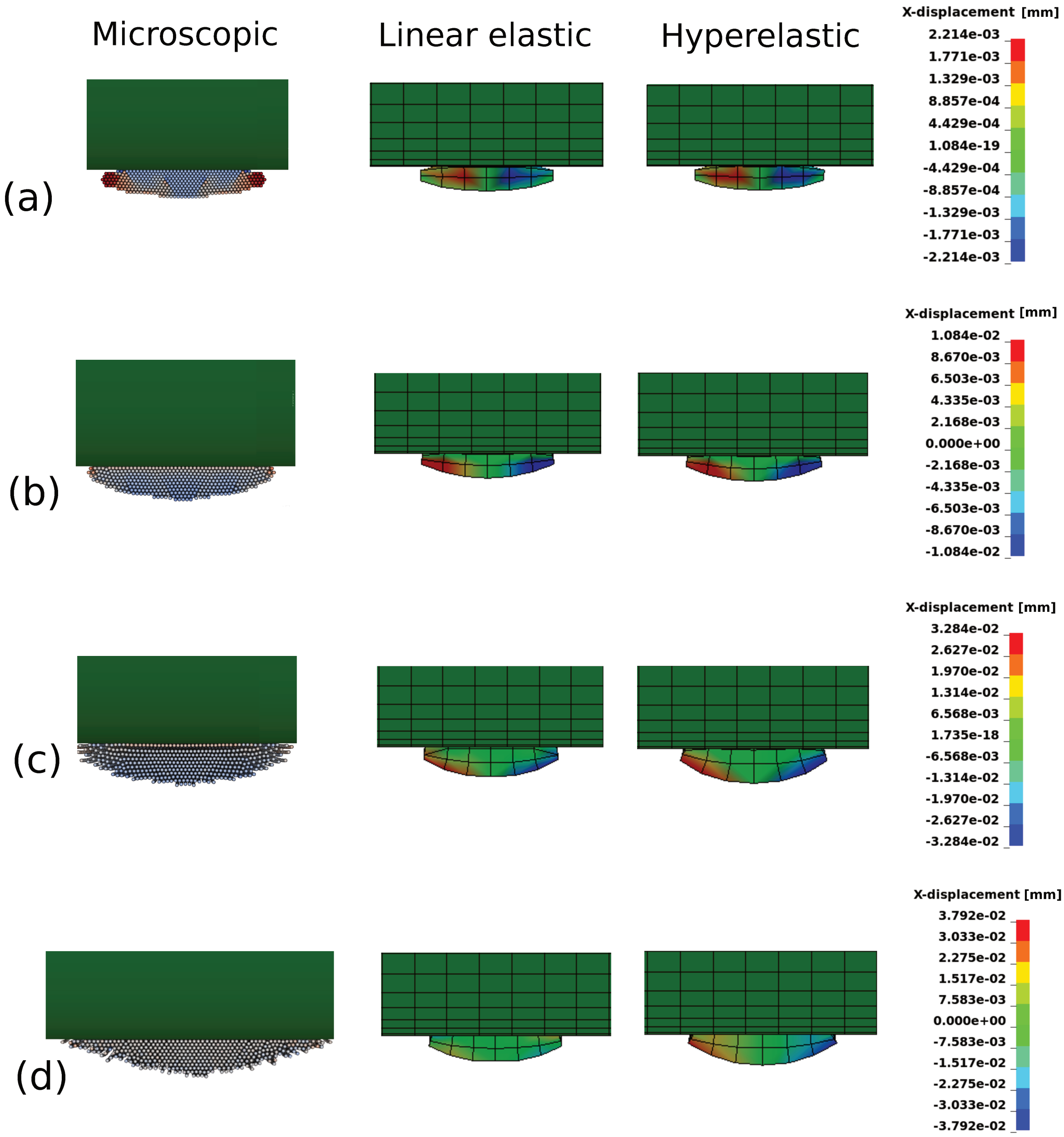

Fig. 4.25 Yarn center cross section at 0.125 µs (a), 0.25 µs (b), 0.5 µs (c), 1.5 µs (d) for microscopic and mesoscopic models.

2 µs. This form of energy presets a lower value for the hyperelastic model, then closer values to those registered in the microscopic approach. Unfortunately an overestimation of the internal energy is obtained for both the mesoscopic models compared to the microscopic approach. This fact can be explained by the flexural modes which are intrinsically included in the continuum approach. These are completely neglected in the microscopic analysis due to the choice of the pin-joined model.
On the other hand, kinetic energy assumes higher values for the micro model. This energy presents the same trend during the contact initialisation phase for both the mesoscopic models, then they differentiate from 0.5 µs. At this point the section rearrangement phase begins and, as saw from the cross section evolution, hyperelastic model behave differently. Here spreading wave initialisation and wider section is recorded in the hyperelastic case which are related to higher kinetic energy values.
Both the mesoscopic models presents the same yarn sonic velocity. Wave reflection time is coherent with the microscopic one then a good representation of the sonic properties is confirmed.

4.7.4 Local energy trends

The evolution of the elementary strain energies density field provided by the hyperelastic model has been analyzed for the long time impact case. It was found that strain energy density associated to fiber elongation propagates as the longitudinal wave while those associated to transverse modes remains confined to the contact zone, Fig. 4.21-4.22. Obviously here the same evolution is found.
An interesting observation concern the evolution of the maximum value of elementary strain energy densities associated to each mode, Fig. 4.27. As for microscopic analyses, the first two stages of the impact at this time scale are evident. During contact initialisation, 0 µs-0.25 µs, both the strain energy maximum values associated to transverse modes drastically increase. Their value is much higher compared to that recorded for longitudinal elongation which remains negligible up to 0.5 µs. This is actually representative of the observed microscopic dynamic where internal energy associated to fiber elongation appears to be negligible during this stage. Fibers bounce stage begins at 0.25 µs when a decreasing trend for transverse compaction and distortion strain energy is observed. During this time longitudinal elongation term keeps to increase up to the end of the stage, 0.5 µs. The regime phase is characterized by internal energy stored under longitudinal elongation and transverse distortion while no contribution is given by transverse compaction. Longitudinal wave reflection is marked by a strong increment of the maximum value associated to longitudinal elongation elementary strain energy.

Fig. 4.28 reports the trends of the maximum transverse compaction strain energy density and microscopic contact energy both adimenzionalized with their maximum values. Contact initialisation stage appears to be shorter in mesoscopic analysis while a good correlation is obtained for the transverse section rearrangement phase. However their trend appear very similar and actually confirms the physical interpretation of the elementary strain energies previously provided.

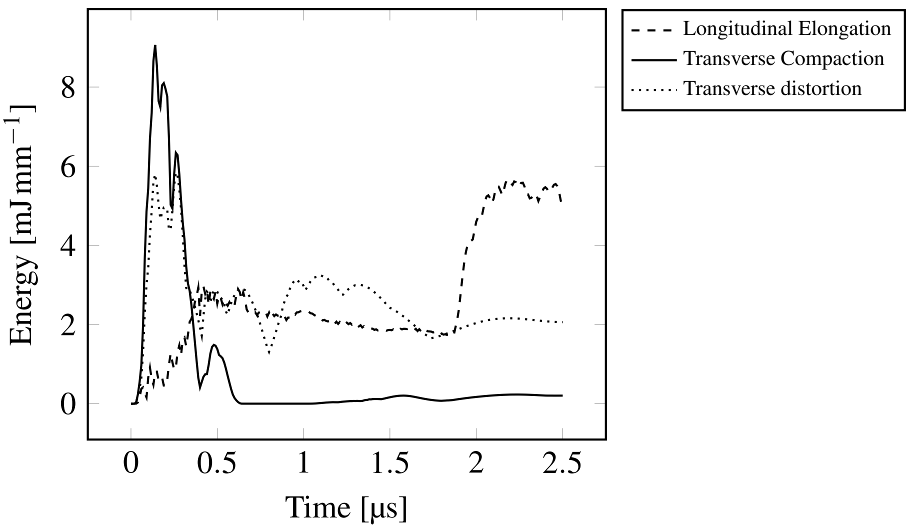

Fig. 4.27 Maximum elementary strain energies during the impact.

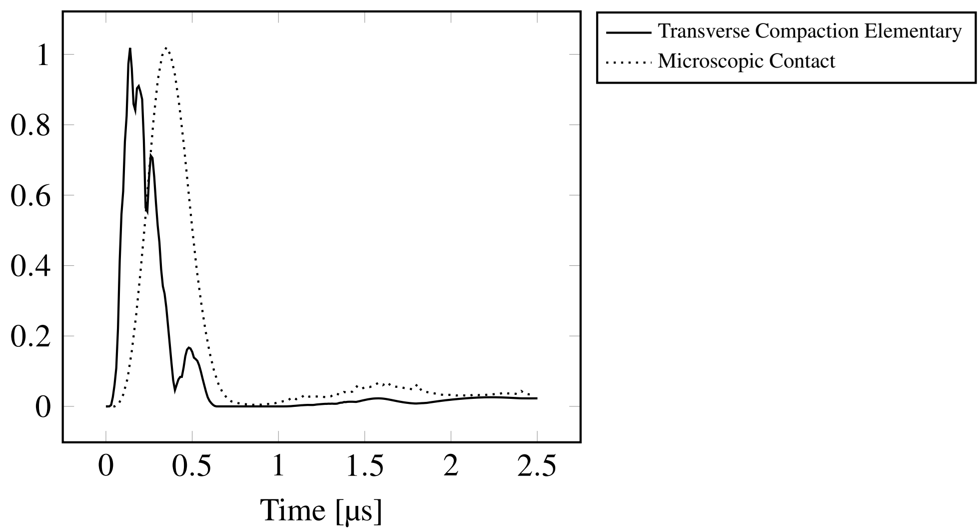

Fig. 4.28 Adimenzionalized value of maximum transverse compaction strain energy and microscopic contact energy.

4.8 Conclusions

In the present chapter a novel hyperelastic constitutive law for yarn mesoscopic models has been presented and implemented as a UMAT in the commercial software LS-DYNA. Aim of the proposed model is to take into account the yarn transverse behaviour during mesoscopic simulations and opens new possibilities in terms of yarn failure modelling. A first theoretical introduction to the model has been followed by the presentation of a novel material parameters identification strategy. The proposed approach consists in solving three different independent identifications problems taking advantage of numerical / analytical solutions and it is able to relate yarn threedimensional properties to fiber level mechanic. A novel failure modellisation strategy has been even introduced. This takes advantage of the hyperelastic formulation to provide failure criteria based on deformation modes rather than stresses nor strains. Thanks to this approach a physical way to model yarn 'multiaxial' failure has been introduced.

The proposed constitutive law has been validated using previous microscopic results and compared classical linear elastic approach. Results shown how the two mesoscopic models are in very good agreement with microscopic results for long term analyses. The energy absorption process and transverse wave propagation are equivalent for the two models, however they differ for the kinematic of the yarn cross section and projectile residual speed. Compared to the linear elastic approach, the proposed hyperelastic model is able to represent the propagation of the spreading wave and is much closer to microscopic projectile residual speed when a proper multiaxial failure criterion is adopted.

The same validation procedure has been even applied to a short term analysis. In terms of energies, the two mesoscopic models are in good agreement between each other however there is still a difference with microscopic results. The hyperelastic constitutive behaviour is able to provide a better representation of the yarn center cross section evolution during the impact and energy trends closer to that observed at the microscale.

One more advantage of the proposed constitutive law is the possibility of following the evolution of elementary strain energies during the impact. These are associated to elementary deformation modes and related to microscopic phenomena. From their trends it is possible to understand the type of load experienced by the yarn and what kind of energy is stored in each part of the fabric.

At this point the hyperelastic model can be applied at the fabric level in order to test its ability in representing the fabric behaviour under impact.

Chapter 5

Mesoscopic fabric level analysis using yarn hyperelastic model

This last chapter will be focused on mesocopic analyses of a Kevlar fabric layer impacted by a spherical projectile. The previously proposed hyperelastic constitutive law for mesoscopic representation of yarn structures will be adopted at the fabric level and its effectiveness and stability will be tested.
Two different impact scenarios will be assumed, namely a penetrating and non-penetrating one.
In the first case failure criterion is not considered while kinematic and energetic trends of the fabric during the impact will be analyzed.
In the second case the projectile striking velocity is sufficient to induce fabric failure, then failure criterion will be included and projectile residual velocity will be even analyzed.
Three different model variations will be considered for each of the two impact scenarios. The first two are based on an hyperelastic and linear elastic representation of the yarns respectively. Here the totality of the filaments have been modeled using a single constitutive law. The third is based on a hybrid formulation of the panel. In this case the hyperelastic constitutive model is confined to the impact zone, where important contributions of yarns transverse modes are expected, while the rest of the layer is traditionally modeled. Comparing the results obtained for the same impact scenario it is possible to validate the hyperelastic approach at the fabric level. The validation procedure will be based on the comparison among macroscopic data as fabric internal, kinetic energy and global displacements. Moreover the advantages in terms of model stability and elementary energies mapping will be finally presented.

5.1 Impact scenario

The impact scenario is presented in Fig. 5.1 [113]. It consist of a single ply of a plain-woven Kevlar S706 fabric impacted by a spherical projectile. The assumed fabric presents a count of 34 yarns per inch in warp and weft direction, an areal density of 180 g/m^2 and is comprised of the same Kevlar KM2 600 yarns previously modeled at the microscopic and mesoscopic scale. In the experimental reference the fabric was clamped into a steel frame with a circular aperture of 50.8 mm which left a circular area exposed to the impact. The bullet is a stainless steel sphere with a diameter ϕ of 5.56 mm, a mass m of 0.692 g. A penetrating and a non-penetrating impact have been analyzed with a striking velocity of 142 $\mathrm{m\,s^{-1}}$ and 63 $\mathrm{m\,s^{-1}}$ respectively.

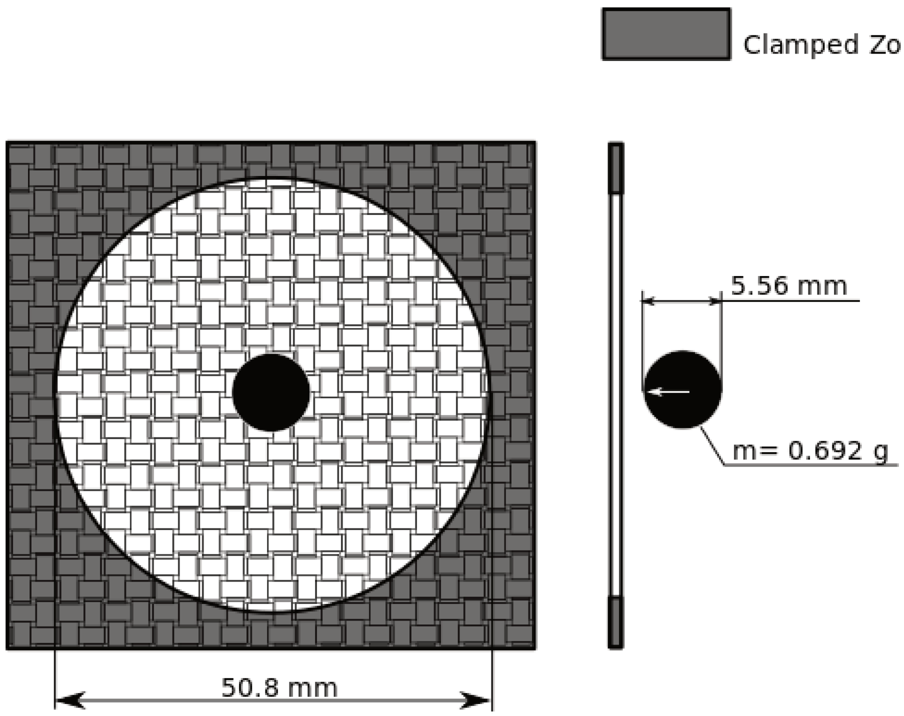

Fig. 5.1 Fabric impact configuration.

The finite element model have been implemented in the commercial software LS-DYNA and is presented in Fig. 5.2. Taking advantage of the problem symmetry, a quarter of the original fabric exposed area has been modeled using a mesoscopic approach. Yarns are assumed as a continuous body and the weaving geometry is explicitly considered. The warp and weft count results in a yarn span of 0.747 mm in both the directions while fabric total thickness is equal to 0.230 mm [100]. Yarns cross section is equal to that presented in Section 4.6 with major and minor axes respectively equal to 0.5337 mm and 0.115 mm which results into a yarn volume fraction ν of 0.93848. Each one of the Kevlar KM2 600 yarns is composed of 400 Kevlar KM2 fibres whose main physical properties are presented in Table 4.2. A detailed description of the procedure used to identify the yarns material parameters have been presented in Section 4.5 - 4.6. Here the main results are resumed in Table 5.1 and Table 5.2 where the material parameters for the hyperelastic and linear elastic yarn model are respectively presented. Yarn failure has not been included for the non-penetrating impact models while maximum longitudinal elongation invariant and maximum principal stress criteria presented in Section 4.6.3 have been adopted in penetrating impact models for hyperelastic and linear elastic yarn modelling respectively.

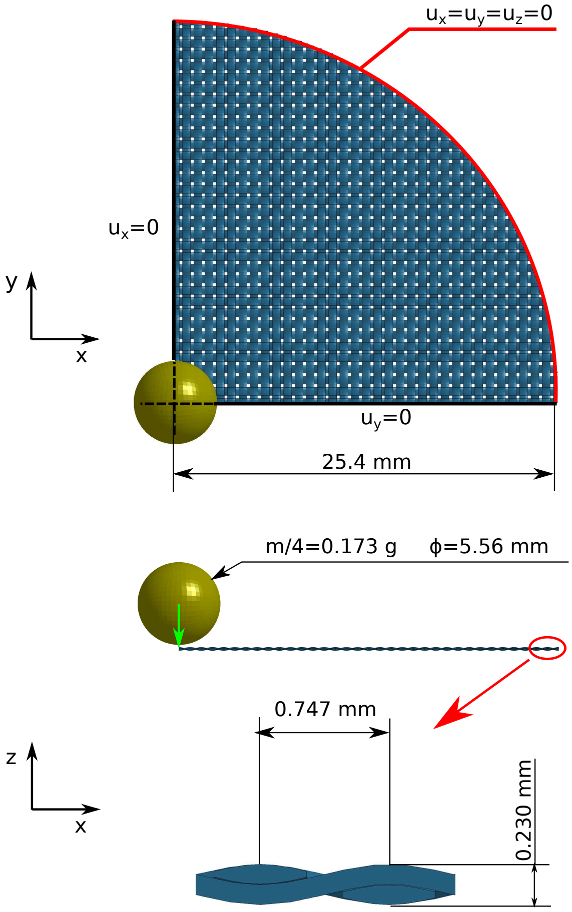

Fig. 5.2 Fabric finite element model.

Table 5.1 Properties of hyperelastic Kevlar KM2 yarn model.

k_{el}(GPa)	k_{tc}(GPa)	p	k_{td}(GPa)
82.341	1.055	2.2	0.649

Table 5.2 Properties of linear elastic Kevlar KM2 yarn model.

E_1 [GPa]	$E_2 = E_3$ [GPa]	$\nu_{23} = \nu_{12} = \nu_{13}$	$G_{23} = G_{13} = G_{12}$[GPa]
79.414	0.794	0	0.126

The same mesh size used for the yarn studies here have been adopted. Yarn cross section is discretized using twelve eight nodes reduced integrated brick element while element size along yarn center line is equal to 0.0906 mm. The whole fabric is comprised of 98059 elements and 173819 nodes.

The spherical projectile is considered to be rigid while its original mass have been divided by four due to symmetry conditions.

Symmetry boundary conditions are applied on the two symmetry planes of the fabric while nodes on the external arc have been fixed in order to simulate clamping. An initial velocity of 63 $\mathrm{m\,s^{-1}}$ along the z axis have been imposed to the projectile while zero displacements along the x-y axes have been imposed due to symmetry.

An automatic surface-to-surface contact has been chosen for the projectile-yarn and yarn-yarn interactions with a static friction coefficient of 0.23 and 0.18 respectively [75].

Three different variations of the described model for both the penetrating and non-penetrating impact have been implemented and their results compared, Fig. 5.3. In the first two a single constitutive law have been employed for the yarns. The proposed hyperelastic formulation and linear elastic constitutive law have been used in the first and in the second variation respectively. On the other side, the third one is based on a mixed representation of the fabric where hyperelastic constitutive law is used in the central zone of the layer while linear elastic approach is adopted in the remaining part. The dimentions of the hyperelastic area have been chosen as the smallest ones which assure no contact among the projectile and the linear elastic zone. In this way it is easily possible to verify the compatibility among the two approaches and adopt a more complex formulation just in the contact zone where complex strain states are expected.

5.2 Results

5.2.1 Non-penetrating case

The hyperelastic, linear elastic and hybrid version of the model reported the same results in terms of global kinematic. Fig. 5.4 reports the vertical displacement of the fabric during the impact for the hyperelastic model. The initialization and propagation of the transverse wave in the fabric plane and the resultant pyramidal shape is clearly observed. The wave begins

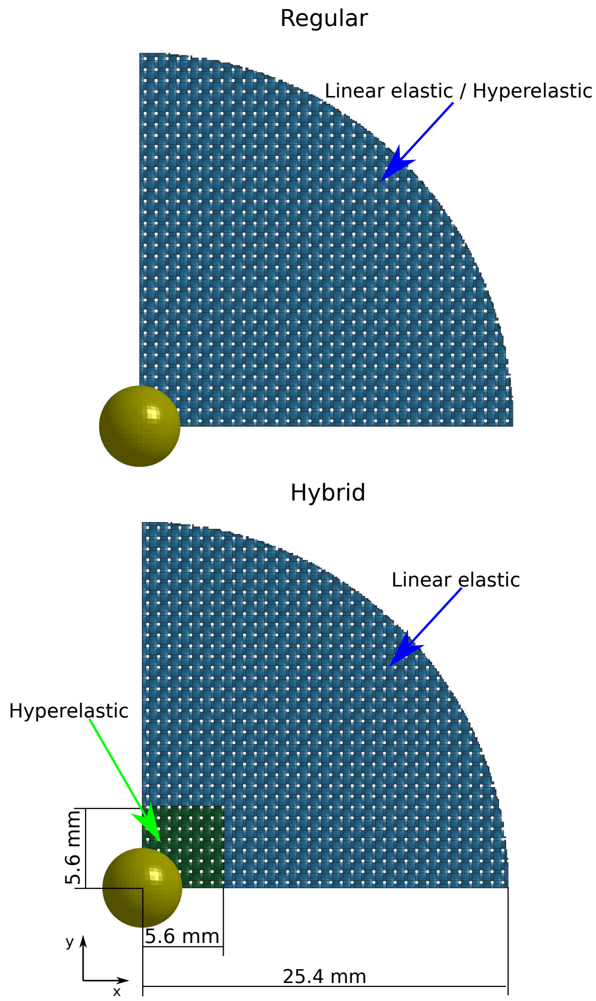

Fig. 5.3 Regulars and Hybrid variations of the fabric model.

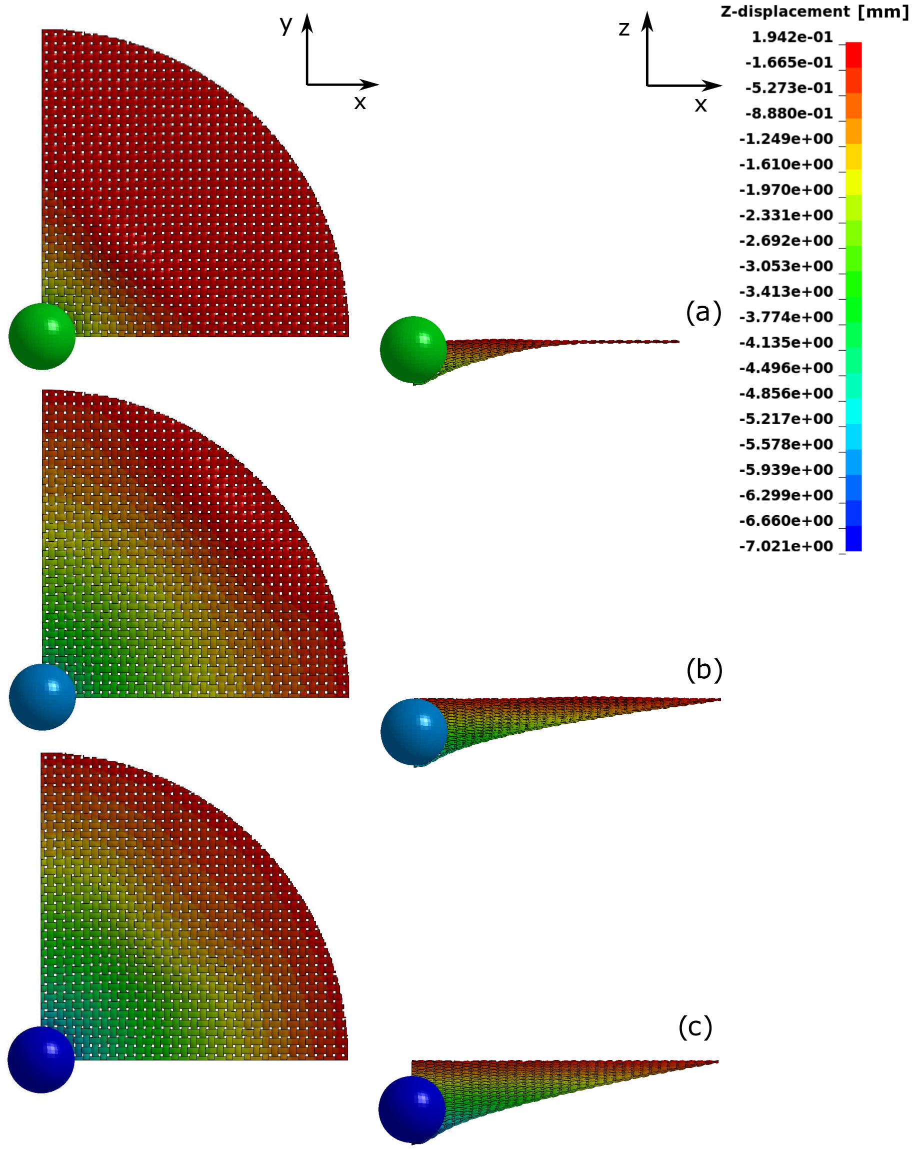

Fig. 5.4 Transverse wave propagation recorded using hyperelastic formulation for the yarns at 60 µs (a), 100 µs (b), 148 µs (c).

to propagate after the first contact among the projectile and the fabric , 0 µs-100 µs, than it reaches the clamped zone, 110 µs, and it is finally reflected, 120 µs-160 µs.

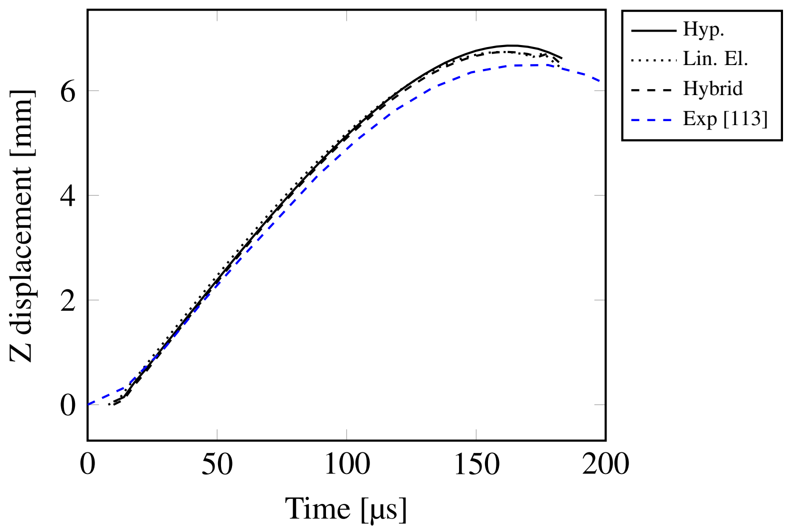

Fig. 5.5 Maximum Z displacement of the fabric impacted at 63 $\mathrm{m\,s^{-1}}$.

Fig. 5.5 reports the maximum displacement along the vertical direction of the fabric during the impact for the three different cases. All numerical models are in very good agreement among each other with a maximum displacement around 6.8 mm instead of the 6.5 mm experimentally recorded [113]. The numerical results are very close to the experimental reference in terms of trends and maximum values.

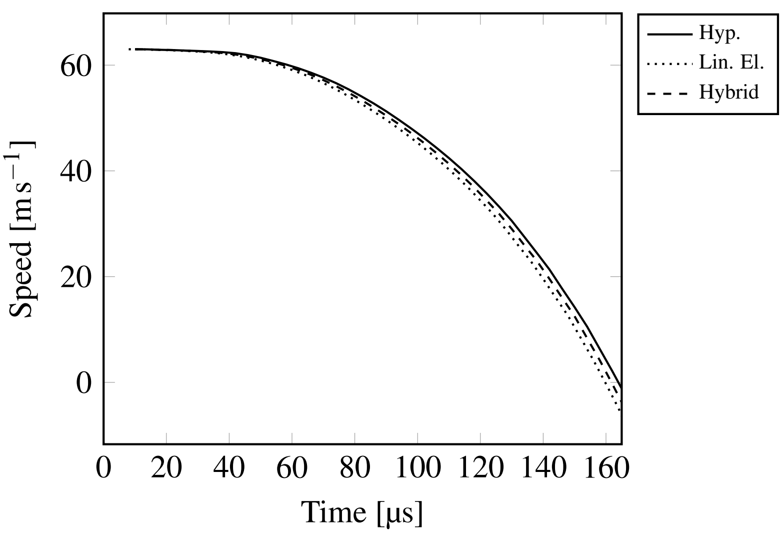

Fig. 5.6 Projectile speed trend for the fabric impacted at 63 $\mathrm{m\,s^{-1}}$.

The projectile speed trends for the three different approaches are presented in Fig. 5.6. Even in this case the hyperelastic, linear elastic and hybrid variations are equivalent among each other.

The evolution of energies absorbed by the fabric during the impact are reported in Fig. 5.7 for the three different versions of the model. Kinetic and internal energies both increase during the first phase of the impact, 0 µs-110 µs. When the transverse wave reaches the clamped boundaries, a reduction and an increment of fabric kinetic and internal energy respectively is observed due to wave reflection. The following energy oscillations are still related to transverse wave reflections. Friction energy appears negligible compared to the others.
It is interesting to underline how the results obtained for the hybrid variation of the model are very similar with those obtained by the linear elastic one. Both presents an internal energy slightly higher than the hyperelastic version. This results in a slightly slower bullet deceleration.

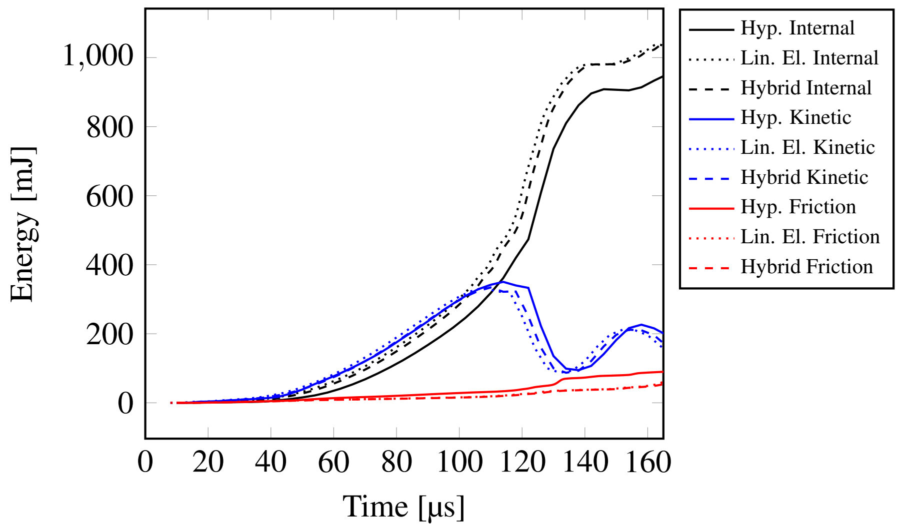

Fig. 5.7 Fabric energy trends for an impact at 63 $\mathrm{m\,s^{-1}}$.

Local energy trends

For the hyperelastic and hybrid variations of the model it is possible to follow the evolution of the elementary strain energies as performed for a single yarn, Section 4.6.2. In order to follow it in the whole fabric, the results of the hyperelastic model variant will be presented hereafter.

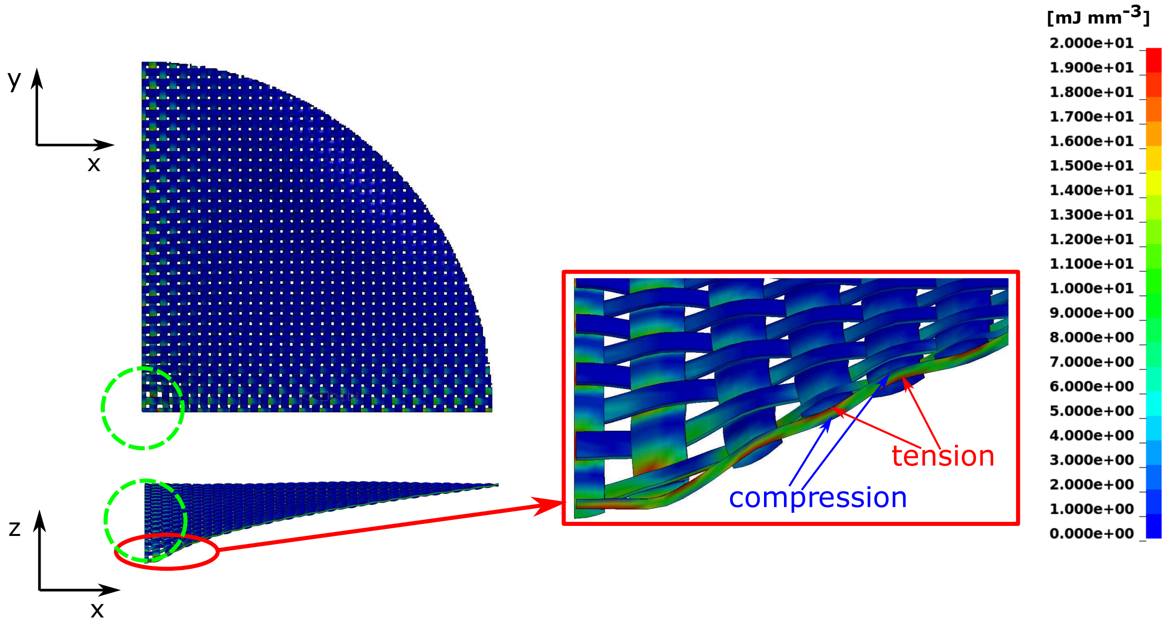

Fig. 5.8 Longitudinal elongation elementary strain energy field at 100 ms.

Fig. 5.8 reports the elementary strain energy density associated to longitudinal elongation in the fabric at 100 µs. At this time a maximum value of 29.02 mJ mm^{-1} is registered near the impact zone while no elongation energy is recorded in secondary yarns far from this point. As expected, primary yarns present the highest values of energy stored as fiber longitudinal elongation. The energy field does not appears to be homogeneous within these yarns, however it presents a periodic pattern along their lengths and cross sections. This result is related to the fabric weaving geometry. Before yarns get strained they are actually de-crimped. The de-crimping process induces a yarn centerline curvature variation which results into an alternations of elongated and compressed zones at the cross-over points, Fig. 5.8.

Fig. 5.9 reports the elementary strain energies associated to transverse compaction and transverse distortion at 100 µs. Highest values of both the elementary energies are recorded where contact with the projectile is established. Here a maximum value of 7.84 mJ mm^{-1} and 6.07 mJ mm^{-1} have been found for transverse compaction and transverse deformation respectively.
Small values of energy are even registered outside the impact zone. Here the elementary strain energy values are around 0.1 mJ mm^{-1}, then one order of magnitude lower than those recorded at the impact point. It is interesting to notice how values of 0.2 mJ mm^{-1} are recorded at the cross over points where warp and weft yarns get in contact. This is actually related to the yarns de-cirmping process which raise the contact pressure at the cross over

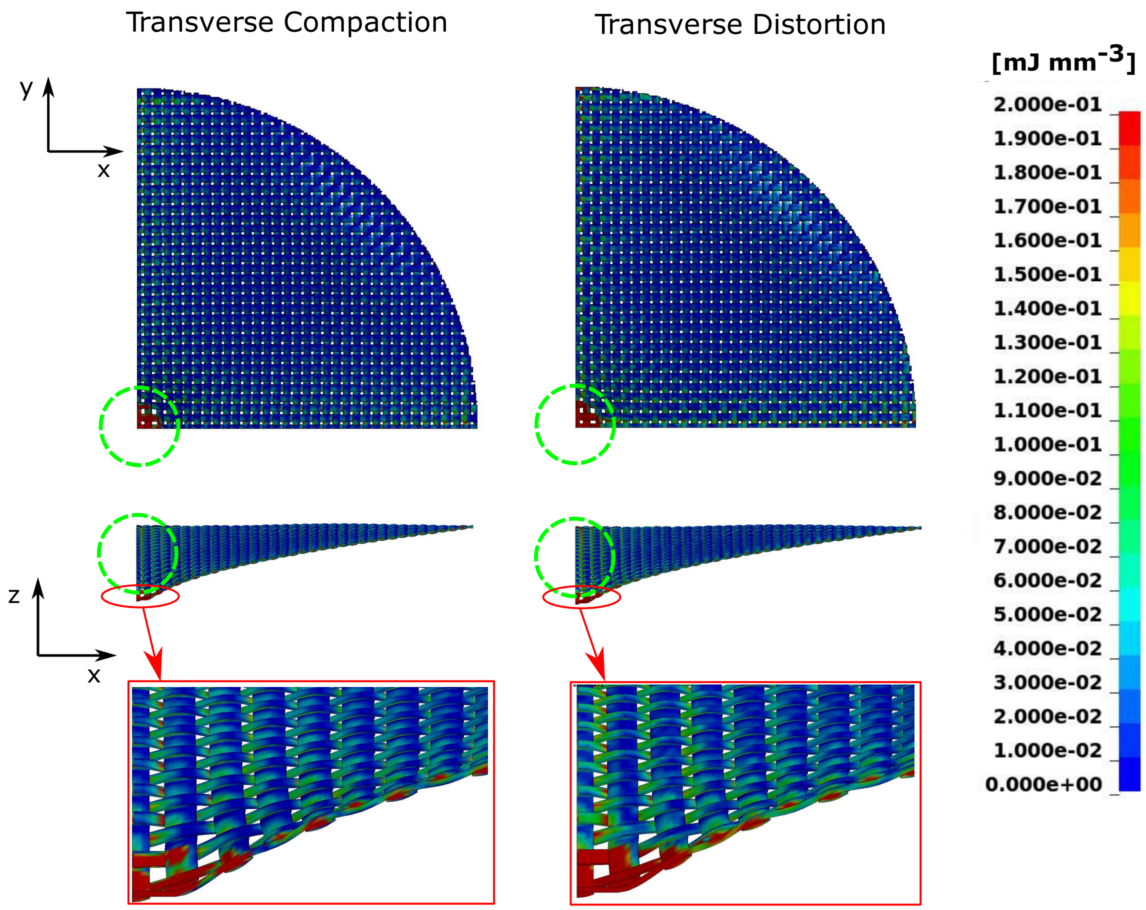

Fig. 5.9 Transverse compaction and transverse distortion elementary strain energy fields at 100 μs.

points among warp and weft filaments, Fig. 5.9.

Fig. 5.10 reports the evolution of the maximum values assumed by the elementary strain energies during the impact. As previously observed for the yarn, the maximum elementary energies are comparable during the first phase of the impact when the projectile get in touch with the fabric, 0 µs - 40 µs. After this time all the maximum recorded energies continuously increase and longitudinal elongation becomes predominant with a value of 134.51 $\mathrm{mJ\,mm^{-1}}$ compared to the 21.59 $\mathrm{mJ\,mm^{-1}}$ and 16.21 $\mathrm{mJ\,mm^{-1}}$ of transverse compaction and distortion respectively.

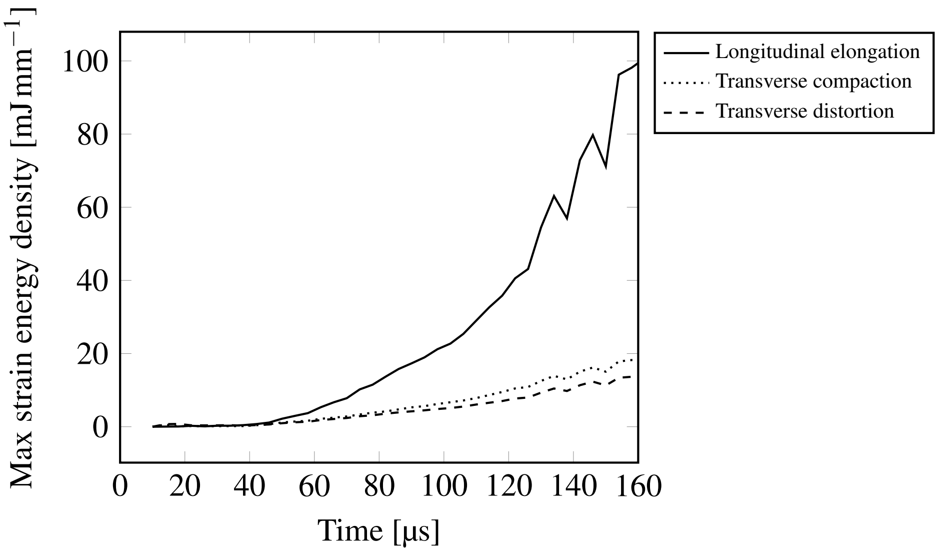

Fig. 5.10 Evolution of maximum values of elementary strain energy densities in a fabric impacted at 63 $\mathrm{m\,s^{-1}}$ by a spherical projectile.

5.2.2 Penetrating case

Fig. 5.11 reports the different phases of the impact observed using the proposed hyperelastic approach. The transverse wave is initialized and propagated while projectile penetration occurs at 44 µs. The same low-velocity penetrating impact dynamic is observed for the other two variations of the models.

Some differences in fabric failure desccription have been found among the three proposed approaches. It is worth to underline how a better description of the failure event is provided by the hyperelastic and hybrid models compared to the linear elastic ones, Fig. 5.12. The first two modelling strategies are able to catch important yarn transverse deformation during

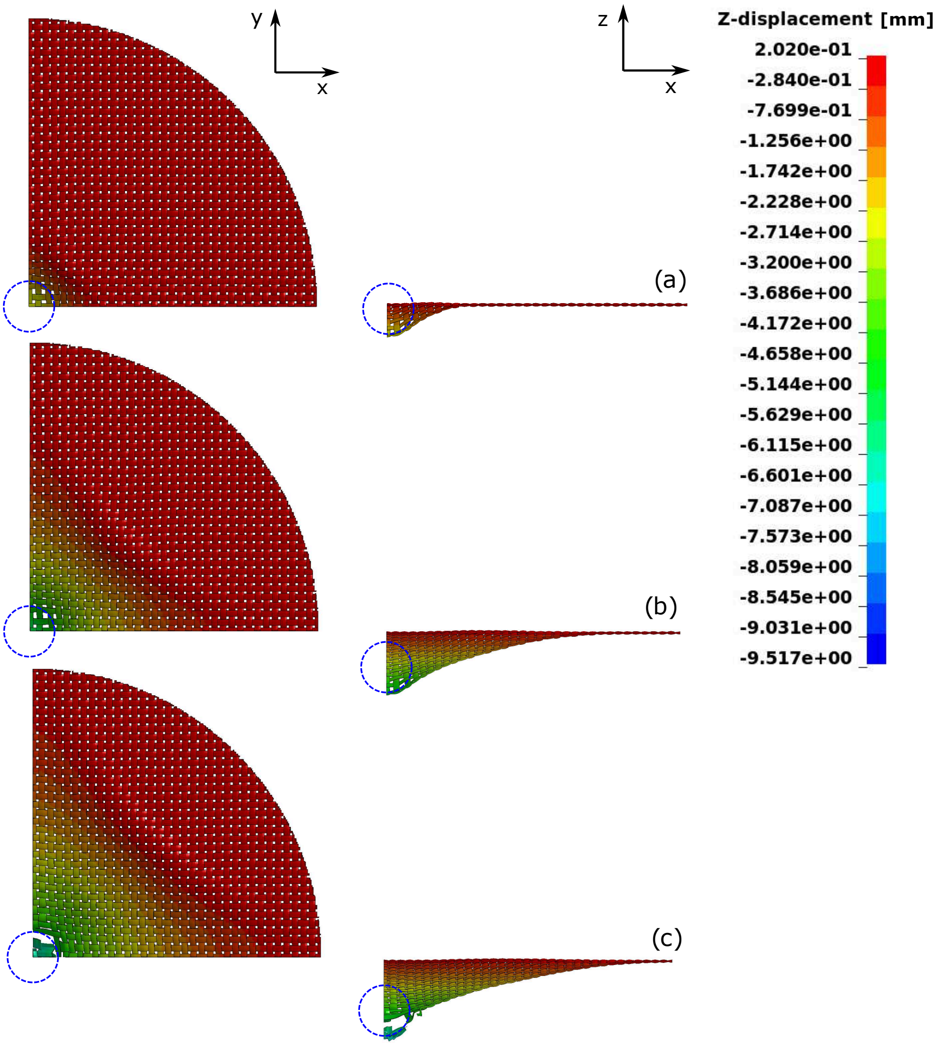

Fig. 5.11 Fabric kinematic recorded at 20 μs(a), 40 μs(b), 48 μs(c) for an impact at 142 $\mathrm{m\,s^{-1}}$ where hyperelastic formulation for the yarns has been adopted.

failure, Fig. 5.12 (a). Moreover these two models resulted in a much more stable simulation compared to the linear elastic one where a long calibration of the hourglass parameters was required to get model stability and physically induced failure.

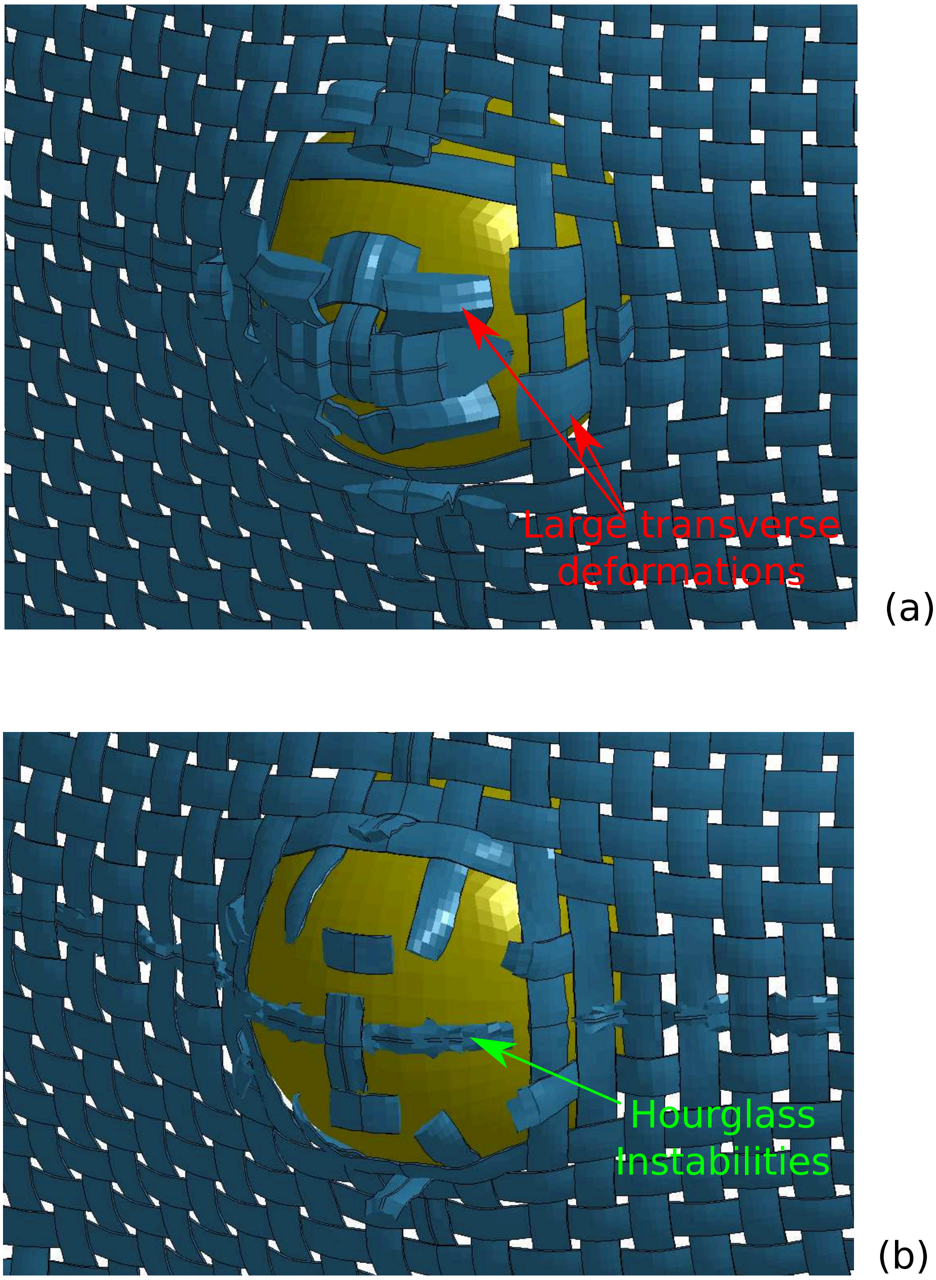

Fig. 5.12 Fabric failure kinematic for hyperelastic/hybrid (a) and linear elastic (b) variation of the model.

In Fig. 5.13 the global results in terms of maximum vertical displacement are compared. All the curves are traced up to the failure time of the fabric. This has been identified as the

time for which a different increasing displacement rate was observed.
All the three models accurately describe the linear trend obtained experimentally, moreover a good agreement is obtained among the three curves up to the failure time. Failure instants resulted to be different for the three models. Penetration occurs at 30 µs for the linear elastic variation and 44 µs for the hyperelastic and hybrid model. This resulted in a maximum displacement at failure time of 4.2 mm, 5.9 mm, 6 mm for the linear elastic, hyperelastic and hybrid model variation respectively. Failure instants are coherent with those observed in Section 4.6.3 where hyperelastic yarn model resulted in higher resistance compared to the linear elastic one. It is worth to underline how the hybrid model failure instant resulted equal to that of the hyperelastic one. This actually emphasize how the yarn properties in the impact zone play a key role in failure initialisation.

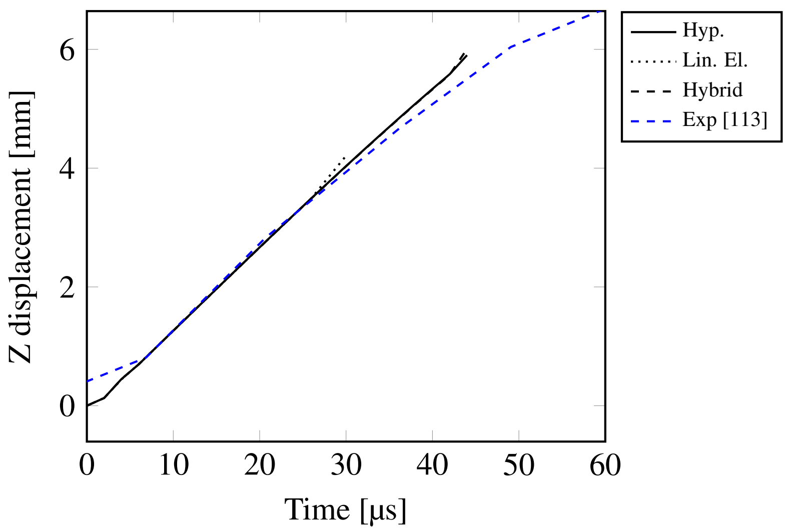

Fig. 5.13 Maximum Z displacement of the fabric impacted at 142 $\mathrm{m\,s^{-1}}$.

Fig. 5.14 reports the bullet speed trend during the simulations. As observed for the maximum vertical displacement, even in this case the three curves are in very good agreement before fabric failure. Different failure initialization times are evident from the curves. Here a residual velocity of 134.31 $\mathrm{m\,s^{-1}}$, 120.33 $\mathrm{m\,s^{-1}}$, 120.75 $\mathrm{m\,s^{-1}}$ for the linear elastic, hyperelastic, hybrid case respectively is obtained. Experimental results showed a residual velocity of 75 $\mathrm{m\,s^{-1}}$ which is unfortunately far lower than the numerical predictions. This obviously represents a critical point for all the three numerical models and it will be discussed at the end of the chapter.

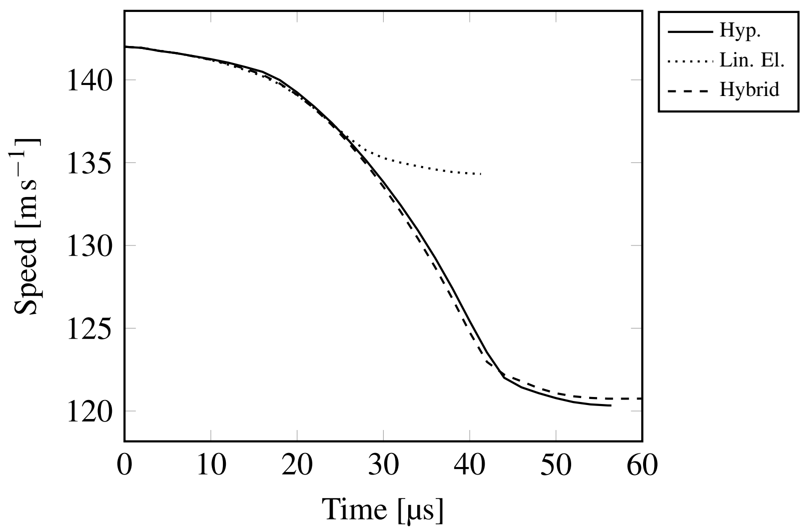

Fig. 5.14 Projectile speed trend for the fabric impacted at 142 m s^{-1}.

Finally energy balance of the fabric during the impact for the three case is presented in Fig. 5.15. For all the three models, fabric internal and kinetic energy raise during the impact up to failure instant (30 µs for the linear elastic variation, 44 µs for the others). When failure occurs fabric internal energy is converted in kinetic one and, at the same time, induced yarn mobility brings to consistent energy dissipation by yarn-to-yarn friction.

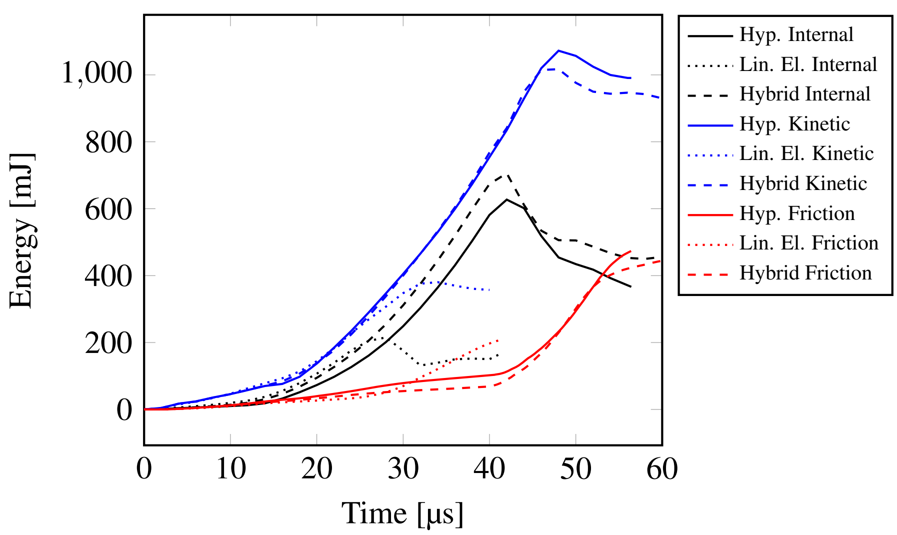

Fig. 5.15 Fabric energy trends for an impact at 142 m s^{-1}.

5.3 Discussions

Results obtained in the current chapter actually confirm the previous observation performed at the yarn level. The proposed hyperelastic approach demonstrates to accurately describe the fabric response in non-penetrating and low-velocity penetrating impact scenarios. From Fig. 5.15-5.7-5.14,5.6 it is clear that the proposed constitutive law gives the same consistent results in terms of energy and projectile speed trends than linear elastic model. In this type of impact scenarios, where a large zone of the fabric is involved in the impact energy absorption process, the energetic contribution of transverse mode is expected to be negligible and the two approaches results to be equivalent, apart from failure modelisation. Concerning this last point, the results obtained in Chapter 4 are confirmed. Assuming the same physical failure criterion for both the constitutive laws, the hyperelastic model presents higher resistance compared to the linear elastic one. This results in lower projectile residual speed and better agreement with the experimental observations. Unfortunately, both penetrating impact models resulted in an overestimation of the projectile residual speed compared to the experimental reference. This problem cannot be related to the inclusion of yarn transverse effect since fiber damage would increase projectile residual speed. According to the author, the overestimation of the projectile residual speed is probably related to some approximation performed in the numerical model. First of them, the fabric geometrical representation. In a first step, the TexGen library [80] has been adopted to model the fabric as a geometrically perfect entity. Then, the obtained geometry has been modified suppressing the excessively distorted elements which could led to numerical instabilities. This results in lower fabric firmness compared to the reality which favorites yarn mobility and premature failure [24, 117]. A more complex approach to fabric geometric modelling should be adopted in order to solve this problem [71, 72]. Other aspects which could give their contributions are yarn mesh type and the hourglass numerical treatment.

Despite the previous mentioned reasons, the difference among the numerically predicted projectile residual speed and the experimental reference appears to be too high. This statement is even more valid if the latest work on the subject are analyzed [21, 71]. Here a good correlation among experimental and numerical results is obtained using the classical linear elastic approach. This is actually an encouraging point, since the residual velocity difference between the proposed and the classical approach is around 10% of the striking one.

Deeper investigation of the proposed law at the fabric level are still required to clarify this aspect. Moreover, the support of internally developed experimental tests will be helpful to the study.

Concerning the advantages offered by the proposed model compared to the classical one, stability is added to those observed in Chapter 4. The proposed hyperelastic model gives a better description of the yarns kinematic near the impact zone combined with a low risk of having elements negative volumes due to high deformation. This is actually related to the physical determination of the material law parameters and to strain energy formulation based on physical invariants. The advantages offered by the porposed model can be even adopted in localized areas of the fabric, as demonstrated by the hybrid models results.

5.4 Conclusions

In the present chapter the proposed hyperelastic constitutive law for yarns structures has been tested at the fabric level. A plain-woven Kevlar S706 fabric has been modeled in two different impact scenarios, namely a sub-ballistic and a low-velocity perforating one, using a mesocopic approach. For each of the two impact scenarios three different version of the model have been developed where hyperelastic, linear elastic and an hybrid hyperelastic/linear elastic formulation were employed for the yarns.
Results showed how the three different formulation of the models are actually equivalent in representing fabric dynamic and energetic history.
Unfortunately all the three proposed approaches overestimate projectile residual velocity according to the experimental references. The state of the art of mesoscopic fabric modelling actually demonstrates the predictive abilities of the linear elastic model for fabric single layers [71]. The current results showed that the proposed approach is at least as good as the linear elastic one while offering new possibilities in terms of failure modelling, postprocessing and more stables simulations.

Chapter 6

Conclusions and Perspectives

The current thesis work focused on the development of a predictive numerical model of dry fabrics under high velocity impact. In the first chapter, the context and the objectives of this dissertation have been presented.
An extensive bibliographic study on textiles materials under impact loading and their modelling is performed in the second chapter.
A mature bibliography exists on these subjects. The impact phenomenon can be essentially resumed as an energy transfer between the colliding object and the fabric layers. The entire projectile energy is absorbed by the fabric when no penetration occurs, otherwise the bullet will save part of its initial energy even after the impact.
The correct prediction of the fabric ballistic performance by a numerical model is intrinsically related to the correct representation of the fabric energy evolution. This is obtained if two conditions are fulfilled by the model:

- The correct representation of the structure inertial and mechanical properties. This ensures the correct trends of the fabric kinetic, internal and friction dissipated energy.

- The correct formulation of a failure criterion. This guarantee that the energy transfer among the structure and the bullet is interrupted at the right time in the case of penetration

Different numerical strategies have been proposed to model a fabric under ballistic impact. Mesoscopic numerical models resulted to be the most popular since they provide a realistic representation of the phenomenon for a reasonable computational cost. This is possible thanks to the main assumption of treating yarns as continuous media. In order to represent a discrete fiber bundle as a continuum an appropriate constitutive behaviour have to be formulated. The universally adopted constitutive law accurately describes yarns longitudinal

properties but it is limited in the representation of their transverse mechanical behaviour. Recent studies have demonstrated how this last point is intrinsically related to fabrics failure and multi-layer textiles response, then its correct representation becomes a critical point for an accurate model. The goal of the current work has been to provide a new constitutive model which overcome the limitation of the classic linear elastic approach while keeping unaltered its advantages, i.e. low computational costs and accurate description of yarn longitudinal behaviour.
The first step of this study was to quantify the yarn cross section effects over textile ballistic properties and the phenomena related to this aspect. In order to provide an answer, two microscopic numerical studies of a single Kevlar KM2 600 yarn transversely impacted have been presented in the third chapter.
Results showed how yarn transverse mechanical behaviour has a role in failure initialization, when long term yarn response is considered. On the other side, short term yarn response is drastically affected by transverse section mechanic both from the energetic and kinematic point of view. From the obtained results, the importance of a correct representation of the yarn transverse behaviour for a predictive fabric numerical model was confirmed.
The presentation and validation of a consistent yarn continuum model for impact applications is the purpose of the fourth chapter. The hyperelastic formulation presented by Charmetant for static applications has been extended to impact analyses and a novel multiscale approach for the determination of all the material parameters has been introduced. The validation of the hyperelastic approach has been performed comparing the results with those obtained in the third chapter. Compared to the classical approach, the introduced constitutive law is actually able to reproduce the evolution of the yarn cross section during the impact while keeping a correct representation of the yarn longitudinal properties. Moreover, the formulation based on physical invariants provides a useful tool to exploit the physic behind the impact, the phenomena related to yarn cross section and new possibilities in terms of failure modelisation.
The fifth chapter has been dedicated to the application of the proposed constitutive law at the fabric level. Results confirmed the observation performed at the yarn level. The proposed hyperelastic approach is able to correctly represent the impact dynamic and fabric energies trends. Moreover, it is more stable and proved a better representation of the fabric failure compared to linear elastic approach. The proposed hyperelastic constitutive law and the linear elastic one can be adopted for different portion of the same yarn without occurring into model instabilities and providing accurate results. This would reduce the global computational cost of a full hyperelastic mesoscopic model. Unfortunately both the models overestimate projectile residual velocity. Hyperelastic fabric model get closer to bibliographic experimental

references, however they are still far from the experimental results. This could be related to a large number of factors which include assumed yarn mesh type, idealized fabric geometry and impact point uncertainty. What is possible to assert is that all the developed models behaved in a similar way.
The state of the art of mesoscopic fabric modelling actually demonstrates the predictive abilities of the linear elastic model for fabric single layers in low speed penetration regime[71]. The current results showed that the proposed approach is at least as good as the linear elastic one for this type of impact scenarios.

In terms of perspectives, the current dissertation opens new scenaries in yarns and fabrics modelisation.
Yarn microscopic models appears to be a promising tool for fiber-level phenomena investigation and multiscale analyses. Today, these models are still affected by an enormous computational cost. In a near future, with the raising of computational power, they could be used to perform sensitivity analyses at the microscopic scale and investigate the fundamental problem of yarn failure. In order to get there a major effort from all the researchers is required. On one side, more experimental data of fibers and yarns mechanical behaviour under static and dynamic loading are needed to feed and validate more complex numerical models. On the other side, new numerical tools are should be proposed to perform fiber-level analyses keeping a reasonable computational cost.
Concerning yarn mesoscopic modeling, different aspects still have to be improved. The proposed constitutive model still lacks in the representation of some physical phenomena observed in microscopic simulation. Firstly, results obtained showed how yarn response is not purely elastic. Fiber-fiber friction induce non-negligible energy dissipation when the first part of an impact is considered. This aspect is part of yarn cross section behaviour and should be included in the constitutive law. Hyperelastic formulations are conservative by definition, then a different approach should be adopted to accomplish this goal. Secondly, the evolution of the yarn cross section obtained by the proposed model does not completely agree with the observation performed at the microscale. The spreading wave observed in yarn continuum model fully develops outside the impact zone, while yarn immediately spreads under the projectile in microscopic model. This particular aspect could be related to the formulation of the hyperelastic law or to the multiscale approach adopted for material parameter identification. Given a general hyperelastic constitutive law, it is not possible to predict apriori yarn deformations near the impact zone. A different formulation could perform better than the proposed one in representing yarn spreading. An alternative solution would be the adoption of a different strategy for material parameter identification. The proposed multiscale approach

relies on microscopic analyses performed on a RVE. This could brings to an overestimation of some material parameters, as material constants associated to transverse distortion mode. A different strategy could be to perform the same numerical analysis using mesoscopic and microscopic approach and optimize mesoscopic material parameters on microscopic results. As an example, long term yarn energetic response to transverse impact could be adopted to determine yarn longitudinal elongation material parameters while fiber-fiber contact energy and transverse displacement due to spreading wave could be adopted to determine transverse compression and distortion constants.

In terms of future works, it would be interesting to investigate the response of single yarn model under transverse impact for different projectile shapes and striking speeds. The evolution of the elementary strain energies and the associated invariants appear to be a useful investigation tool to determine the loading conditions imposed by a specific projectile shape. This information could be adopted for different purposes such as the investigation of mechanisms behind yarns inelastic failure or the formulation of multiaxial failure criteria. For this second case, experimental observations, as those provided in [56], could be adopted to tune the parameters α and β presented in Sec. 4.4.2 or, if needed, a novel failure criterion could be proposed. Future investigations at the fabric level should include the analysis of single and multi-layer fabrics using the proposed yarn continuum model. The elementary strain energy fields could be employed to elucidate about the load imposed by different projectiles to a fabric. In the same way, it would be possible to understand how a particular weave geometry affect the impact energy absorption process. Finally, the application of the proposed yarn mesoscopic model in multi-layer systems appears to be mandatory. A sensitivity analysis on material parameters related to yarn transverse properties would elucidate about the role of yarn cross section in this impact scenario. Following analyses should aim to the investigation and the comprehension of the impact phenomenon.

Bibliography

[1] Abbott, N., Donovan, J., and Shoppee, M. (1974). The effect of temperature and strain rate on the tensile properties of Kevlar and PBI yarns. Defense Technical Information Center.

[2] Aimene, Y., Hagege, B., Sidoroff, F., Vidal-Sallé, E., Boisse, P., and Dridi, S. (2008). Hyperelastic approach for composite reinforcement forming simulations. International Journal of Material Forming, 1(SUPPL. 1):811–814.

[3] Aimène, Y., Vidal-Sallé, E., Hagège, B., Sidoroff, F., and Boisse, P. (2009). A Hyperelastic Approach for Composite Reinforcement Large Deformation Analysis. Journal of Composite Materials.

[4] ANDRE, D. (2012). Mod{é}lisation par {é}l{é}ments discrets des phases d ' {é}bauchage et de doucissage de la silice. pages 1–34.

[5] André, D., Jebahi, M., Iordanoff, I., Charles, J.-l., and Néauport, J. (2013). Using the discrete element method to simulate brittle fracture in the indentation of a silica glass with a blunt indenter. Computer Methods in Applied Mechanics and Engineering, 265(8):136–147.

[6] Barauskas, R. and Abraitiene, A. (2007). Computational analysis of impact of a bullet against the multilayer fabrics in LS-DYNA. International Journal of Impact Engineering, 34(7):1286–1305.

[7] Bazhenov, S. (1997). Dissipation of energy by bulletproof aramid fabric. Journal of Materials Science, 32(15):4167–4173.

[8] Bazhenov, S. L., Dukhovskii, I. A., Kovalev, P. I., and Rozhkov, A. N. (2001). The fracture of SVM aramide fibers upon a high-velocity transverse impact. Polymer science.Series A, Chemistry, physics, 43(1):61–71.

[9] Bazhenov, S. L., Goncharuk, G. P., and Bobrov, A. V. (2015). Effect of transverse compression on the tensile strength of aramid yarns. Doklady Physical Chemistry, 462(1):115–117.

[10] Boussu, F. (2014). Compréhension des paramètres de produit et de procédé de fabrication des tissus 3D interlocks chaine. Applications en tant que renfort fibreux de solutions de protection à l ' impact. pages 0–173.

[11] Briscoe, B. J. and Motamedi, F. (1992). The ballistic impact characteristics of aramid fabrics: The influence of interface friction. Wear, 158(1-2):229–247.

[12] C. Criscione, J., S. Douglas, A., and C. Hunter, W. (2001). Physically based strain invariant set for materials exhibiting transversely isotropic behavior. Journal of the Mechanics and Physics of Solids, 49(July):871–897.

[13] Carr, D. J. (1999). Failure mechanisms of yarns subjected to ballistic impact. Journal of Materials Science Letters, 18(7):585–588.

[14] Charmetant, A., Vidal-Sall??, E., and Boisse, P. (2011). Hyperelastic modelling for mesoscopic analyses of composite reinforcements. Composites Science and Technology, 71(14):1623–1631.

[15] Cheeseman, B. A. and Bogetti, T. A. (2003). Ballistic impact into fabric and compliant composite laminates. Composite Structures, 61(1-2):161–173.

[16] Chen, W., Hudspeth, M., Guo, Z., Lim, B. H., Horner, S., and Zheng, J. Q. (2017). Multi-scale experiments on soft body armors under projectile normal impact. International Journal of Impact Engineering, 108:63–72.

[17] Chen, X. (2016). Advanced Fibrous Composite Materials for Ballistic Protection.

[18] Cheng, M. and Chen, W. (2006). Modeling transverse behavior of Kevlar® KM2 single fibers with deformation-induced damage. International Journal of Damage Mechanics, 15(2):121–132.

[19] Cheng, M., Chen, W., and Weerasooriya, T. (2004). Experimental investigation of the transverse mechanical properties of a single Kevlar KM2 fiber. International Journal of Solids and Structures, 41(22-23):6215–6232.

[20] Cheng, M., Chen, W., and Weerasooriya, T. (2005). Mechanical Properties of Kevlar® KM2 Single Fiber. Journal of Engineering Materials and Technology, 127(2):197.

[21] Chocron, S., Figueroa, E., King, N., Kirchdoerfer, T., Nicholls, A. E., Sagebiel, E., Weiss, C., and Freitas, C. J. (2010). Modeling and validation of full fabric targets under ballistic impact. Composites Science and Technology, 70(13):2012–2022.

[22] Chocron, S., Kirchdoerfer, T., King, N., and Freitas, C. J. (2011). Modeling of Fabric Impact With High Speed Imaging and Nickel-Chromium Wires Validation. Journal of Applied Mechanics, 78(September 2011):051007.

[23] Chocron, S., Ranjan Samant, K., Nicholls, A. E., Figueroa, E., Weiss, C. E., Walker, J. D., and Anderson, C. E. (2009). Measurement of strain in fabrics under ballistic impact using embedded nichrome wires. Part I: Technique. International Journal of Impact Engineering, 36(10-11):1296–1302.

[24] Chu, C. K. and Chen, Y. L. (2010). Ballistic-proof effects of various woven constructions. Fibres and Textiles in Eastern Europe, 83(6):63–67.

[25] Chu, T.-l., Ha-Minh, C., and Imad, A. (2016). A numerical investigation of the inuence of yarn mechanical and physical properties on the ballistic impact behavior of a Kevlar KM2® woven fabric. Composites Part B: Engineering, 95:144–154.

[26] Chu, Y., Min, S., and Chen, X. (2017). Numerical study of inter-yarn friction on the failure of fabrics upon ballistic impacts. Materials and Design, 115:299–316.

[27] Cundall, P. and Strack, O. (1979). A discrete numerical model for granular assemblies. Géotechnique, 29:47–65.

[28] Cunniff, P. (1992). An analysis of the system effects in woven fabrics under ballistic impact. Textile Research Journal, 62(9):495–509.

[29] Cunniff, P. (1999a). Decoupled response of textile body armor. Proc. 18th Int. Symp. on Ballistics, (January 1999):0–7.

[30] Cunniff, P. (1999b). Dimensionless Parameters for Optimization of Textile-Based Body Armor Systems. Proceeding of the 18th International Symposium on Ballistics, (January 1999):1303–1310.

[31] Cunniff, P. M. (1996). A Semiempirical Model for the Ballistic Impact Performance of Textile-Based Personnel Armor. Textile Research Journal, 66(1):45–58.

[32] Cunniff, P. M. and Committee, T. I. B. (1999). A Design Tool for the Development of Fragmentation Protective Body Armor. 18th International Symposium on Ballistics, 2(January 1999):1295–1302.

[33] Cuong, H. M., Imad, A., Boussu, F., Kanit, T., and Crepin, D. (2012). Numerical study on the effects of yarn mechanical transverse properties on the ballistic impact behaviour of textile fabric. Journal of Strain Analysis for Engineering Design, 47(7):524–534.

[34] Darijani, H. and Naghdabadi, R. (2010). Hyperelastic materials behavior modeling using consistent strain energy density functions. Acta Mechanica, 213(3-4):235–254.

[35] Das, S., Jagan, S., Shaw, A., and Pal, A. (2015a). Determination of inter-yarn friction and its effect on ballistic response of para-aramid woven fabric under low velocity impact. Composite Structures, 120:129–140.

[36] Das, S., Jagan, S., Shaw, A., and Pal, A. (2015b). Determination of inter-yarn friction and its effect on ballistic response of para-aramid woven fabric under low velocity impact. Composite Structures, 120:129–140.

[37] Deteresa, S. J., Allen, S. R., Farris, R. J., and Porter, R. S. (1984). Compressive and torsional behaviour of Kevlar 49 fibre. Journal of Materials Science, 19(1):57–72.

[38] Du Pont (2012). Kevlar Technical Guide.

[39] Duan, Y., Keefe, M., Bogetti, T. A., Cheeseman, B. A., and Powers, B. (2006a). A numerical investigation of the influence of friction on energy absorption by a high-strength fabric subjected to ballistic impact. International Journal of Impact Engineering, 32(8):1299–1312.

[40] Duan, Y., Keefe, M., Bogetti, T. A., and Powers, B. (2006b). Finite element modeling of transverse impact on a ballistic fabric. International Journal of Mechanical Sciences, 48(1):33–43.

[41] Durville, D. (2010). Simulation of the mechanical behaviour of woven fabrics at the scale of fibers. International Journal of Material Forming, 3(SUPPL. 2):1241–1251.

[42] Erlich, D., Shockey, D., and Simon, J. (2003). Slow Penetration of Ballistic Fabrics. Textile Research Journal, 73:179–184.

[43] Gasser, A., Boisse, P., and Hanklar, S. (2000). Mechanical behaviour of dry fabric reinforcements. 3D simulations versus biaxial tests. Computational Materials Science, 17(1):7–20.

[44] Grujicic, M., Glomski, P. S., Pandurangan, B., Bell, W. C., Yen, C. F., and Cheeseman, B. A. (2011). Multi-length scale computational derivation of Kevlar® yarn-level material model. Journal of Materials Science, 46(14):4787–4802.

[45] Grujicic, M., Hariharan, A., Pandurangan, B., Yen, C. F., Cheeseman, B. A., Wang, Y., Miao, Y., and Zheng, J. Q. (2012). Fiber-level modeling of dynamic strength of kevlar{®} KM2 ballistic fabric. Journal of Materials Engineering and Performance, 21(7):1107–1119.

[46] Ha-Minh, C., Boussu, F., Kanit, T., Crépin, D., and Imad, A. (2011a). Analysis on failure mechanisms of an interlock woven fabric under ballistic impact. Engineering Failure Analysis, 18(8):2179–2187.

[47] Ha-Minh, C., Imad, A., Boussu, F., and Kanit, T. (2015). Experimental and numerical investigation of a 3D woven fabric subjected to a ballistic impact. International Journal of Impact Engineering.

[48] Ha-Minh, C., Imad, A., Kanit, T., and Boussu, F. (2013). Numerical analysis of a ballistic impact on textile fabric. International Journal of Mechanical Sciences, 69:32–39.

[49] Ha-Minh, C., Kanit, T., Boussu, F., and Imad, A. (2011b). Numerical multi-scale modeling for textile woven fabric against ballistic impact. Computational Materials Science, 50(7):2172–2184.

[50] Hamila, N. and Boisse, P. (2007). A meso-macro three node finite element for draping of textile composite preforms. Applied Composite Materials, 14(4):235–250.

[51] Hearle, J. (2001). High-performance fibre.

[Holzapfel] Holzapfel, G. Nonlinear solid mechanics A continuum Approach for Engineers.

[53] Hosseinzadeh, M., Ghoreishi, M., and Narooei, K. (2016). Investigation of hyperelastic models for nonlinear elastic behavior of demineralized and deproteinized bovine cortical femur bone. Journal of the Mechanical Behavior of Biomedical Materials, 59:393–403.

[54] Hudspeth, M., Agarwal, A., Andrews, B., Claus, B., Hai, F., Funnell, C., Zheng, J., and Chen, W. (2014). Degradation of yarns recovered from soft-armor targets subjected to multiple ballistic impacts. Composites Part A: Applied Science and Manufacturing, 58:98–106.

[55] Hudspeth, M., Chen, W., and Zheng, J. (2015a). Why the Smith theory over-predicts instant rupture velocities during fiber transverse impact. Textile Research Journal, 86:743–754.

[56] Hudspeth, M., Chu, J.-m., Jewell, E., Lim, B., Ytuarte, E., Tsutsui, W., Horner, S., Zheng, J., and Chen, W. (2016). Effect of projectile nose geometry on the critical velocity and failure of yarn subjected to transverse impact. Textile Research Journal, 87:953–972.

[57] Hudspeth, M., Li, D., Spatola, J., Chen, W., and Zheng, J. (2015b). The effects of off-axis transverse deflection loading on the failure strain of various high-performance fibers. Textile Research Journal, 86(9):897–910.

[58] Isvilanonda, V., Iaquinto, J. M., Pai, S., Mackenzie-Helnwein, P., and Ledoux, W. R. (2016). Hyperelastic compressive mechanical properties of the subcalcaneal soft tissue: An inverse finite element analysis. Journal of Biomechanics, 49(7):1186–1191.

[59] Ivanov, I. and Tabiei, A. (2004). Loosely woven fabric model with viscoelastic crimped fibres for ballistic impact simulations. International Journal for Numerical Methods in Engineering, 61(10):1565–1583.

[60] Justin McKee, P., Sokolow, A. C., Yu, J. H., Long, L. L., and Wetzel, E. D. (2016). Finite Element Simulation of Ballistic Impact on Single Jersey Knit Fabric. Composite Structures, 162:98–107.

[61] Leigh Phoenix, S. and Porwal, P. K. (2003). A new membrane model for the ballistic impact response and V50 performance of multi-ply fibrous systems. International Journal of Solids and Structures, 40(24):6723–6765.

[62] Lim, C. T., Shim, V. P. W., and Ng, Y. H. (2003). Finite-element modeling of the ballistic impact of fabric armor. International Journal of Impact Engineering, 28:13–31.

[63] Lim, C. T., Tan, V. B. C., and Cheong, C. H. (2002). Perforation of high-strength double-ply fabric system by varying shaped projectiles. International Journal of Impact Engineering, 27(6):577–591.

[64] Lim, J., Zheng, J. Q., Masters, K., and Chen, W. W. (2011). Effects of gage length, loading rates, and damage on the strength of PPTA fibers. International Journal of Impact Engineering, 38(4):219–227.

[65] Luding, S. (2008). Introduction to discrete element methods: Basic of contact force models and how to perform the micro-macro transition to continuum theory. European Journal of Environmental and Civil ..., (Md):785–826.

[66] Mansouri, M. R., Montazerian, H., Schmauder, S., and Kadkhodapour, J. (2018). 3D-printed multimaterial composites tailored for compliancy and strain recovery. Composite Structures, 184(September 2017):11–17.

[67] McAllister, Q. P., Gillespie, J. W., and VanLandingham, M. R. (2012). Evaluation of the three-dimensional properties of Kevlar across length scales. Journal of Materials Research, 27(14):1824–1837.

[68] Miao, Y., Zhou, E., Wang, Y., and Cheeseman, B. A. (2008). Mechanics of textile composites: Micro-geometry. Composites Science and Technology, 68(7-8):1671–1678.

[69] Nilakantan, G. (2013). Filament-level modeling of Kevlar KM2 yarns for ballistic impact studies. Composite Structures, 104:1–13.

[70] Nilakantan, G. (2017). World's First Predictive and Validated Yarn-level FEA Modeling of the V0-V100 Probabilistic Penetration Response of Fully-Clamped Kevlar Fabric.

[71] Nilakantan, G. (2018). Experimentally validated predictive finite element modeling of the V0-V100 probabilistic penetration response of a Kevlar fabric against a spherical projectile. International Journal of Protective Structures.

[72] Nilakantan, G., Cox, B. N., and Sudre, O. (2017). Generation of Realistic Stochastic Virtual Microstructures using a Novel Thermal Growth Method for Woven Fabrics and Textile Composites. (October).

[73] Nilakantan, G. and Gillespie, J. W. (2012). Ballistic impact modeling of woven fabrics considering yarn strength, friction, projectile impact location, and fabric boundary condition effects. Composite Structures, 94(12):3624–3634.

[74] Nilakantan, G., Keefe, M., Bogetti, T. A., and Gillespie, J. W. (2010). Multiscale modeling of the impact of textile fabrics based on hybrid element analysis. International Journal of Impact Engineering, 37(10):1056–1071.

[75] Nilakantan, G., Keefe, M., Wetzel, E. D., Bogetti, T. A., and Gillespie, J. W. (2012). Effect of statistical yarn tensile strength on the probabilistic impact response of woven fabrics. Composites Science and Technology, 72(2):320–329.

[76] Nilakantan, G. and Nutt, S. (2014a). Effects of clamping design on the ballistic impact response of soft body armor. Composite Structures, 108(1):13–150.

[77] Nilakantan, G. and Nutt, S. (2014b). Effects of fabric target shape and size on the V50 ballistic impact response of soft body armor. Composite Structures, 116(1):661–669.

[78] Nilakantan, G. and Nutt, S. (2014c). State of the Art in the Deterministic and Probabilistic Ballistic Impact Modeling of Soft Body Armor : Filaments to Fabrics. American Society for Composites 29th Technical Conference.

[79] Nilakantan, G., Wetzel, E. D., Bogetti, T. A., and Gillespie, J. W. (2013). A deterministic finite element analysis of the effects of projectile characteristics on the impact response of fully clamped flexible woven fabrics. Composite Structures, 95:191–201.

[80] Nottingham, T. (2007). Sherburn, Martin (2007) Geometric and Mechanical Modelling of Textiles. PhD thesis, University of Nottingham.

[81] Ogden, R. W., Saccomandi, G., and Sgura, I. (2004). Fitting hyperelastic models to experimental data. Computational Mechanics, 34(6):484–502.

[82] Parsons, E. M., King, M. J., and Socrate, S. (2013). Modeling yarn slip in woven fabric at the continuum level: Simulations of ballistic impact. Journal of the Mechanics and Physics of Solids, 61(1):265–292.

[83] Parsons, E. M., Weerasooriya, T., Sarva, S., and Socrate, S. (2010). Impact of woven fabric: Experiments and mesostructure-based continuum-level simulations. Journal of the Mechanics and Physics of Solids, 58(11):1995–2021.

[84] Phoenix, S., Heisserer, U., van der Werff, H., and van der Jagt-Deutekom, M. (2017). Modeling and Experiments on Ballistic Impact into UHMWPE Yarns Using Flat and Saddle-Nosed Projectiles. Fibers, 5(1):8.

[85] Pritchard, M., Sarsby, R. W., and Anand, S. C. (2000). Handbook of Technical Textiles.

[86] Prosser, R. A. (1988). Penetration of Nylon Ballistic Panels by Fragment-Simulating Projectiles: Part II: Mechanism of Penetration. Textile Research Journal, 58(3):161–165.

[87] Rao, M. P., Duan, Y., Keefe, M., Powers, B. M., and Bogetti, T. A. (2009). Modeling the effects of yarn material properties and friction on the ballistic impact of a plain-weave fabric. Composite Structures, 89(4):556–566.

[88] Rashid, B., Destrade, M., and Gilchrist, M. D. (2013). Mechanical characterization of brain tissue in simple shear at dynamic strain rates. Journal of the Mechanical Behavior of Biomedical Materials, 28:71–85.

[89] Roylance, D. (1977). Ballistics of Transversely Impacted Fibers. Textile Research Journal, 47(10):679–684.

[90] Roylance, D. (1980). Penetration Mechanics of Textile Structures.

[91] Roylance, D. K., Wilde, A. F., and Tocci, G. C. (1973). Ballistic impact of textile structures.

[92] Shahkarami, A. and Vaziri, R. (2007). A continuum shell finite element model for impact simulation of woven fabrics. International Journal of Impact Engineering, 34(1):104–119.

[93] Shim, V. P. W., Tan, V. B. C., and Tay, T. E. (1995). Modelling deformation and damage characteristics of woven fabric under small projectile impact. International Journal of Impact Engineering, 16(4):585–605.

[94] Smith, J., Carl, A., and Shouse, P. J. (1964). Stress-Strain Relationships in Yarns Subjected to Rapid Impact Loading Part XI: Strain Distributions Resulting from Rifle Bullet Impact. Journal of Research of the National Bureau of Standards, pages 743–757.

[95] Smith, J. C. (1961). Stress-Strain Relationship in Yarns Subjected to Rapid Impact Loading Part VII: Stress-Strain Curves and Breaking -Energy Data for Textile Yarns. National Bureau of Standards, 31:721–734.

[96] Smith, J. C. (1963). Stress-strain relationships in yarns subjected to rapid impact loading part x: Stress-strain curves obtained by impact with rifle bullets. National Bureau of Standards, 33:919–934.

[97] Smith, J. C., McCracking, F. L., and Schiefer, H. F. (1955). Stress-Strain Relationships in Yarns Subjected to Rapid Impact Loading. Part V: Wave Propagation In Long Textile Yarns Impacted Transversely. Journal of Research of the National Bureau of Standards, 60(5):701–708.

[98] Sockalingam, S., Bremble, R., Gillespie, J. W., and Keefe, M. (2016a). Transverse compression behavior of Kevlar KM2 single fiber. Composites Part A: Applied Science and Manufacturing, 81:271–281.

[99] Sockalingam, S., Chowdhury, S. C., Gillespie, J. W., and Keefe, M. (2016b). Recent advances in modeling and experiments of Kevlar ballistic fibrils, fibers, yarns and flexible woven textile fabrics - a review. Textile Research Journal, 87:984–1010.

[100] Sockalingam, S., Gillespie, J. W., and Keefe, M. (2014a). On the transverse compression response of Kevlar KM2 using fiber-level finite element model. International Journal of Solids and Structures, 51(13):2504–2517.

[101] Sockalingam, S., Gillespie, J. W., and Keefe, M. (2015). Dynamic modeling of Kevlar KM2 single fiber subjected to transverse impact. International Journal of Solids and Structures, 67-68(May):297–310.

[102] Sockalingam, S., Gillespie, J. W., and Keefe, M. (2016c). Influence of multiaxial loading on the failure of Kevlar KM2 single fiber. Textile Research Journal, 88:483–498.

[103] Sockalingam, S., Gillespie Jr, J. W., and Keefe, M. (2014b). Fiber-level Tow Modeling of Kevlar KM2 Subjected to High Velocity Impact. SAMPE Seattle 2014, Seattle, Washington, June 02-05, 2014, (January 2014).

[104] Sockalingam, S., Jr, J. W. G., and Keefe, M. (2016d). Modeling the fiber length-scale response of Kevlar KM2 yarn during transverse impact. Textile Research Journal, 88:483–498.

[105] Song, B., Park, H., Lu, W.-Y., and Chen, W. (2011). Transverse Impact Response of a Linear Elastic Ballistic Fiber Yarn. Journal of Applied Mechanics, 78(5):051023.

[106] Tabiei, A. and Nilakantan, G. (2008). Ballistic Impact of Dry Woven Fabric Composites: A Review. Applied Mechanics Reviews, 61(1):010801.

[107] Tan, V. B. C., Lim, C. T., and Cheong, C. H. (2003). Perforation of high-strength fabric by projectiles of different geometry. International Journal of Impact Engineering, 28(2):207–222.

[108] Walker, J. D. and Chocron, S. (2011). Why Impacted Yarns Break at Lower Speed Than Classical Theory Predicts. Journal of Applied Mechanics, 78(September 2011):51021.

[109] Wang, Y., Chen, X., Young, R., and Kinloch, I. (2016a). A numerical and experimental analysis of the influence of crimp on ballistic impact response of woven fabrics. Composite Structures, 135:8–16.

[110] Wang, Y., Miao, Y., Huang, L., Swenson, D., Yen, C.-F., Yu, J., and Zheng, J. Q. (2016b). Effect of the inter-fiber friction on fiber damage propagation and ballistic limit of 2-D woven fabrics under a fully confined boundary condition. International Journal of Impact Engineering, 97:66–78.

[111] Wang, Y., Miao, Y., Swenson, D., Cheeseman, B. A., Yen, C. F., and LaMattina, B. (2010). Digital element approach for simulating impact and penetration of textiles. International Journal of Impact Engineering, 37(5):552–560.

[112] Yang, C. C., Ngo, T., and Tran, P. (2015). Influences of weaving architectures on the impact resistance of multi-layer fabrics. Materials and Design, 85:282–295.

[113] Yu, J. H., Dehmer, P. G., and Yen, C.-f. (2010). High-speed Photogrammetric Analysis on the Ballistic Behavior of Kevlar Fabrics Impacted by Various Projectiles. Technical Reports United States Army Research Laboratory.

[114] Zeng, X. S., Tan, V. B. C., and Shim, V. P. W. (2006). Modelling inter-yarn friction in woven fabric armour. International Journal for Numerical Methods in Engineering, 66(8):1309–1330.

[115] Zheng, Q.-S. (1994). Theory of Representations for Tensor Functions—A Unified Invariant Approach to Constitutive Equations. Applied Mechanics Reviews, 47(11):545.

[116] Zhou, G., Sun, X., and Wang, Y. (2004). Multi-chain digital element analysis in textile mechanics. Composites Science and Technology, 64(2):239–244.

[117] Zhou, Y. and Chen, X. (2015). A numerical investigation into the influence of fabric construction on ballistic performance. Composites Part B: Engineering, 76:209–217.

TITRE FRANÇAIS

Résumé :

Ce travail de thèse est dédié au développement d’un modèle numérique prédictif du comportement de tissu sec soumis à l’impact à haute vitesse. Parmi les différentes stratégies adoptées pour modéliser un tissu, les modèles mésoscopiques sont les plus populaires du fait de leur capacité à représenter fidèlement l’évolution de l’impact combinée à un coût de calcul raisonnable. L’objet de cette thèse est de développer une nouvelle loi constitutive capable de surpasser les limites du modèle linéaire élastique classique tout en maintenant une bonne représentation des propriétés longitudinales du toron et un coût de calcul acceptable. La première étape a été de comprendre les phénomènes physiques et de quantifier en particulier les effets liés à la section droite du toron sur les propriétés balistiques d’un tissu. Les résultats obtenus ont confirmé que la mécanique de la section droite a des répercussions sur l’initialisation de la rupture du fil mettant en jeu des énergies significatives pendant la première phase d’un impact. A partir des résultats précédents, un nouveau modèle constitutif de toron adapté à des applications dynamiques a été développé. Une formulation hyper-élastique, précédemment utilisée pour des analyses statiques a été étendue au cas de l’impact et une nouvelle approche multi échelle a été proposée pour la détermination des paramètres du modèle. Par la suite, le modèle de fil proposé a été implémenté au niveau du tissu. Il est ainsi capable de représenter correctement la dynamique d’impact , l’évolution des énergies en jeu et la rupture du tissu. La stabilité numérique du modèle a également pu être appréciée. Il devient ainsi un outil pratique et efficace pour la prédiction des performances balistiques de tissus.

Mots clés : Multi échelle, Modélisation, Tissus, Impact, Fils

TITRE ANGLAIS

Abstract :

This thesis work focuses on the development of a new predictive numerical model for dry fabrics under high velocity impact . Among the different approaches adopted , the fabric mesoscopic models (yarn level models) result to be the most popular due to their ability to carefully represent the impact evolution combined with a reasonable computational cost . In order to represent a group of disjointed fibers as a continuum , a proper constitutive model is required . According to recent studies , yarn cross section behaviour should be carefully treated in any numerical model which aims to the prediction of the fabric ballistic performance . The goal of the current work has been to provide a new constitutive model which overcome the limitation of the classic linear elastic approach while keeping unaltered its advantages , i . e . low computational costs and accurate description of yarn longitudinal behaviour . The first step of this study was to quantify the yarn cross section effects over textile ballistic properties and the phenomena related to this aspect. Results showed how yarn transverse mechanical behaviour has a role in failure initialization and energies trends , especially during the first phase of an impact . Starting from the previous observations , a new consistent yarn continuum model for impact applications has been developed with a novel multiscale approach for the determination of its material parameters. The last part has been dedicated to the application of the proposed constitutive law at the fabric level .

The proposed hyperelastic approach is able to correctly represent the impact dynamic and fabric energies trends without occurring into model instabilities.

Keywords : Multiscale, Fabric, Impact, Yarn

ARTS ET MÉTIERS ParisTech

ParisTech INSTITUT DES SCIENCES ET TECHNOLOGIES PARIS INSTITUTE OF TECHNOLOGY